



**UNIVERSIDADE FEDERAL DO PARÁ
INSTITUTO DE GEOCIÊNCIAS
PROGRAMA DE PÓS-GRADUAÇÃO EM GEOLOGIA E GEOQUÍMICA**

DISSERTAÇÃO DE MESTRADO Nº 474

**PETROGRAFIA, QUÍMICA MINERAL E PARÂMETROS DE
CRISTALIZAÇÃO DA SUÍTE PLANALTO, PROVÍNCIA
CARAJÁS**

Dissertação apresentada por:

INGRID ROBERTA VIANA DA CUNHA

Orientador: Prof. Dr. Roberto Dall'Agnol (UFPA)

Coorientadora: Prof.^a Dr.^a Gilmara Regina Lima Feio (UNIFESSPA)

**BELÉM
2015**

Dados Internacionais de Catalogação de Publicação (CIP)
Biblioteca do Instituto de Geociências/SIBI/UFPA

Cunha, Ingrid Roberta Viana da, 1988-
Petrografia, química mineral e parâmetros de cristalização da
suíte Planalto, Província Carajás / Ingrid Roberta Viana da Cunha. –
2015.

xvii, 92 f. : il. ; 30 cm

Inclui bibliografias

Orientador: Roberto Dall'Agnol
Coorientadora: Gilmara Regina Lima Feio

Dissertação (Mestrado) – Universidade Federal do Pará,
Instituto de Geociências, Programa de Pós-Graduação em Geologia
e Geoquímica, Belém, 2015.

1. Petrologia - Pará. 2. Rochas Ígneas - Pará. 3.
Geologia estratigráfica – Arqueano. 4. Província Carajás. I. Título.

CDD 22. ed. 552.098115



Universidade Federal do Pará
Instituto de Geociências
Programa de Pós-Graduação em Geologia e Geoquímica


**PETROGRAFIA, QUÍMICA MINERAL E PARÂMETROS DE
CRISTALIZAÇÃO DA SUÍTE PLANALTO, PROVÍNCIA
CARAJÁS**

**DISSERTAÇÃO APRESENTADA POR
INGRID ROBERTA VIANA DA CUNHA**

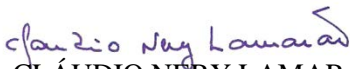
**Como requisito parcial à obtenção do Grau de Mestre em Ciências na Área de
GEOQUÍMICA E PETROLOGIA.**

Data de Aprovação: 28 / 07 / 2015

Banca Examinadora:


Prof. ROBERTO DALL'AGNOL
(Orientador-UFPA)


Prof. NILSON FRANCISQUINI BOTELHO
(Membro-UnB)


Prof. CLÁUDIO NERY LAMARÃO
(Membro-UFPA)

À minha amada mãe

AGRADECIMENTOS

- *Agradeço a Deus por todas as bênçãos concedidas ao longo da minha caminhada.*
- *À minha família, em especial aos meus pais, por terem ensinado que esforço, dedicação, sacrifícios e humildade associados à busca pelo conhecimento são as chaves para obter sucesso.*
- *À Universidade Federal do Pará (UFPA), ao Instituto de Geociências, ao Programa de Pós-graduação em Geologia e Geoquímica, por todo suporte disponibilizado para a elaboração da dissertação.*
- *À Coordenação de Aperfeiçoamento de Pessoal de Nível Superior (CAPES) pela concessão de bolsa de estudo.*
- *Ao prof. Dr. Roberto Dall’Agnol pela orientação, confiança e principalmente, pelos conhecimentos transmitidos.*
- *À profa. Dr. Gilmara Regina Lima Feio, por ter direcionado as fases iniciais desta pesquisa. E também, pelos ensinamentos, conversas e conselhos...*
- *Ao Instituto Nacional de Ciência e Tecnologia de Geociências da Amazônia/Geociam (Processo N°573733/2008-2) pelo apoio financeiro.*
- *Ao Grupo de Pesquisa Petrologia de Granitoides (GPPG), do Instituto de Geociências da Universidade Federal do Pará, pelo suporte técnico-científico.*
- *As colegas de grupo (GPPG), Mayara Fraeda Barbosa Teixeira e Fabriciana Vieira Guimarães pelo companheirismo e amizade.*
- *Aos amigos, Bruna Nogueira, Luísa Barros, Carlos Junior, Paulo Soares, Carla Braga, Aldemir Sotero, Renato Sol e Camila Vilar, por terem feito essa jornada mais leve e divertida.*
- *Ao geólogo e amigo, Rafael Estumano Leal, pela contribuição dada na elaboração do artigo científico incluso nesta dissertação.*
- *Ao geólogo e melhor amigo, Juvenal Neto, pelo companheirismo, amizade e incentivo compartilhados. E acima de tudo, agradeço a confiança e sinceridade transmitida a mim ao longo desses anos...*
- *Aos amigos Ramon Carvalho e Leandro Melo, pelos momentos de descontração e pela amizade.*
- *Por fim, agradeço a todos que contribuíram direta ou indiretamente para a elaboração deste trabalho.*

Confie no Senhor de todo o coração e não se apoie na sua própria inteligência. Lembre de Deus em tudo o que fizer, e Ele lhe mostrará o caminho certo.

Provérbios 3: 5-6

RESUMO

A Suíte Planalto está localizada no Domínio Canaã dos Carajás da Província Carajás. A suíte tem idade neoarqueana (2,73 Ga), e os granitos que a constituem possuem caráter ferroso e afinidade com granitos tipo-A e são intrusivos em unidades mesoarqueanas e no Supergrupo Itacaiúnas. Associa-se espacialmente com rochas charnoquíticas do Diopsídio-Norito Pium e com a Suíte Pedra Branca. As rochas da Suíte Planalto são hololeucocráticas a leucocráticas com dominância de monzogranitos e sienogranitos e presença de raros álcali-feldspato-granitos. Ao microscópio, apresentam feições texturais magmáticas parcialmente preservadas, porém a textura granular hipidiomórfica média a grossa original tende a ser substituída por texturas protomiloníticas a miloníticas, com formação de porfiroblastos ovalados de granulação média a grossa de microclina envoltos por matriz fina a base de quartzo e feldspatos intensamente recristalizados. A Suíte Planalto apresenta valores de suscetibilidade magnética (SM) variáveis, os quais, associados com as características petrológicas, permitiram distinguir dois grupos: (1) Grupo formado em condições reduzidas, que engloba as amostras contendo ilmenita e desprovidas de magnetita, com baixos valores de SM; (2) Grupo moderadamente oxidado, que se distingue do anterior por apresentar os mais altos valores de SM, justificados pela presença de magnetita associada à ilmenita. A ilmenita ocorre como cristais anédricos a subédricos dos tipos texturais ilmenita individual ou ilmenita composta, sendo esta última menos comum e restrita às rochas do grupo 2. A magnetita, por sua vez, ocorre como cristais subédricos a anédricos ou, mais raramente, euédricos com evidência de martitização, localmente com bordas e núcleos corroídos. Ilmenita e magnetita exibem composições próximas de seus membros extremos ideais, embora a ilmenita mostre proporções variáveis de pyrophanita (MnTiO_3). Os cristais de titanita ocorrem nos grupos 1 e 2 circundando os cristais de ilmenita, ou então, como finos grãos anédricos inclusos em anfibólio e biotita, que formam agregados máficos. Os conteúdos modais de titanita são muito variáveis em ambos os grupos e não há correlação entre titanita e opacos modais. Além disso, as composições químicas de titanita, em particular suas baixas razões Fe/Al, sugerem que este mineral foi reequilibrado por processos subsolidus. Os anfibólios da Suíte Planalto são cálcicos com composição variando entre potássio-hastingsita (dominante) e cloro-potássio-hastingsita (subordinada) e razões $\text{Fe}/(\text{Fe}+\text{Mg}) > 0,8$. A biotita também apresenta altas razões Fe/Mg ($> 0,7$) e é classificada como annita. Os porfiroclastos de plagioclásios são oligoclásio (An_{25-10}) e os grãos da matriz recristalizada mostram composição variando entre oligoclásio ou albita (An_{259-2}). Os dados obtidos, mostram que os granitos do grupo 1 da Suíte Planalto

foram formados em condições reduzidas, abaixo do tampão FMQ. Os granitos do grupo 2 cristalizaram em condições mais oxidantes, coincidentes com às do tampão FMQ ou ligeiramente acima, ou alternativamente, também foram formados em fO_2 abaixo de FMQ, submetidos a condições ligeiramente mais oxidantes no *subsolidus*. Pressões de 900 MPa a 700 MPa e de 500 e 300 MPa foram estimadas, respectivamente, para a origem dos magmas da Suíte Planalto e para a colocação e cristalização final dos seus plutons. Geotermômetros sugerem temperaturas iniciais de cristalização variando de 900°C e 830°C, sendo que a temperatura do *solidus* foi provavelmente próxima de 700 °C. O conteúdo de água do magma foi estimado em 4 % em peso, podendo atingir possivelmente até 4% em peso. A comparação mineralógica entre a Suíte Planalto e granitos neoarqueanos similares da Província Carajás mostram que a Suíte Planalto e o Complexo Granítico Estrela foram formados em condições muito similares. As composições de anfibólio e biotita dos granitos Planalto e Estrela são enriquecidas em alumínio e assemelham-se neste aspecto aqueles do pluton Matok do Limpopo Belt. Diferem, usando este mesmo critério dos granitos rapakivi tipo-A proterozoicos. Em termos das condições de fugacidade de oxigênio, a Suíte Planalto e o Complexo Granítico Estrela se aproximam dos granitos rapakivi mesoproterozoicos e dos granitos paleoproterozóicos reduzidos a moderadamente oxidados da Província Carajás e diferem dos granitos oxidados daquela província e também dos granitoides do pluton Matok. Conclui-se que a Suíte Planalto é similar aos granitos neoarqueanos ferrosos ou do tipo-A da Província Carajás e, exceto por seu caráter reduzido, diferem em suas características mineralógicas e nos parâmetros de cristalização de alguns exemplos clássicos de granitos tipo-A e exceto por seu caráter reduzido, são semelhantes aos granitoides neoarqueanos Fe-K e Mg-K. O fato de se ter um ambiente colisional em Carajás e também no Limpopo Belt durante o neoarqueano sugere que as similaridades observadas entre os granitos de ambas províncias pode refletir um condicionamento geológico e tectônico.

Palavras chaves: Arqueano. Granite tipo-A. Petrologia magnética. Parâmetros de cristalização. Província Carajás.

ABSTRACT

The Planalto Suite is located in the Canaã dos Carajás Domain of the Carajás Province in the southeastern part of the Amazonian Craton. The suite has Neoproterozoic age (~2.73 Ga), ferroan character and affinity with A-type granites. Magnetic petrology studies allowed the distinction of two groups: (1) Ilmenite granites devoid of magnetite and showing low magnetic susceptibility (MS) values (MS between 0.6247×10^{-3} and 0.0102×10^{-3} SI; average of 0.1522×10^{-3}); (2) Magnetite-ilmenite-bearing granites which display comparatively higher but still moderate MS values (between 15.700×10^{-3} and 0.8036×10^{-3} SI; average of 5.1717×10^{-3}). Textural evidence indicates that amphibole, ilmenite, titanite, and, in the rocks of Group 2, also magnetite formed during magmatic crystallization. However, titanite chemical composition suggests that it was re-equilibrated by subsolidus processes. The amphibole varies from potassian-hastingsite to chloro-potassian-hastingsite and shows $\text{Fe}/(\text{Fe}+\text{Mg}) > 0.8$. Biotite also shows high $\text{Fe}/(\text{Fe}+\text{Mg})$ ratios and is classified as annite although relatively enriched in Al compared to the annite end member. Plagioclase porphyroclasts are oligoclase (An_{25-10}) and the grains of the recrystallized matrix display oligoclasic or albitic composition (An_{9-2}). Mineral chemistry, magnetic petrology and whole rock geochemistry indicate that the dominant group 1 granites of the Planalto Suite were formed under reduced conditions below the FMQ buffer. The group 2 granites crystallized under more oxidizing conditions on or slightly above the FMQ buffer. Pressures of 900-700 MPa for the origin and of 500-300 MPa for the emplacement were estimated for the Planalto magmas. Geothermometers suggest initial crystallization temperatures between 900 °C and 830 °C and water content in the magma higher than 4 wt %. The mineralogical comparison between the Planalto Suite and the Archean subalkaline Estrela Granitic Complex of the Carajás Province reveals strong compositional analogies indicating that they were probably formed under similar conditions. The amphibole and biotite compositions of Planalto and Estrela granites are relatively enriched in Al being comparable with those of the Neoproterozoic Matok Pluton of the Limpopo Belt. They differ using the same criteria of the Proterozoic rapakivi A-type granites. On the other hand, in terms of $\text{Fe}/(\text{Fe}+\text{Mg})$ ratio, the Planalto and Estrela granites approach the reduced Mesoproterozoic rapakivi granites and the reduced to moderately oxidized Paleoproterozoic granites of, respectively, the Velho Guilherme and Serra dos Carajás suites and differ from the oxidized granites (Jamon Suite) of the Carajás province and also of Matok pluton. It is concluded that the Planalto Suite and similar Neoproterozoic granites of the Carajás Province differ in mineralogical characteristics and crystallization parameters of some classic examples of A-type granites and, except for its reduced character, they are akin to the

Neoproterozoic Fe-K and Mg-K granitoids of the Limpopo Belt, as exemplified by the Matok granitoids. This indicates that the collisional setting of Carajás and Limpopo exerted strong influence in the nature of the Neoproterozoic granitoid magmas.

Keywords: Archean. A-type granites. Magnetic petrology. Crystallization parameters. Carajás Province.

LISTA DE ILUSTRAÇÕES

CAPÍTULO 1

- Figura 1.1 - Mapa de localização e acesso à área de estudo.....2
- Figura 1.2 - a) Localização da Província Carajás no Cráton Amazônico; b) Mapa geológico simplificado da Província Carajás, mostrando os Domínios Rio Maria e Carajás, posteriormente subdivididos em subdomínios Sapucaia e Canaã dos Carajás e Bacia Carajás; o retângulo corresponde a área de estudo detalhada na figura 1c; (c) Mapa geológico da área de Canaã dos Carajás, mostrando a Suíte Planalto e a localização das amostras analisadas por Microsonda Eletrônica.....6
- Figura 1.3 - Mapa geológico da área de Canaã dos Carajás com destaque para as amostragens realizadas na Suíte Planalto.....7

CAPÍTULO 2

- Figure 2.1 – a) Location of the Carajás Province in the Amazonian Craton; b) Simplified geological map of the Carajás Province, showing the Rio Maria and Carajás domains, the latter subdivided in the Sapucaia and Canaã dos Carajás subdomains, and Carajás Basin; the rectangle corresponds to the studied area detailed in figure 1c; (c) Geological map of the Canaã dos Carajás area, displaying the Planalto Suite and the location of samples analyzed by electronmicroprobe.....19
- Figure 2.2 - QAP and Q-(A+P)-M' modal diagrams for the Planalto Suite. A – Alkaline feldspar; P- Plagioclase; Q – Quartz; M' = M – (apatite, muscovite and carbonates).....21
- Figure 2.3 - a) Macroscopic aspect of a granite from the Planalto Suite (Facies HBMzG, Group 1; cf. abbreviations in Supplementary data, Table S1); b) Relatively well preserved microcline phenocryst in a recrystallized matrix (Facies HBSG, Group 2); c) Phenocryst of mesoperthitic microcline with inclusion of amphibole and incipient development of chessboard albite (Facies HLAG, Group 2); d) Recrystallized quartz ribbon in a granite with mylonitic texture (Facies HBSG, Group 2); e) Clots of mafic minerals with dominance of amphibole and biotite associated with subhedral titanite and euhedral zircon and apatite (Facies BHMzG, Group 2); f) Lamellae of biotite associated with subhedral grains of titanite and amphibole (Facies BHMzG, Group 2). Photomicrographs in crossed nicols (b, c, d) or parallel nicols (e, f).....23

Figure 2.4 - Magnetic Susceptibility histogram for samples of the Planalto Suite.....	24
Figure 2.5 - Modal opaques (volume %) vs. magnetic susceptibility (SI units) diagram for the Planalto Suite.....	25
Figure 2.6 - a) and b) Corona of titanite surrounding ilmenite crystal associated with amphibole (Facies BHMzG, Group 1); c) and d) Mafic clot with amphibole, subhedral magnetite and composite ilmenite (Facies HLAG, Group 2); e) and f) Poikilitic amphibole crystals with abundant subhedral inclusions of magnetite, composite ilmenite and felsic minerals; to note the coarser subhedral crystals of magnetite found generally in the borders of the amphibole (Facies HLAG, Group 2); a), c) and e) Transmitted light microscopy with parallel nicols; b), d) and f) Backscattered images obtained in scanning electron microscope. Ilm Cext = external composite ilmenite.....	27
Figure 2.7 - Classification diagram for amphiboles of the Planalto Suite.....	29
Figure 2.8 - Compositional variation of the biotite of the Planalto Suite. a) $^{IV}Al - Fe/(Fe+Mg)$ diagram; b) Al total x Mg diagram; Abbreviations: Sid - siderophyllite; East - eastonite; Phlog - phlogopite; Ann -annite; TSM - tetrasilicic mica; Zw - zinnwaldite.....	30
Figure 2.9 - Fe vs Al diagram for the titanite of the Planalto Suite, with fields of magmatic and metamorphic titanite compositions. Symbols for the Planalto varieties as in Figure 8.....	53
Figure 2.10 - $Fe/(Fe+Mg) \times Al$ diagram for amphiboles of the Planalto Suite, showing possible crystallization pressure ranges of amphibole without temperature correction (see text).....	44
Figure 2.11 - Compositional variation of amphibole and biotite of the Planalto Suite; a) $Fe/(Fe+Mg)$ ratio versus Al^{IV} diagram showing the low fO_2 character of Planalto amphibole; amphiboles of A-type granites of Carajás (Jamon Suite) and mid-Proterozoic granites of the United States are shown for comparison; b) $Fe/(Fe+Mg)$ versus $Al^{IV} + Al^{VI}$ diagram showing the biotite composition of Planalto granites and those from A-type granites of Carajás (Jamon Suite) and United States.....	46

Figure 2.12 – Diagram T vs $\log fO_2$ showing possible temperature intervals of formation and estimated fO_2 conditions for the Planalto Suite granites. Curves of the main stability buffers and different Fe phases in function of the oxidation stage in the Fe-Si-O system. Grayish lines illustrate the evolution of the Planalto granites of Groups 1 and 2 in two different hypotheses (see text). QIF = quartz-ilmenite-fayalite; FMQ = fayalite-magnetite-quartz; MH = magnetite-hematite.....47

Figure 2.13 – Comparison between amphibole and biotite from the Planalto granites and similar granites. a) $Fe/(Fe+Mg) \times Al^{IV}$ diagram showing the distribution of Planalto amphibole and the fields of amphibole composition of granites selected for comparison; b) $Fe/(Fe+Mg)$ vs $Al^{IV} + Al^{VI}$ diagram comparing the distribution of Planalto biotite with that of similar ferroan or A-type granites.....54

LISTA DE TABELAS**CAPÍTULO 2**

Table 2.1: Representative electron microprobe analyses of amphiboles of the Planalto Suite.....	31
Table 2.2: Electron microprobe analyses of biotite of the Planalto Suite.....	32
Table 2.3: Representative electron microprobe analyses of plagioclase of the Planalto Suite.....	33
Table 2.4: Representative electron microprobe analyses of titanite of the Planalto Suite.....	36
Table 2.5: Representative electron microprobe analyses of ilmenite and magnetite of the Planalto Suite.....	38
Table 2.6: Estimate of pressure and temperature of crystallization for the granites of the Planalto Suite.....	41

SUMÁRIO

DEDICATÓRIA	iv
AGRADECIMENTOS	v
EPÍGRAFE	vi
RESUMO	vii
ABSTRACT	ix
LISTA DE ILUSTRAÇÕES	xi
LISTA DE TABELAS	xiv
CAPÍTULO 1	
1. INTRODUÇÃO	1
1.1 APRESENTAÇÃO	1
1.2 CONTEXTO GEOLÓGICO REGIONAL	2
1.3 PROBLEMÁTICA E JUSTIFICATIVA DA PROPOSTA	4
1.4 OBJETIVOS	5
1.5 MATERIAIS E MÉTODOS	5
1.5.1 Pesquisa Bibliográfica	8
1.5.2 Estudo Petrográfico	8
1.5.3 Química Mineral	9
1.5.3.1 Microscopia Eletrônica de Varredura (MEV).....	9
1.5.3.2 Microsonda Eletrônica.....	9
1.5.3.3 Estimativa dos parâmetros de cristalização.....	9
1.5.4 Geoquímica em rocha total	10
CARTA DE ACEITE	11
CAPÍTULO 2	
ARTIGO CIENTÍFICO: MINERAL CHEMISTRY AND MAGNETIC PETROLOGY OF THE ARCHEAN PLANALTO SUITE, CARAJÁS PROVINCE – AMAZONIAN	

CRATON: IMPLICATIONS FOR THE EVOLUTION OF FERROAN ARCHEAN GRANITES.....	31
ABSTRACT	13
2.1 INTRODUCTION	14
2.2 GEOLOGIC SETTING	15
2.3 GEOLOGY OF THE PLANALTO SUITE	17
2.4 PETROGRAPHY	20
2.4.1 Modal composition and petrographic classification	20
2.4.2 Textural aspects	21
2.5 MAGNETIC PETROLOGY.....	24
2.6 MINERAL CHEMISTRY	28
2.6.1 Amphibole	28
2.6.2 Biotite	29
2.6.3. Plagioclase	30
2.6.4 Titanite.....	34
2.6.5 Ilmenite	37
2.6.6 Magnetite.....	37
2.7 DISCUSSION	39
2.7.1 Estimation of crystallization parameters of the Planalto Suite	39
2.7.1.1 Temperature	39
2.7.1.2 Pressure	42
2.7.1.3 Oxygen fugacity (fO_2).....	44
2.7.1.4 Water content	48
2.7.2 Comparison between the Planalto Suite and similar granites	49
2.7.2.1 Comparison between the Planalto Suite and similar granites of the Carajás Province	49
2.7.2.2 Comparison between the Planalto Suite and similar granites of other provinces in the world	51

2.8 CONCLUSIONS	55
Acknowledgments	57
References	57
SUPPLEMENTARY DATA	66
CAPÍTULO 3	
3. CONCLUSÃO	72
REFERÊNCIAS	75
APÊNDICES	79
APÊNDICE A: COORDENADAS DOS PONTOS AMOSTRADOS E ESTUDOS REALIZADOS	80
APÊNDICE B: TABELAS COM ANÁLISES QUÍMICAS POR EDS EM MICROSCOPIA ELETRÔNICA DE VARREDURA DA SUÍTE PLANALTO	82
APÊNDICE C: TABELAS COM ANÁLISES QUÍMICAS POR WDS EM MICROSSONDA ELETRÔNICA DA SUÍTE PLANALTO	87
APÊNDICE D: COMPARAÇÃO ENTRE AS ANÁLISES OBTIDAS POR EDS EM MEV E WDS EM MICROSSONDA ELETRÔNICA, PARA OS ANFIBÓLIOS DA SUÍTE PLANALTO	89
APÊNDICE E: COMPARAÇÃO ENTRE AS ANÁLISES OBTIDAS POR EDS EM MEV E WDS EM MICROSSONDA PARA BIOTITA DA SUÍTE PLANALTO	91

CAPÍTULO 1

1.INTRODUÇÃO

1.1 APRESENTAÇÃO

A presente pesquisa foi voltada para a Suíte Planalto (Figura 1.1) localizada no Domínio Canaã dos Carajás (DCC), inserido no contexto geológico da Província Carajás (PC), de idade arqueana e dividida em três domínios, Domínio Canaã dos Carajás (DCC), Domínio Sapucaia (DS) e Domínio Rio Maria (DRM) (Dall'Agnol *et al.* 2013). O Granito Planalto foi descrito originalmente por Huhn *et al.* (1999) e a denominação de Suíte Planalto foi atribuída por Feio *et al.* (2012).

Uma série de estudos já foram realizados em granitos da Suíte Planalto (Huhn *et al.* 1999, Gomes 2003, Oliveira 2003, Sardinha *et al.* 2004, Silva 2011, Feio *et al.* 2012, Santos, P.A. 2013, Cunha 2013), porém ainda permanecem algumas lacunas no conhecimento daquela unidade. Entre as principais lacunas constam seu comportamento em termos de petrologia magnética, abordado em estudo prévio por Cunha (2013), e a melhor definição dos seus parâmetros de cristalização. Em razão disso, pretende-se neste trabalho aprimorar o conhecimento sobre a Suíte Planalto, aprofundando as discussões sobre sua petrologia magnética e realizando sua caracterização mineralógica, obtendo composições químicas quantitativas das principais fases minerais que a constituem, de modo a discutir suas condições de formação (fugacidade de oxigênio, pressão, temperatura e influência das fases voláteis). Para tanto foram realizadas análises pontuais químicas semiquantitativas por *Energy Dispersive Spectrometry* (EDS) em microscópio eletrônico de varredura e análises químicas quantitativas por *Wavelength Dispersive Spectroscopy* (WDS) em microsonda eletrônica nas principais fases minerais da Suíte Planalto.

Este trabalho foi fomentado pelo INCT de Geociências da Amazônia (GEOCIAM) e por CAPES (Bolsa de mestrado da autora) e está integrado a outros estudos que estão sendo desenvolvidos no Domínio Canaã dos Carajás pelo Grupo de Pesquisa Petrologia de Granitoides (GPPG) do Instituto de Geociências da Universidade Federal do Pará.

A presente dissertação inclui um capítulo introdutório (CAPÍTULO 1), onde são abordados o contexto geológico regional, resumindo os principais aspectos geológicos da Província Carajás, problemática, objetivos da pesquisa, e os procedimentos metodológicos. O CAPÍTULO 2 inclui um artigo científico submetido a periódico internacional, intitulado: Mineral chemistry and crystallization parameters of the Archean Planalto Suite, Carajás

Province, Amazonian Craton. Finalmente, o CAPÍTULO 3 apresenta as conclusões da dissertação.

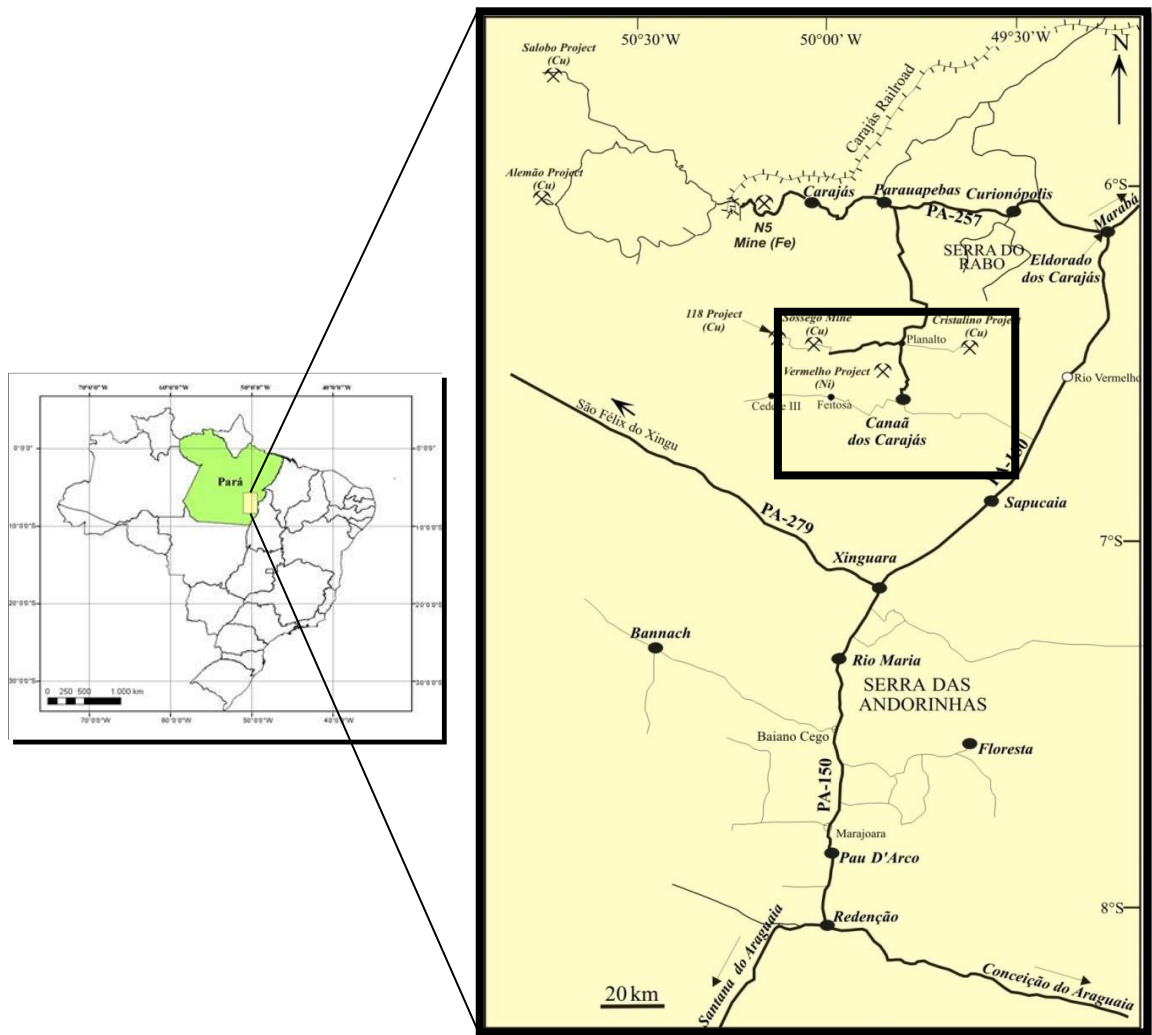


Figura 1.1 - Mapa de localização e acesso à área de estudo.
Fonte: Modificado de Almeida 2010.

1.2 CONTEXTO GEOLÓGICO REGIONAL

A Província Carajás (PC) está localizada na porção sul oriental do Cráton Amazônico (Figura 1.2), no sudeste do estado do Pará, e constitui o principal núcleo arqueano do cráton. Devido a seu vasto potencial metalogênético, diversos estudos vêm sendo realizados na região com o objetivo ampliar o conhecimento com relação à evolução crustal e processos geológicos que levaram à formação da Província Carajás. Como resultado, diversas propostas de compartimentação tectônica para a PC foram apresentadas ao longo das últimas décadas (Costa *et al.* 1995, Souza *et al.* 1996, Althoff *et al.* 2000, Dall’Agnol *et al.* 2006, 2013).

Souza *et al.* (1996) subdividiram a Província Carajás em dois blocos distintos, denominados de Rio Maria e Carajás. Posteriormente, Dall’Agnol *et al.* (2006) subdividiram o Domínio Carajás em Bacia Carajás e Domínio de Transição, este último designando a região compreendida entre o Domínio Rio Maria e a Bacia Carajás, interpretada como uma possível extensão do terreno mesoarqueano de Rio Maria intensamente deformado pelos eventos neoarqueanos que levaram à formação e fechamento da Bacia Carajás. Vasquez *et al.* (2008) acataram proposta de Santos *et al.* (2003) que dividiu a Província Carajás em dois domínios tectônicos distintos, e assumiram a existência do Domínio Rio Maria e Domínio Carajás no mapa geológico do estado do Pará. Contudo, Feio *et al.* (2013) mostraram que na área de Canaã dos Carajás, situada imediatamente a sul da Bacia Carajás, o magmatismo Mesoarqueano é distinto daquele encontrado no Domínio Rio Maria e levantaram a hipótese de que a mesma poderia representar um domínio distinto do de Rio Maria. Sugeriram, ainda, que uma extensão da crosta de Canaã dos Carajás corresponderia provavelmente ao substrato da Bacia Carajás de idade neoarqueana.

Além disso, os avanços nos trabalhos de caracterização dos principais granitoides arqueanos presentes no Domínio de Transição (Oliveira *et al.* 2010; Gabriel & Oliveira, 2014; Santos, P. A. *et al.* 2013; Teixeira *et al.* 2013; Silva, A.C. *et al.* 2014; Santos, P. J. L. *et al.* 2014; Rodrigues *et al.* 2014) permitiram que Dall’Agnol *et al.* (2013) observassem importantes diferenças estruturais e litológicas entre o DT e o Domínio Rio Maria, que os levou a propor uma nova compartimentação tectônica, dividindo o Domínio de Transição em dois domínios distintos: (1) Domínio Sapucaia ~2,95 a 2,73 Ga; (2) Domínio Canaã dos Carajás ~ 3,0 to 2,73 Ga. A Bacia de Carajás representaria um terceiro domínio do antigo Domínio Carajás e os três domínios mencionados teriam tido evolução distinta daquela do Domínio Rio Maria.

Segundo Dall’Agnol *et al.* (2013), o Domínio Sapucaia (2,95 a 2,73 Ga) apresenta fortes analogias em termos de litologias dominantes com o Domínio Rio Maria, porém, as rochas que o constituem foram intensamente deformadas durante o neoarqueano e seccionadas pelos granitoides das suítes Vila Jussara e Planalto. Uma descrição detalhada da geologia e das características geoquímicas dos principais granitoides presentes naquele domínio são fornecidas por Gabriel & Oliveira (2013, 2014), Santos, P. A. *et al.* (2013), Teixeira *et al.* (2013), Silva, A. C. *et al.* (2014), Santos, P. J. L. *et al.* (2014) e não serão retomadas aqui porque os granitos estudados da Suíte Planalto se situam no Domínio Canaã dos Carajás e, portanto, fora do Domínio Sapucaia.

O Domínio Canaã dos Carajás foi intensamente deformado pelos eventos neoarqueanos que levaram à formação e fechamento da Bacia Carajás. Na área de Canaã dos Carajás (Figuras 1.2c e 1.3), Feio *et al.* (2013) distinguiram quatro principais eventos magmáticos, três de idade mesoarqueana e um de idade neoarqueana: (1) em 3,05-3,0 Ga, teria havido a formação do protólito do Complexo Pium e do Tonalito Bacaba (~ 3,0 Ga; Moreto *et al.* 2011) e de rochas com idades semelhantes; (2) o segundo evento (2,96-2,93 Ga) foi marcado pela cristalização do Granito Canaã dos Carajás e pela formação do Trondhjemito Rio Verde; (3) no terceiro evento (2,87-2,83 Ga), houve a formação do Complexo Tonalítico Campina Verde, do Trondhjemito Rio Verde e dos granitos Cruzadão, Bom Jesus e Serra Dourada; (4) no Neoarqueano, entre 2,75-2,73 Ga, ocorreu à formação dos granitos subalcalinos da Suíte Planalto, dos granitos sódicos da Suíte Pedra Branca e de rochas charnoquíticas associadas espacialmente com o Complexo Pium. Posteriormente, Santos, R.D. *et al.* (2013) e Galarza *et al.* (2013) obtiveram idades neoarqueanas para diferentes variedades de rochas do Complexo Pium e concluíram que o mesmo seria formado essencialmente por charnockitos e não por granulitos. Eles reforçaram, assim, interpretação prévia de Ricci & Carvalho (2006), admitida por Vasquez *et al.* (2008), de que o Complexo Pium seria de origem ígnea e neoarqueano, contrapondo-se a interpretação de Pidgeon *et al.* (2000) de que corresponderia a complexo metamórfico formado durante o Mesoarqueano.

1.3 PROBLEMÁTICA E JUSTIFICATIVA DA PROPOSTA

Estudos desenvolvidos por Feio *et al.* (2012) e Cunha (2013) permitiram um avanço considerável no entendimento da natureza e origem dos granitos pertencentes a Suíte Planalto. Entretanto, ainda há necessidade de aprofundar questões relativas aos parâmetros físicos, tais como pressão, temperatura e fugacidade de oxigênio em que se deu a cristalização dessa suíte.

A Suíte Planalto é formada por diversos plutons de idade neoarqueana os quais exibem foliação penetrativa EW-NNW com mergulhos subverticais, localmente acompanhada por lineação mineral e bandas de cisalhamento do tipo-C. É composta por monzogranitos e sienogranitos com conteúdo modal variável de biotita e hornblenda, tendo como minerais acessórios principais zircão, apatita, allanita, ilmenita ± magnetita ± titanita 1 ± fluorita. Os minerais secundários são representados por epidoto, muscovita ± escapolita ± carbonatos ± titanita 2 ± turmalina.

Geoquimicamente, os granitos da Suíte Planalto são subalcalinos, ferrosos [$\text{FeO}_v/(\text{FeO}_t+\text{MgO}) > 0,88$] e similares aos granitos reduzidos do tipo-A (Dall'Agnol &

Oliveira 2007). Porém, Feio *et al.* (2012) propõem que tais granitos sejam classificados como biotita-hornblenda granitos hidratados de série charnockítica ao invés de granitos tipo-A, pois os mesmos foram colocados durante evento colisional identificado no Domínio Canaã dos Carajás e, além disso, apresentam íntima relação com rochas charnockíticas.

Para avançar na compreensão da petrologia da Suíte Planalto, é essencial a caracterização químico-mineralógica das fases minerais presentes em seus granitos, pois a composição química dos minerais permitirá estabelecer os principais parâmetros de cristalização atuantes nestas rochas.

Além disso, os resultados de análises quantitativas obtidas por microsonda eletrônica (*Wavelength Dispersive Spectroscopy* - WDS) foram comparados com aqueles resultantes de análises semiquantitativas (Cunha 2013), utilizando microscópio eletrônico de varredura (*Energy Dispersive Spectrometry* - EDS), permitindo avaliar melhor o alcance e limitações das análises por EDS.

Os avanços obtidos na caracterização das principais fases minerais da Suíte Planalto contribuirão para o melhor entendimento da evolução magmática da suíte e para ampliar o conhecimento das rochas granitoides arqueanas da Província Carajás e deverão assim melhorar a compreensão da evolução da mesma.

1.4 OBJETIVOS

O principal objetivo desta pesquisa é determinar as composições químicas de biotita, anfibólio, titanita, plagioclásio e minerais opacos (ilmenita e magnetita) e, com isso, estimar com maior precisão as condições de fugacidade de oxigênio, pressão e temperatura em que se deu a cristalização da Suíte Planalto. Pretende-se ainda comparar os resultados de análises químicas semiquantitativas por EDS em MEV (Cunha 2013) com aqueles obtidos em análises químicas quantitativas por WDS em microsonda eletrônica para avaliar o grau de precisão das análises semiquantitativas.

1.5 MATERIAIS E MÉTODOS

Os procedimentos metodológicos executados neste trabalho envolveram pesquisa bibliográfica e estudos laboratoriais. Estes compreenderam a aplicação de métodos petrográficos e microanálises utilizando microscopia eletrônica de varredura e microsonda eletrônica.

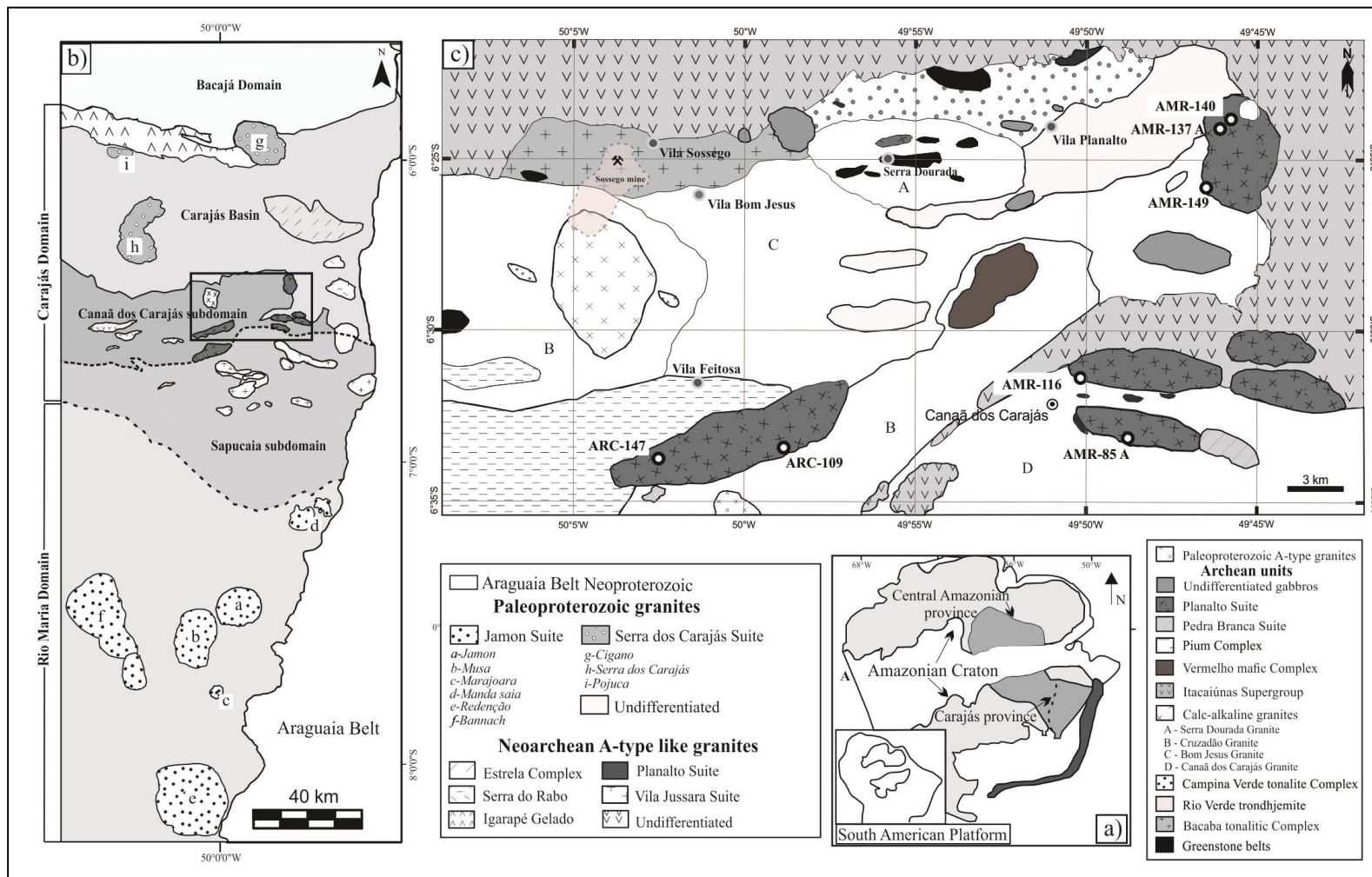


Figura 1.2 - a) Localização da Província Carajás no Cráton Amazônico; b) Mapa geológico simplificado da Província Carajás, mostrando os Domínios Rio Maria e Carajás, posteriormente subdivididos em subdomínios Sapucaia e Canaã dos Carajás e Bacia Carajás; o retângulo corresponde a área de estudo detalhada na figura 1c; (c) Mapa geológico da área de Canaã dos Carajás, mostrando a Suíte Planalto e a localização das amostras analisadas por Microsonda Eletrônica.

Fonte figura c: Feio et al. (2013).

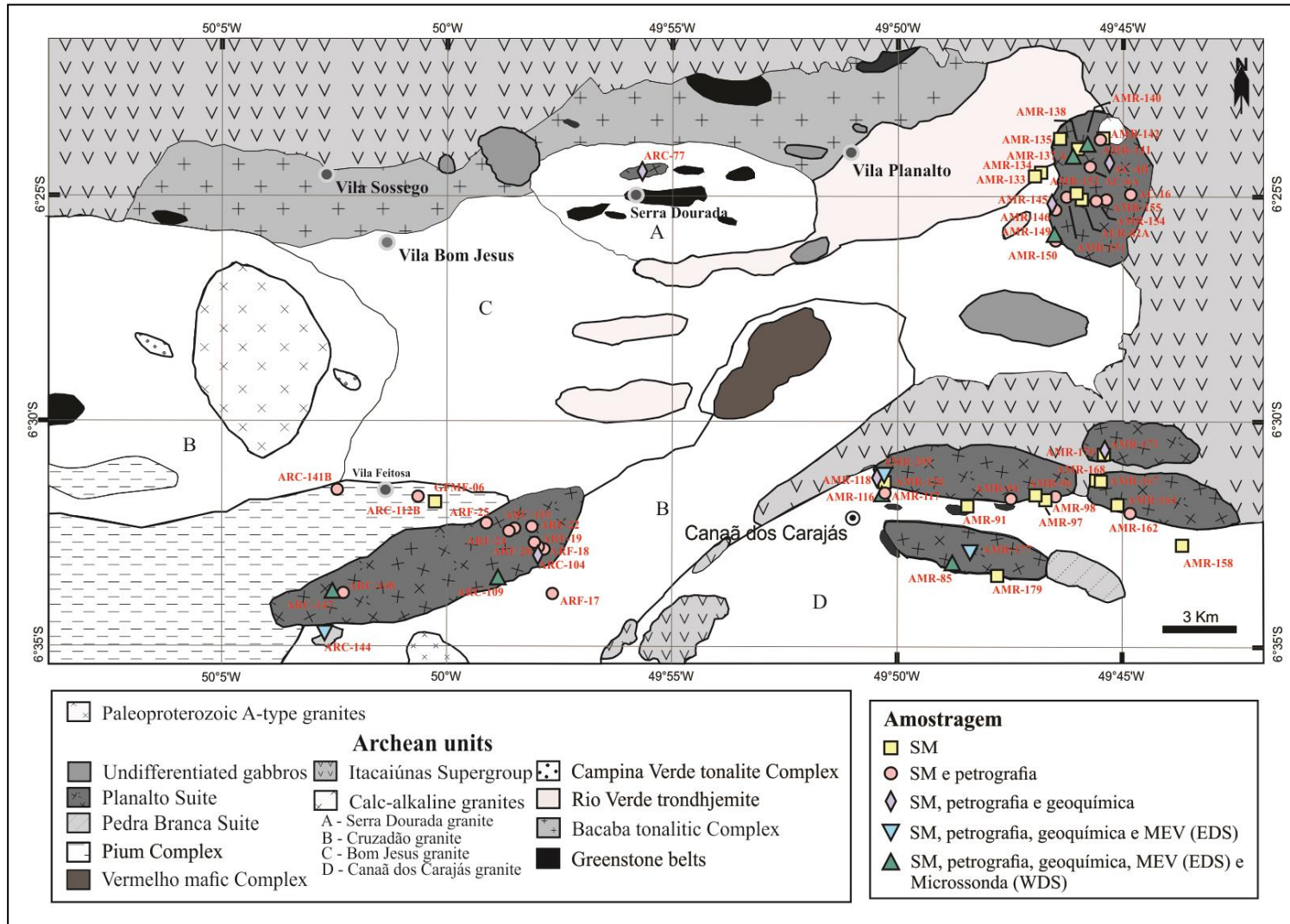


Figura 1.3 - Mapa geológico da área de Canaã dos Carajás com destaque para as amostragens realizadas na Suíte Planalto.
 Fonte: Feio et al. (2013).

1.5.1 Pesquisa Bibliográfica

Durante o desenvolvimento da pesquisa foi realizado um levantamento bibliográfico da geologia arqueana da Província Carajás com ênfase no magmatismo subalcalino e, particularmente, em suas características petrográficas e mineralógicas. Trabalhos abordando a geologia regional da porção sudeste do Cráton Amazônico, bem como estudos petrográficos e petrológicos de rochas graníticas tipo-A (Barros *et al.* 1997, 2009; Dall’Agnol *et al.* 1994, 1997, 1999, 2005; Oliveira, D.C. *et al.* 2010; Sardinha *et al.* 2006) e de granitoides associados com rochas charnockíticas (Frost *et al.* 2000, Frost & Frost 2008, Rajesh & Santosh 2004, Rajesh *et al.* 2014; Vander Auwera *et al.* 2014) serviram de base para elaboração dessa dissertação. Adicionalmente, foram pesquisados na literatura temas relacionados à aplicação da composição mineralógica como marcadora das condições de formação dos magmas.

1.5.2 Estudo Petrográfico

Os estudos mineralógicos foram precedidos e acompanhados por estudos petrográficos minuciosos das amostras de diferentes variedades da Suíte Planalto. Tais estudos complementaram aqueles efetuados anteriormente por Oliveira, M.A. (2003), Gomes (2003) e Feio *et al.* (2012) e foram feitos no Laboratório de Petrologia Magnética do IG-UFGA com uso de lupa binocular e microscópio ótico petrográfico em luz transmitida e refletida. Com base nisso, foram selecionadas amostras representativas das principais variedades petrográficas para estudos complementares.

O estudo microscópico consistiu na descrição mineralógica detalhada das diversas variedades de granitos e na análise das relações texturais, intercrescimentos, texturas de exsolução e/ou substituição, procurando esclarecer a evolução de tais rochas. Foi dada atenção aos seus diferentes minerais constituintes, porém com maior ênfase nas principais fases máficas e nos minerais opacos. As composições modais disponíveis em trabalhos anteriores (Oliveira, M.A. 2003 Gomes 2003; G.R.L. Feio, Comunicação Escrita de dados inéditos) foram compiladas e foram efetuadas análises modais adicionais em amostras selecionadas para estudos complementares, utilizando contador automático de pontos da marca *Swift* (1500 a 2.000 pontos por lâmina delgada). Posteriormente, as rochas submetidas a análises modais foram classificadas com base nas recomendações da Subcomissão de Nomenclatura de Rochas Ígneas da IUGS (Streckeisen, 1976; Le Maitre *et al.* 2002).

1.5.3 Química Mineral

1.5.3.1 Microscopia Eletrônica de Varredura (MEV)

As imagens de elétrons retroespalhados auxiliaram na observação das relações texturais entre fases minerais. As composições semiquantitativas de anfibólio, biotita, plagioclásio, titanita e minerais opacos foram obtidas por meio de análises de *Energy Dispersive Spectrometry* (EDS). As análises foram realizadas no Laboratório de microanálises do Instituto de Geociências da Universidade Federal do Pará (IG/UFPA), utilizando-se microscópio eletrônico LEO modelo 1430, sob condições de voltagem de 20kv. As observações e análises foram realizadas em lâminas polidas confeccionadas na Oficina de Laminação do IG/UFPA, posteriormente metalizadas com carbono. Com base nas composições químicas foram elaboradas fórmulas estruturais dos minerais e feita sua classificação preliminar (Cunha 2013). Os dados obtidos nessa etapa visaram complementar os já disponíveis (Cunha 2013).

1.5.3.2 Microsonda Eletrônica

As análises químicas foram realizadas em amostras da Suíte Planalto, anteriormente analisadas por EDS em MEV. As análises químicas quantitativas pontuais em microsonda eletrônica utilizaram *Wavelength Dispersive Spectroscopy* (WDS) e foram realizadas no Laboratório de Microsonda Eletrônica no Instituto de Geociências da Universidade de Brasília (IG-UnB), utilizando o equipamento Jeol JXA-8230 com cinco espectrômetros WDS e um EDS. As condições operacionais foram: tempo de aceleração 15 kV e tempo de análise 5 segundos. Os cristais utilizados para análises foram LIFH para V, Mn, Fe, Ni e Ba; PETJ para K, Ca, Ti e Sr; TAP para Na, Si, Al e Mg; LDE1 para F. Os padrões utilizados para calibração do instrumento foram andradita (Si e Ca), microclina (Al e K), hematita (Fe), olivina (Mg), albita (Na), pirophanita (Ti e Mn), Vanadinita (V e Cl), topázio (F). Os minerais analisados foram anfibólio, biotita, plagioclásio, titanita, ilmenita e magnetita. O programa MINPET, versão 2.2 (Richard 1995) foi utilizado para obter as fórmulas estruturais dos minerais. As classificações dos minerais foram efetuadas seguindo as proposições da International Mineralogical Association (Leake et al., 1997, 2003; Rieder 1999).

1.5.3.3 Estimativa dos parâmetros de cristalização

Para estimativa dos parâmetros de cristalização foram utilizadas diferentes abordagens disponíveis na literatura, as quais são discutidas em detalhe no capítulo 2.

1.5.4 Geoquímica em rocha total

Os dados geoquímicos utilizados nesta dissertação foram inteiramente baseados em análises publicadas anteriormente (Feio et al. 2012), sendo os métodos analíticos descritos naquele trabalho.

CARTA DE ACEITE
- PRIMEIRA SUBMISSÃO

Dear Mrs. Ingrid Roberta Viana da Cunha,

We have received your article "**Mineral chemistry and crystallization parameters of the Archean Planalto Suite, Carajás Province - Amazonian Craton**" for consideration for publication in Journal of South American Earth Sciences.

Your manuscript will be given a reference number once an editor has been assigned.

Thank you for submitting your work to this journal.

Kind regards,

Elsevier Editorial System

Journal of South American Earth Sciences

- SEGUNDA SUBMISSÃO

Dear Mrs. Ingrid Roberta Viana da Cunha,

Your submission "**Mineral chemistry and magnetic petrology of the Archean Planalto Suite, Carajás Province - Amazonian Craton: implications for the evolution of ferroan Archean granites**" will be handled by Regional Editor Reinhardt A. Fuck, D. Sc..

Thank you for submitting your work to this journal.

Kind regards,

Elsevier Editorial System

Journal of South American Earth Sciences

CAPÍTULO 2

ARTIGO: MINERAL CHEMISTRY AND MAGNETIC PETROLOGY OF THE ARCHEAN PLANALTO SUITE, CARAJÁS PROVINCE – AMAZONIAN CRATON: IMPLICATIONS FOR THE EVOLUTION OF FERROAN ARCHEAN GRANITES

Ingrid Roberta Viana da Cunha

Roberto Dall'Agnol

Gilmara Regina Lima Feio

Submetido: Journal of South American Earth Sciences

MINERAL CHEMISTRY AND MAGNETIC PETROLOGY OF THE ARCHEAN PLANALTO SUITE, CARAJÁS PROVINCE – AMAZONIAN CRATON: IMPLICATIONS FOR THE EVOLUTION OF FERROAN ARCHEAN GRANITES.

Ingrid Roberta Viana da Cunha^{1,2*}, Roberto Dall’Agnol^{1,2,3}, Gilmara Regina Lima Feio^{1,4}

¹Grupo de Pesquisa Petrologia de Granitoides, Instituto de Geociências (IG), Universidade Federal do Pará (UFPA), Rua Augusto Corrêa, 01. CEP 66075-110. Belém, PA, Brazil.

²Programa de Pós-graduação em Geologia e Geoquímica, IG-UFPA. Belém, PA, Brazil.

³Vale Institute of Technology, Belém, PA, Brazil.

⁴Universidade Federal do Sul-Sudeste do Pará (UNIFESSPA), Marabá, PA, Brazil.

ABSTRACT: The Planalto Suite is located in the Canaã dos Carajás Domain of the Carajás Province in the southeastern part of the Amazonian Craton. The suite has Neoproterozoic age (~2.73 Ga), ferroan character and affinity with A-type granites. Magnetic petrology studies allowed the distinction of two groups: (1) Ilmenite granites devoid of magnetite and showing low magnetic susceptibility (MS) values (MS between 0.6247×10^{-3} and 0.0102×10^{-3} SI; average of 0.1522×10^{-3}); (2) Magnetite-ilmenite-bearing granites which display comparatively higher but still moderate MS values (between 15.700×10^{-3} and 0.8036×10^{-3} SI; average of 5.1717×10^{-3}). Textural evidence indicates that amphibole, ilmenite, titanite, and, in the rocks of Group 2, also magnetite formed during magmatic crystallization. However, titanite chemical composition suggests that it was re-equilibrated by subsolidus processes. The amphibole varies from potassian-hastingsite to chloro-potassian-hastingsite and shows $Fe/(Fe+Mg) > 0.8$. Biotite also shows high $Fe/(Fe+Mg)$ ratios and is classified as annite although relatively enriched in Al compared to the annite end member. Plagioclase porphyroclasts are oligoclase (An_{25-10}) and the grains of the recrystallized matrix display oligoclastic or albitic composition (An_{9-2}). Mineral chemistry, magnetic petrology and whole rock geochemistry indicate that the dominant group 1 granites of the Planalto Suite were formed under reduced conditions below the FMQ buffer. The group 2 granites crystallized under more oxidizing conditions on or slightly above the FMQ buffer. Pressures of 900-700 MPa for the origin and of 500-300 MPa for the emplacement were estimated for the Planalto magmas. Geothermometers suggest initial crystallization temperatures between 900 °C and 830 °C and water content in the magma higher than 4 wt %. The mineralogical comparison between the Planalto Suite and the Archean subalkaline Estrela Granitic Complex of the Carajás Province reveals strong compositional analogies indicating that they were probably formed under similar conditions. The amphibole and biotite compositions of Planalto and Estrela granites are relatively enriched in Al being comparable with those of the Neoproterozoic Matok Pluton of the Limpopo Belt. They differ using the same criteria of the Proterozoic

rapakivi A-type granites. On the other hand, in terms of Fe/(Fe+Mg) ratio, the Planalto and Estrela granites approach the reduced Mesoproterozoic rapakivi granites and the reduced to moderately oxidized Paleoproterozoic granites of, respectively, the Velho Guilherme and Serra dos Carajás suites and differ from the oxidized granites (Jamon Suite) of the Carajás province and also of Matok pluton. It is concluded that the Planalto Suite and similar Neoproterozoic granites of the Carajás Province differ in mineralogical characteristics and crystallization parameters of some classic examples of A-type granites and, except for its reduced character, they are akin to the Neoproterozoic Fe-K and Mg-K granitoids of the Limpopo Belt, as exemplified by the Matok granitoids. This indicates that the collisional setting of Carajás and Limpopo exerted strong influence in the nature of the Neoproterozoic granitoid magmas.

Keywords: Archean, A-type granites, Magnetic petrology, Crystallization parameters, Carajás Province.

*Corresponding author: ingridvcunha@gmail.com

2.1 INTRODUCTION

A-type granites were originally associated to anorogenic tectonic settings and were admitted to be formed under low oxygen fugacity conditions from magmas with low water content (Loiselle and Wones, 1979). Subsequently, they were related to post-collisional environments (Whalen et al., 1987; Eby, 1992; King et al., 1997; Nardi et al., 2009) and it was proposed the existence of oxidized A-type granites that could have moderate to high water contents (Anderson and Smith, 1995, Anderson and Morrison, 2005; Dall'Agnol et al., 1997, 1999, 2012; Dall'Agnol and Oliveira, 2007).

Several Neoproterozoic granites, geochemically similar to A-type granites, have been described in the Carajás Province, situated in the southeastern part of the Amazonian Craton. They occur as batholiths and stocks in the central-northern sector of the province (Figure 2.1b) and are represented by the Estrela Complex, the Serra do Rabo and Igarapé Gelado granites (Barros et al., 1997, 2001, 2009; Sardinha et al., 2006), and the Planalto Suite (Huhn et al., 1999; Feio et al., 2012, 2013; Feio and Dall'Agnol, 2012). Overall, they have high FeO/(FeO+MgO) ratio, subalkaline affinity and metaluminous to peraluminous character.

Mineral chemistry is an important tool for definition of intensive parameters of crystallization of granitic rocks (Czamanske et al., 1973; Anderson and Bender, 1989;

Anderson and Smith, 1995; Anderson and Morrison, 2005; Clowe et al., 1988; Dall'Agnol et al., 1999, 2005; Elliot et al., 1998; Frost et al., 1999, 2000; Lamarão and Dall'Agnol, 2004; Papoutsas and Pe-Piper, 2014). The composition of the main mineral phases of granitic rocks can give relevant information about the nature and physicochemical conditions of magmas. Amphiboles are the main ferromagnesian phase in many granitic rocks and their presence indicate derivation from hydrated magmas (Naney, 1983; Dall'Agnol et al., 1999; Klimm et al., 2003). They can also be an important geochemical evolution index of parental magma (Martin, 2007). Similarly, the composition of biotite and the nature of iron-titanium oxide minerals are strongly dependent of oxygen fugacity conditions in the magma and can also give information about the nature of the granite magmatic series (Nachit, 1985; Nachit et al., 1994; Stussi and Cuney, 1996).

The aim of this paper is to determine the chemical and textural characteristics of the main mineral phases of the Planalto Suite granites and to discuss their magnetic petrology. These data and geological information are used to estimate the intensive parameters acting during the crystallization of its magmas. Additionally, a comparative study between the studied granites and similar A-type granites, including those associated with charnockitic rocks is also done. Besides the granites of the Carajás Province, the Neoproterozoic HBG granitoids and the AMC Suite of the Rogaland Anorthosite Province (Norway), the Mesoproterozoic rapakivi granites, and the Neoproterozoic Matok pluton of the Limpopo Belt (Africa) are also shown for comparison. We intend to contribute to the understanding of the origin of these ferroan granites possibly related with charnockites and their contrasts with classical A-type granites.

2.2 GEOLOGIC SETTING

The Carajás Province (CP) is located in the southeastern part of the Amazonian Craton (Figure 2.1a), southeast of Pará state, Brazil. It is the main Archean nucleus of the craton (Almeida et al., 2011; Feio et al., 2013; and references therein) and contains large mines of iron, copper, nickel and manganese. Several studies have been conducted in this region in order to improve the knowledge of the geology, magmatism, crustal evolution and metallogenesis of this province (DOCEGEO, 1988; Botelho et al., 2005; Vasquez et al., 2008; Xavier et al., 2010; Oliveira, M.A. et al., 2009; Almeida et al., 2011; Feio et al., 2013; Moreto et al., 2011, 2015).

The Carajás province is divided in two domains (Souza et al., 1996; Dall'Agnol et al., 2000; Santos et al., 2003; Vasquez et al., 2008): The Rio Maria domain situated in the

southern part of the province and the Carajás domain in the northern sector (Figure 2.1b). The Rio Maria domain was formed during ca. 3,000 Ma to 2,860 Ma in the Mesoarchean (Machado et al., 1991; Macambira and Lafon, 1995; Almeida et al., 2011). It is constituted of greenstone belts and tonalitic-trondhjemitic assemblages (TTG), leucogranodiorites, high-Mg granitoids and potassic granites (Althoff et al., 2000; Souza et al., 2001; Dall'Agnol et al., 2006; Oliveira, M.A., et al., 2010; Almeida et al., 2011, 2013). The main difference between the Rio Maria and Carajás domains is that the latter also initiated its formation during the Mesoarchean and extended into the Neoarchean.

More recently, Feio et al. (2013) have demonstrated that the Mesoarchean magmatism of the Canaã dos Carajás area of the Carajás domain is quite distinct of that of Rio Maria. At the same time, the results of extensive geological mapping and new geochronological and geochemical data obtained in the southern part of the Carajás Domain, in the Sapucaia area (Oliveira et al., 2010; Gabriel et al., 2014; Santos, P. A. et al., 2013; Silva, A. C. et al., 2014; Santos, P. J. L. et al., 2014; Rodrigues et al., 2014) had put in evidence that the structural and textural features, including penetrative deformation and strong recrystallization, of that area are quite distinct of those observed in Rio Maria.

With this in mind, Dall'Agnol et al. (2013) proposed the subdivision of the Carajás domain in the Carajás Basin and the Canaã dos Carajás and Sapucaia subdomains (Figure 2.1b). The main assemblages of the Carajás Basin have Neoarchean ages (~2.76 Ga; Gibbs et al., 1986; Machado et al., 1991) and are composed dominantly of mafic to intermediate metavolcanic rocks and banded iron formations, both included in the Itacaiunas Supergroup. The latter is intruded by the Neoarchean (~2.75-2.73 Ga) Estrela, Igarapé Gelado and Serra do Rabo granites which are geochemically akin to the Planalto Suite. According to Dall'Agnol et al. (2013), the main units of the Sapucaia subdomain (2,950 Ma to 2,730 Ma) are similar in lithologic terms to the dominant rocks in the Rio Maria Domain, but the former were strongly affected by Neoarchean tectonic events and were intruded by granitoids of Vila Jussara and Planalto suites. The Canaã dos Carajás subdomain had a more complex evolution and three Mesoarchean magmatic events were distinguished in it (Feio et al., 2013): (1) at ~3,000 Ma, the formation of the Bacaba Tonalite (Moreto et al., 2011); (2) at 2,960 to 2,930 the emplacement of the Canaã dos Carajás Granite and the Rio Verde Trondhjemitic; (3) at 2,870 Ma to 2,830 Ma the crystallization of the Campina Verde Tonalitic Complex, Rio Verde Trondhjemitic and Cruzadão, Bom Jesus and Serra Dourada granites. Finally, during the Neoarchean, at 2,750 Ma to 2,720 Ma, were formed the subalkaline granitoids (Planalto and

Vila Jussara suites), sodic granitoids distinct of TTG in composition (Pedra Branca Suite) and charnockitic assemblages (Pium Complex; Feio et al., 2012, 2013; Santos, R.D. et al., 2013).

The Planalto Suite is geochemically similar to A-type granites, but it is spatially associated with charnockitic rocks and it could possibly correspond to hydrated granites related to the mentioned series (Feio et al., 2012). Furthermore, the rocks of the suite exhibit EW-NNW penetrative foliation with subvertical dips and locally mineral lineation and C-type shear bands (Feio et al., 2012), features that are not commonly observed in A-type granites of extensional settings.

There is geophysical and geological evidence of a collision between the Rio Maria and Carajás domains but the main features and age of this event are poorly constrained. Recently, Tavares (2015) proposed that the collision occurred more probably at ~2.87 to 2.83 Ga, as indicated by the ages of the granite magmatism observed in the Canaã dos Carajás subdomain (Feio et al., 2013). The Carajás Basin is generally interpreted as a rift-related continental basin formed at ~2.76 Ga (Gibbs et al., 1986; Docegeo, 1988; Dall’Agnol et al., 2006; Tavares, 2015) and later closed possibly by collisional processes.

There is, however, a controversial issue related to the closing of the basin and Neoproterozoic granite evolution. Barros et al. (2001, 2009) admit that the Neoproterozoic granites are collisional, syntectonic A-type granites deformed during emplacement at ~2.75-2.73 Ga. They argue that the final textural aspects observed in those granites were acquired during cooling and consider that the granites are not metamorphosed rocks. More recently, Tavares (2015) proposed that the Neoproterozoic granites are A-type rift-related granites deformed and metamorphosed during the closing of the Carajás Basin at ~2.68-2.63 Ga. In our way of thinking, there is no a clear answer for this controversy at this stage. Anyway, it put in evidence that secondary subsolidus or metamorphic processes could have affected and changed the original magmatic compositions of the minerals that constitute the Planalto Suite.

2.3 GEOLOGY OF THE PLANALTO SUITE

The Planalto Suite, located south of the Carajás Basin in the Canaã dos Carajás subdomain, consists of seven plutons and a stock, intrusive in Mesoproterozoic units and in the Neoproterozoic Itacaiúnas Supergroup (Figure 2.1c). In the southwestern part of the studied area, the Planalto suite granites are in contact with the charnockitic rocks of the Pium Complex (norites, quartz-norites, quartz-gabbros, and more evolved hypersthene-bearing rocks; Feio et al., 2012; Santos, R.D. et al., 2013).

Huhn et al. (1999) described a granite pluton located near Vila Planalto and obtained through the Pb-Pb zircon method a crystallization age of 2747 ± 2 Ma for the thereafter called Planalto Granite. Oliveira (2003) made the first petrographic study of the type-area pluton, including a preliminary overview of its magnetic petrology. Sardinha (2004) characterized the granitic stock located southern of Vila Feitosa (Figure 2.1c) and correlated it with the Planalto Granite and, by analogy, with the Neoproterozoic A-type granites of the Estrela Granitic Complex and similar granites.

Feio et al. (2012) made a detailed geologic, geochemical and geochronological characterization of the Planalto granites and named them Planalto Suite. The age of the hornblende-biotite syenogranite ARC-109 was determined by the zircon Pb-evaporation method (2731 ± 1 Ma; Feio et al., 2012) and by SHRIMP U-Pb in zircon (2730 ± 5 Ma; Feio et al., 2013). More information and additional references about the suite can be obtained in that paper. The plutons of the suite have less than 10 km in the largest dimension, are lenticular, generally elongated E-W concordantly to the dominant regional trend and bounded by shear zones. The Planalto granites show penetrative subvertical foliation sometimes accompanied by a high-angle stretching mineral lineation and C-type shear bands. The plutons of the suite are spatially associated with the noritic, quartz-noritic and enderbitic rocks of the Pium complex, and with the Pedra Branca suite. These units and the Planalto Suite granites were affected by high-angle thrust faulting. The Planalto granites include different kind of mafic enclaves: angular and partially digested enclaves of Pium mafic rocks and oval-shaped or angular enclaves crowded of alkali-feldspar megacrysts indicating mingling processes.

To the south of the studied area (Figure 2.1b), several granitoid bodies were described and initially correlated with the Planalto granite (Oliveira et al., 2010). However, preliminary geochemical and geochronological data (F. V. Guimarães, written commun; Teixeira et al., 2013; Silva, et al., 2014) confirmed the existence of relevant contrasts with the Planalto Suite and those granitoid plutons were grouped in the Vila Jussara Suite that will not be discussed in the present paper.

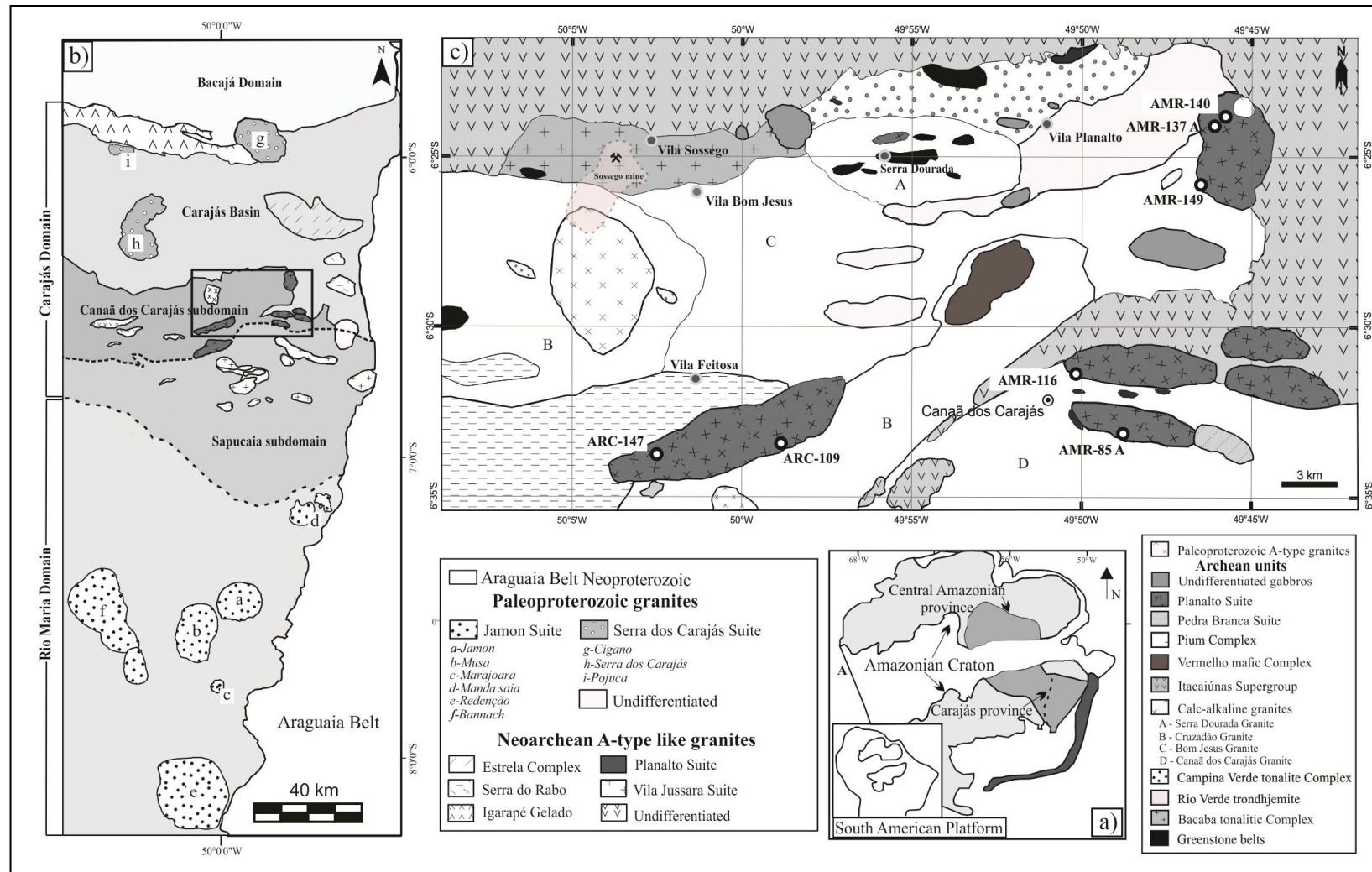


Figure 2.1 - a) Location of the Carajás Province in the Amazonian Craton; b) Simplified geological map of the Carajás Province, showing the Rio Maria and Carajás domains, the latter subdivided in the Sapucaia and Canaã dos Carajás subdomains, and Carajás Basin; the rectangle corresponds to the studied area detailed in figure 1c; (c) Geological map of the Canaã dos Carajás area (Feio et al., 2013), displaying the Planalto Suite and the location of samples analyzed by electron microprobe.

2.4 PETROGRAPHY

The mineralogical studies were preceded by detailed petrographic studies of representative samples from different varieties of the Planalto suite (Feio et al., 2012). The optical microscopy study was done with transmitted and reflected light to allow a better characterization of iron oxide minerals. 56 thin sections including 14 polished ones were studied. Only samples with available whole rock chemical compositions were selected for mineral chemistry. Modal analyses were executed by the authors or compiled from previous works of the same research group. A minimum of 1550 points were counted in each thin section to determine the modal composition and the rocks were classified according to the recommendations of the Subcommittee on the Systematics of Igneous Rocks of IUGS (Le Maitre et al., 2002). Complementary textural and compositional mineralogical studies were performed using a Scanning Electron Microscope LEO model 1430, with a constant accelerating voltage of 20 kV, at the Microanalyses Laboratory of the Geoscience Institute of the Federal University of Pará.

2.4.1 Modal composition and petrographic classification

The Planalto Suite granites have coarse- to medium-grained, locally fine-grained, inequigranular texture and show pinkish color with dark spots related to mafic minerals (Figure 2.3a). The modal data were plotted on QAP (Le Maitre et al., 2002; Streckeisen, 1976; Figure 2.2) and demonstrate little compositional variation with dominance of monzogranites and syenogranites and rare occurrence of alkali feldspar granites. According to mafic minerals proportions, the samples were classified as: biotite-hornblende monzogranite (BHMzG) and syenogranite (BHSg); hornblende-biotite monzogranite (HBMzG), syenogranite (HBSg), leucosyenogranite (HBLSG) and alkali feldspar granite (HBAG); biotite monzogranite (BMzG) and syenogranite (BSG); hornblende syenogranite (HSG) and alkali feldspar leucogranite (HALG). The granites of the suite vary from leucocratic to hololeucocratic and have mafic mineral content generally between 5 % and 20 % ($M' < 20$, Supplementary data; Table S1), that are considered normal for granites (Le Maitre et al., 2002). 8 analysed samples show lower mafic mineral content ($M' < 5\%$) and are classified as leucogranites and 4 other samples have mafic content clearly higher than the average ($M' > 20$; Supplementary data; Table S1).

Two granite Groups were distinguished on the basis of magnetic susceptibility and oxide minerals assemblages (see below) and their modal compositions are presented in the Table S1. Both groups have monzogranites, syenogranites, and alkali feldspar granites, with

variable proportions of hornblende and biotite. Excluding iron-titanium oxide minerals, that will be discussed in the magnetic petrology section, the main accessory minerals in both groups are zircon + apatite ± allanite ± titanite, and the secondary minerals are epidote ± scapolite ± tourmaline ± chlorite ± carbonates ± fluorite ± white mica.

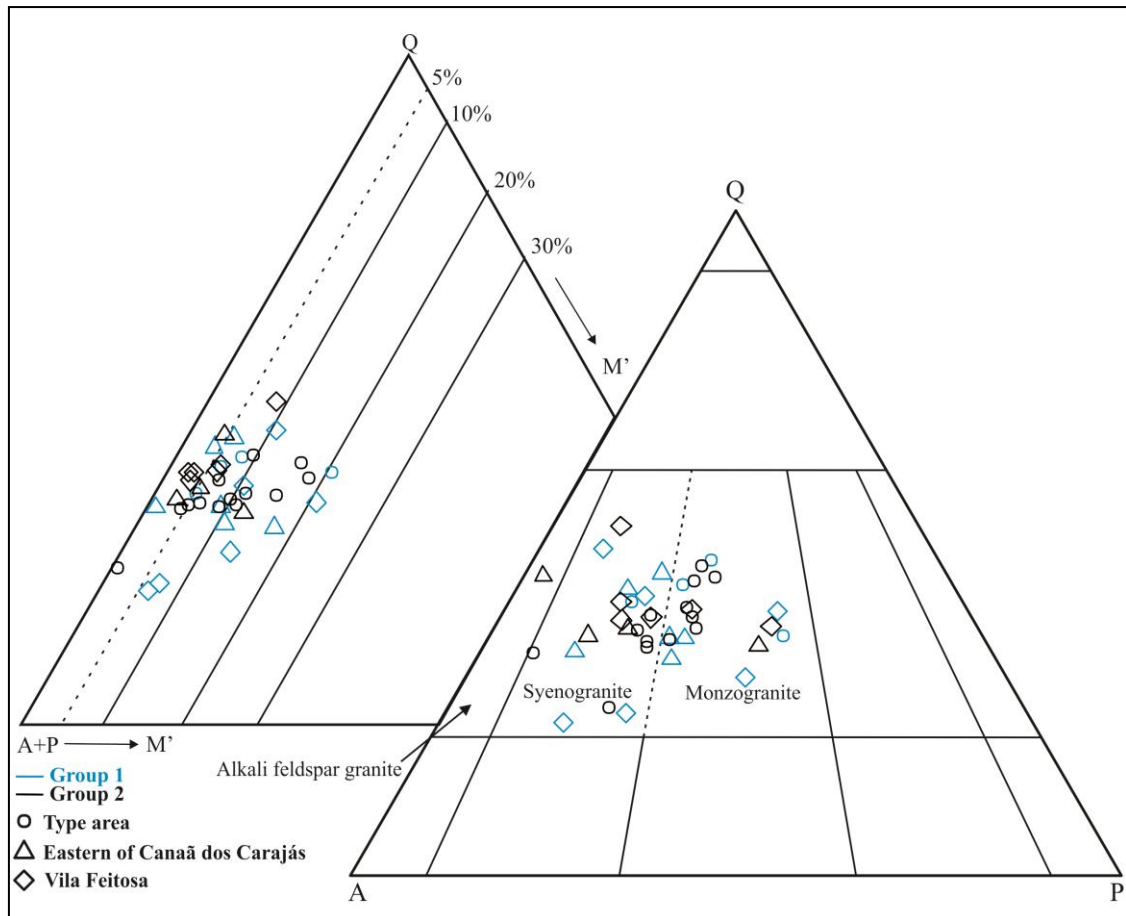


Figure 2.2 - QAP (fields according to Le Maitre et al., 2002) and Q-(A+P)-M' modal diagrams for the Planalto Suite. A – Alkali feldspar; P- Plagioclase; Q – Quartz; M' = M – (apatite + muscovite + carbonates).

2.4.2 Textural aspects

The Planalto Suite rocks exhibit magmatic textures barely preserved. The original medium- to coarse-grained granular hypidiomorphic texture (Figure 2.3b) tends to be replaced by protomylonitic to mylonitic textures, with oval-shaped microcline and rarely plagioclase porphyroclasts which exhibit variable degrees of recrystallization along boundaries and fractures and are surrounded by a fine matrix composed of intensely recrystallized quartz and feldspar. Microcline crystals exhibit commonly perthitic exsolution textures and tartan twinning. In addition, patch perthites occur occasionally in the alkali feldspar and suggest the

incipient development of subsolidus chessboard albite (Figure 2.3c). Bulbous myrmekitic intergrowths are observed near the boundaries of the microcline and along microfractures.

The plagioclase porphyroclasts are medium- to fine-grained (< 2mm) and generally weakly to moderately altered to white mica. The recrystallized fine-grained feldspars crystals show in most cases polygonal contour and tend to develop mosaic textures. Locally, there are microfractures filled by aggregates of new formed grains, which show evidence of deformation. Quartz is found as porphyroclasts, ribbons, and as part of the recrystallized matrix (Figure 2.3d). Occasionally, the contours of the magmatic quartz crystals are preserved and the original crystals are replaced by an aggregate of new grains. In the most deformed rocks, some crystals exhibit intense undulatory extinction and mosaic textures with triple points.

The amphibole crystals are medium- to fine-grained (< 2.0 mm) and exhibit pleochroism varying from light green (X) to olive green (Y) and bluish-green (Z). Most of them are fresh subautomorphic crystals (Figure 2.3e). However, poikilitic crystals (Figure 2.6e, f) which include felsic minerals and ilmenite with subordinate magnetite in the group 2 granites also occur. Commonly, biotite and amphibole are oriented along with other mafic minerals and together with felsic deformed aggregates define the foliation of the rock. The amphibole was locally more intensely deformed and transformed to oval porphyroclasts. Moreover, some crystals are partially replaced by biotite during the late-magmatic or subsolidus stage.

Biotite lamellae are fine- to medium-grained (<1.5 mm) with pleochroism ranging from light yellow (X) to dark brown (Z). They are generally not altered and predominantly subhedral with inclusions of feldspars and opaque minerals, locally displaying corroded rims and titanite and opaque minerals along cleavages. Overall, the mica is found in mafic clots with amphibole, titanite, opaque minerals, zircon, apatite, and rarely allanite (Figure 2.3f).

With respect to the accessory minerals, besides Fe-Ti oxide minerals, discussed in the magnetic petrology section, titanite is also significant. There are no apparent textural differences between the titanites of the Group 1 and Group 2 granites of the Planalto Suite. In both groups, titanite occurs as anhedral irregular grains surrounding ilmenite crystals (corona-type texture; Figure 2.6a, b) or as subhedral crystals associated with mafic clots (Figure 2.3e, f). The zircon and apatite are very fine-grained (< 0.1 mm), euhedral and prismatic crystals which occur as inclusions in amphibole, biotite, plagioclase, and opaques. Allanite crystals

reach up to 1.5 mm, have rounded shape and constitute predominantly anhedral crystals with pleochroism ranging from yellowish-brown (X) to reddish-brown (Z).

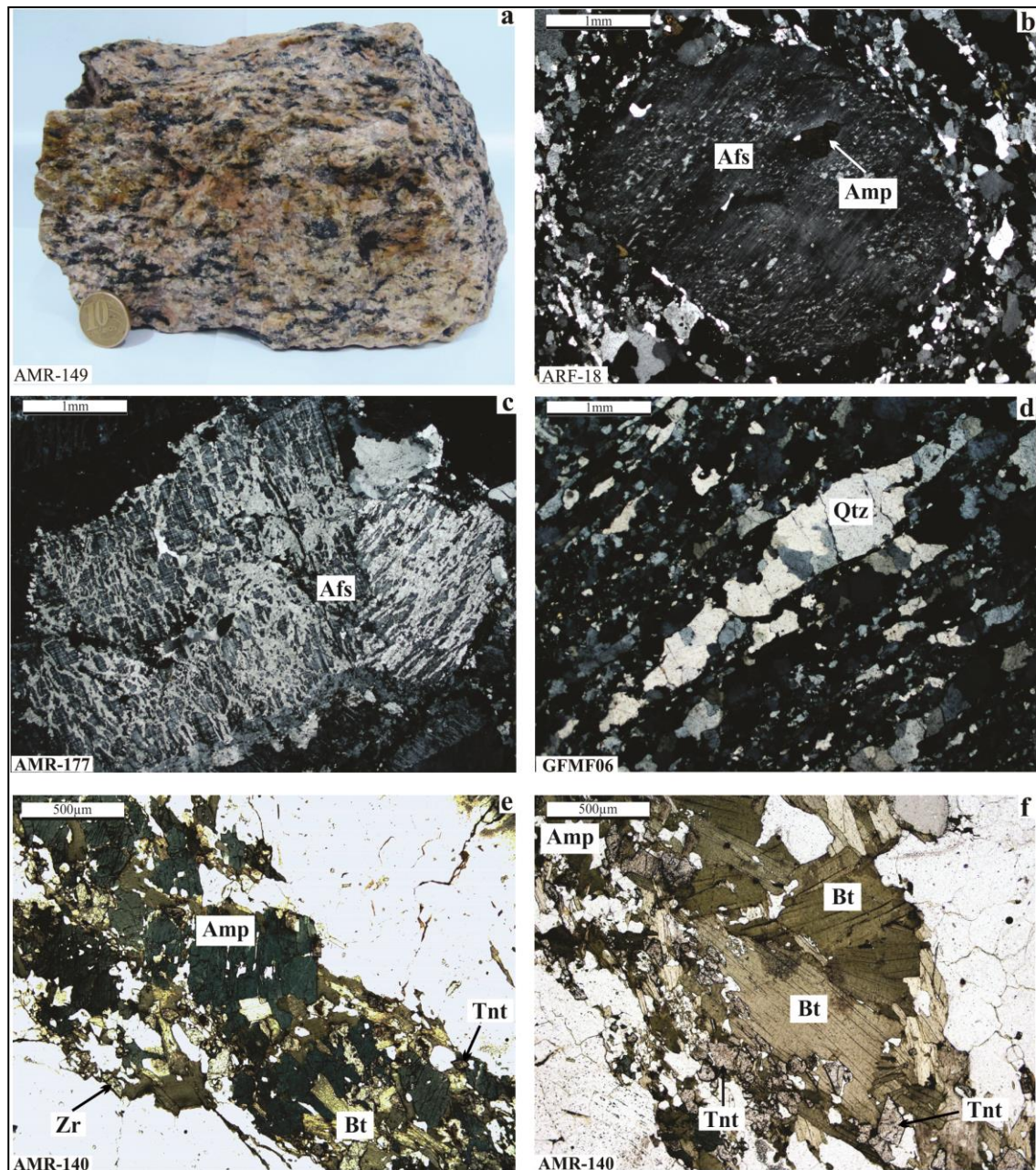


Figure 2.3 - a) Macroscopic aspect of a granite from the Planalto Suite (Facies HBMzG, Group 1; cf. abbreviations in Supplementary data, Table S1); b) Relatively well preserved microcline phenocryst in a recrystallized matrix (Facies HBSG, Group 2); c) Phenocryst of mesoperthitic microcline with inclusion of amphibole and incipient development of chessboard albite (Facies HLAG, Group 2); d) Recrystallized quartz ribbon in a granite with mylonitic texture (Facies HBSG, Group 2); e) Clots of mafic minerals with dominance of amphibole and biotite associated with subhedral titanite and euhedral zircon and apatite (Facies BHMzG, Group 2); f) Lamellae of biotite associated with subhedral grains of titanite and amphibole (Facies BHMzG, Group 2). Photomicrographs in crossed nicols (b, c, d) or parallel nicols (e, f). Mineral abbreviations according to Kretz (1983).

2.5 MAGNETIC PETROLOGY

Magnetic petrology is the integration of magnetic susceptibility (MS) studies with the characterization of iron-titanium oxide minerals and conventional petrology in order to determine the composition, abundance, microstructure and paragenesis of magnetic minerals, as well as to define the genesis, alteration and/or replacement process of magnetic minerals in rocks (Clark, 1999). Magnetic susceptibility is related to the quantity, nature, grain-size and distribution of ferromagnetic minerals content. The Fe-Ti oxide mineral equilibrium is controlled by physical and chemical conditions which define the stability of mineral assemblages and is indirectly reflected in the MS values. Furthermore, rocks exhibit similar magnetic characteristics to their ferromagnetic mineral content.

MS measurements of 77 representative samples of the Planalto Suite were performed at the Magnetic Petrology Laboratory of the Geoscience Institute of the Federal University of Pará, using a susceptibilimeter SM-30 (ZH Instruments), which is able to measure materials with MS values ranging to 1×10^{-7} SI. Data analysis was performed using the Mintab 17 software (free version). The MS was measured directly in sawn regular surfaces of hand samples. Samples with veins or evidence of significant hydrothermal alteration were avoided. The results of MS measurements are presented in the Supplementary Table S2.

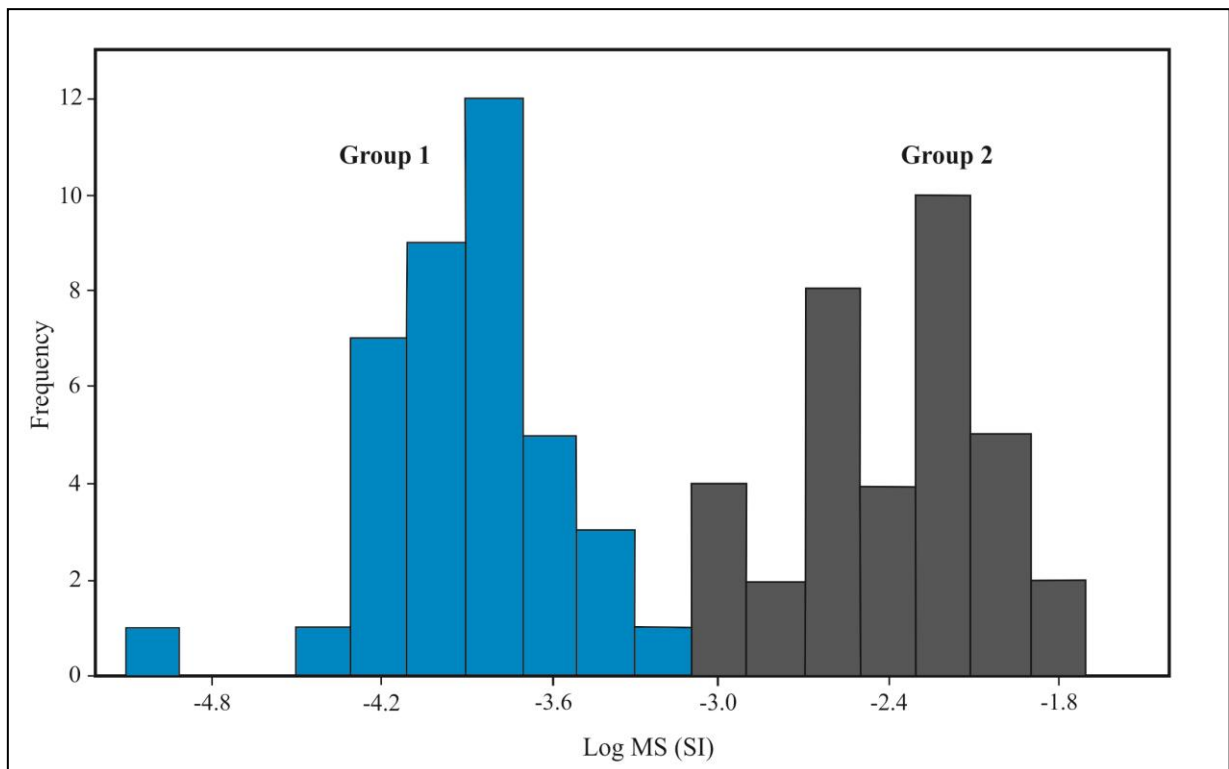


Figure 2.4 - Magnetic Susceptibility histogram for samples of the Planalto Suite.

The Planalto Suite has MS values in the range between 0.0102×10^{-3} SI and 15.700×10^{-3} SI, with a mean value of 2.7263×10^{-3} SI. Statistically, the measured granite samples show a polymodal distribution between log -4.99014 and -1.8041 and MS data plotted on a normal probability graph allowed to distinguish three populations (Supplementary data; Figure S1). However, the petrographic characteristics and the frequency histogram (Figure 2.4) indicate the existence of only two groups of samples. The Group 1 includes the two populations with lower MS values varying between 0.0102×10^{-3} and 0.6247×10^{-3} SI. The Group 2 is distinguished by showing the highest MS values varying between 0.8036×10^{-3} and 15.700×10^{-3} SI.

In the group 1, ilmenite is the sole significant iron-titanium oxide mineral whereas in the group 2, magnetite occurs associated to ilmenite. The modal content of Fe-Ti oxide minerals in both groups of Planalto Suite is also distinct. The Group 1 has lower modal contents (on average 0.12 %) and only in one sample it exceeds 0.3 % (Table S1). On the other hand, in the group 2, the average opaques modal content is 0.39 % and half of the samples show opaques modal content equal or higher than 0.3 % (Supplementary data; Table S1). The binary diagram MS values versus opaque modal contents (Figure 2.5) indicate a poor correlation between those variables.

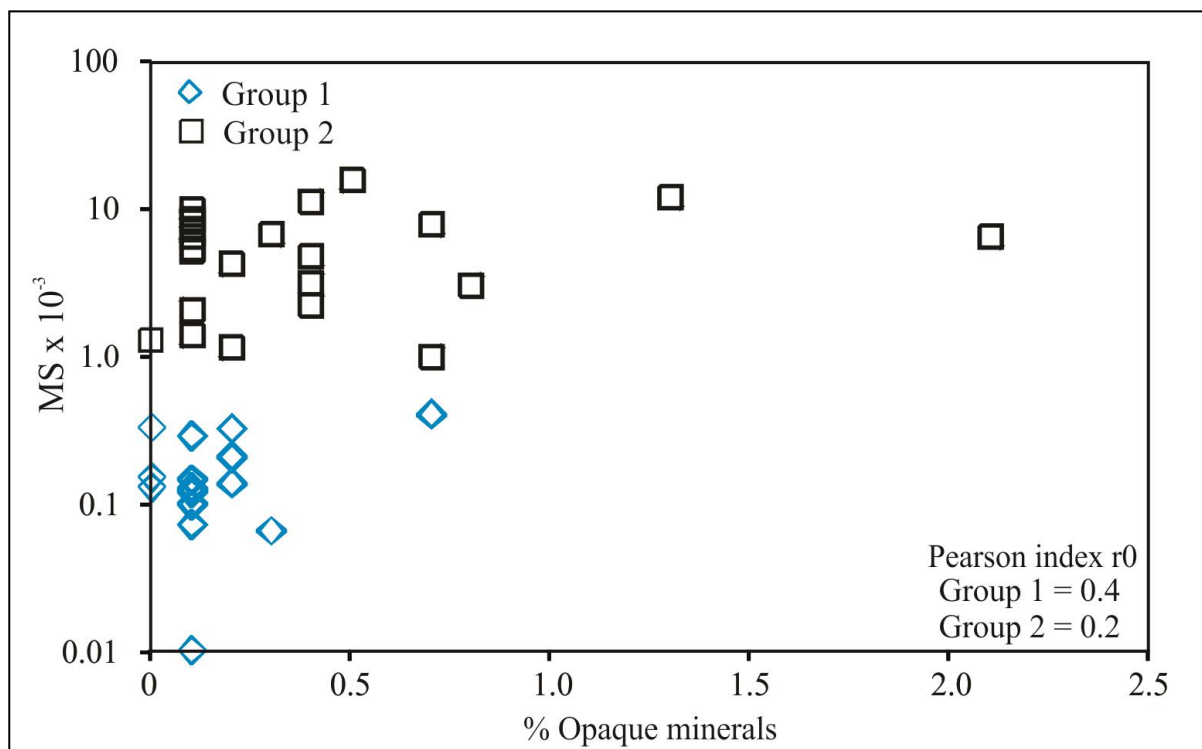


Figura 2.5 - Modal opaques (volume %) vs. magnetic susceptibility (SI units) diagram for the Planalto Suite.

Titanite is irregularly distributed in both groups with large variations. Moreover, in the two groups the average modal contents are similar and they have a relatively large number of samples without significant modal contents of titanite (Supplementary data; Table S1). There is no clear correlation between modal contents of titanite and opaque minerals in both groups. Careful examination in SEM put in evidence that most subhedral titanite crystals are zoned and have Al-enriched layers in the borders and Fe-rich zones in the center of the crystals. This is a clear evidence that titanite was re-equilibrated most probably by subsolidus processes that should favor Al-enrichment and were responsible by the increase of Al/Fe ratio in this mineral.

In the Planalto Suite, the opaque minerals are fine- to very fine-grained, rarely reaching 1 mm. Marthite, pyrite and chalcopyrite occur sparsely and only in the Group 2. In the Group 1, ilmenite occurs as anhedral grains generally associated with amphibole and biotite. Individual ilmenite (Haggerty, 1991; Dall'Agnol et al., 1997) is the main textural variety identified and it is generally enveloped by coronas of titanite (Figure 2.6a, b). Locally, anhedral fine-grained ilmenite occurs as inclusions in amphibole and biotite. In the Group 2, ilmenite crystals are commonly anhedral and show coronas of titanite, similar to Group 1 crystals, or occur associated with magnetite (subhedral composite ilmenite showing even contacts with magnetite and sometimes evidence of initial oxidation; Figures 2.6c, d). Anhedral to subhedral fine-grained ilmenite and magnetite crystals are included in poikilitic amphibole (Figures 2.6e, f). On the other hand, magnetite occurs as subhedral or anhedral crystals generally associated with amphibole clots. Marthite partially replaces magnetite grains.

Composite ilmenite is generally explained as resulting of the oxy-exsolution process that affected titanomagnetite during cooling of magmas or igneous rocks (Buddington and Lindsley, 1964; Haggerty, 1981; Dall'Agnol et al., 1997). However, Haggerty (1991) proposed, as an alternative hypothesis, that composite ilmenite could also form directly from the magma implying that it could be an igneous phase. On the other hand, the presence in the group 2 granites of subhedral amphibole, magnetite, and ilmenite associate crystals (Figure 2.6c, d, e, f) is a strong textural evidence of coeval crystallization of these minerals and indicates that magnetite and ilmenite are magmatic phases modified during cooling. We can thus admit that titanomagnetite and ilmenite-hematite solid solutions have crystallized directly from the Planalto magma and were modified, respectively, by oxy-exsolution or exsolution processes during cooling.

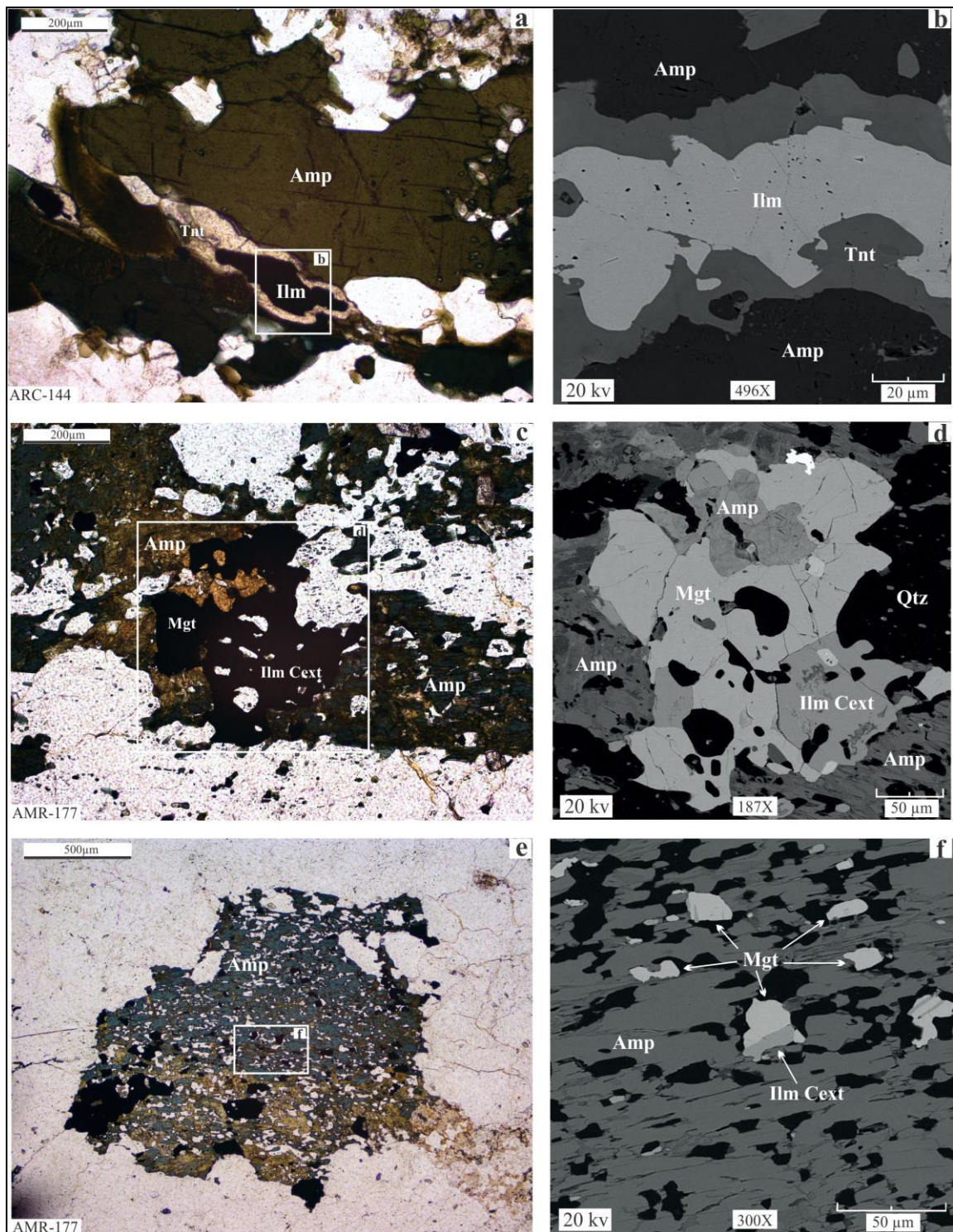


Figure 2.6 - a) and b) Corona of titanite surrounding ilmenite crystal associated with amphibole (Facies BHMzG, Group 1); c) and d) Mafic clot with amphibole, subhedral magnetite and composite ilmenite (Facies HLAG, Group 2); e) and f) Poikilitic amphibole crystals with abundant subhedral inclusions of magnetite, composite ilmenite and felsic minerals; to note the coarser subhedral crystals of magnetite found generally in the borders of the amphibole (Facies HLAG, Group 2); a), c) and e) Transmitted light microscopy with parallel nicols; b), d) and f) Backscattered images obtained in scanning electron microscope. Mineral abbreviations according to Kretz (1983). Ilm Cext = external composite ilmenite.

2.6 MINERAL CHEMISTRY

Seven representative samples of the Planalto Suite were selected for mineral chemical analyses on the basis of petrographic, magnetic petrology and whole rock geochemical data (chemical analyses compiled from Feio et al., 2012). These samples are from the plutons of the type area (AMR-140; AMR-149; AMR-137A), Vila Feitosa (ARC-109; ARC-147), and eastern of Canaã dos Carajás (AMR-116; AMR-85A). The analyzed minerals were amphibole, biotite, plagioclase, titanite, ilmenite, and magnetite.

Polished thin sections of the selected samples were initially submitted to semiquantitative chemical analysis by energy dispersive spectroscopy (EDS) in a Scanning Electron Microscope LEO 1430, of the Microanalyses Laboratory of the Geosciences Institute of the Federal University of Pará and further on to wavelength dispersive spectroscopy (WDS) quantitative analyses at the Electronic Microprobe Laboratory of the Geosciences Institute of the University of Brasilia, using a JEOL JXA-8230 microprobe with 5 WDS and one EDS spectrometers. All thin sections were previously metallized with carbon for both SEM and electron microprobe analyses. Analyses by EDS were performed at 20 kV voltage conditions and the WDS analyses, under the following operating conditions: column accelerating voltage of 15 kV; current 10 nA ; analysis time 10 seconds; beam diameter 5 microns for feldspars and 1 micron for all other minerals; matrix effects were corrected by ZAF model; analytical precision was $\pm 1\%$ and $\pm 10\%$ for major and minor elements respectively. The crystals used for analyses were LIFH for V, Mn, Fe, Ni and Ba, PETJ for K, Ca, Ti, Cr, Cl and Sr, TAP for Na, Si, Al, Mg and LDE1 for F. The standards used for instrument calibration were andradite (Si and Ca), microcline (Al and K), hematite (Fe), olivine (Mg), albite (Na), pyrophanite (Ti and Mn), vanadinite (V and Cl), topaz (F).

2.6.1 Amphibole

Amphiboles were analyzed with free-H₂O content, and the structural formula was calculated on the basis of 23 oxygen atoms, according to Leake et al. (1997) and Hawthorne et al. (2012). The Fe⁺³/Fe⁺² ratios were estimated on the basis of the charge balancing (Schumacher, 1997). For structural formula calculation, the cations were set in a total of 13 - CNK. The amphibole classification follows the IMA criteria (Hawthorne et al., 2012) which indicate that the Planalto Suite has a calcium amphibole (${}^B\text{Ca}/{}^B(\text{Ca}+\text{Na}) \geq 0.75$) with a hastingsitic composition (Table 2.1). Potassian-hastingsite is largely dominant, whereas chloro-potassian-hastingsite occurs only in the sample AMR-85A (Group 2). A relevant aspect is the dominance of Cl over F in the analyzed amphiboles (Table 2.1), which is also

observed in biotite composition (Table 2.2). This feature is not common in A-type granites (e.g. the Paleoproterozoic granites of the Carajás Province; Dall’Agnol et al., 2005) where F is generally the main volatile component. Using the criteria proposed by Leake et al. (1997), the Planalto amphiboles are also classified as hastingsite (Figure 2.7). The core and rim compositions do not show significant variations and the Fe/(Fe+Mg) ratios range between 0.845 and 0.941 and $Al_{total} > 2,00$ (Table 2.1). The calcic amphiboles of the Planalto Suite show evidence of edenitic and tschermakitic exchange.

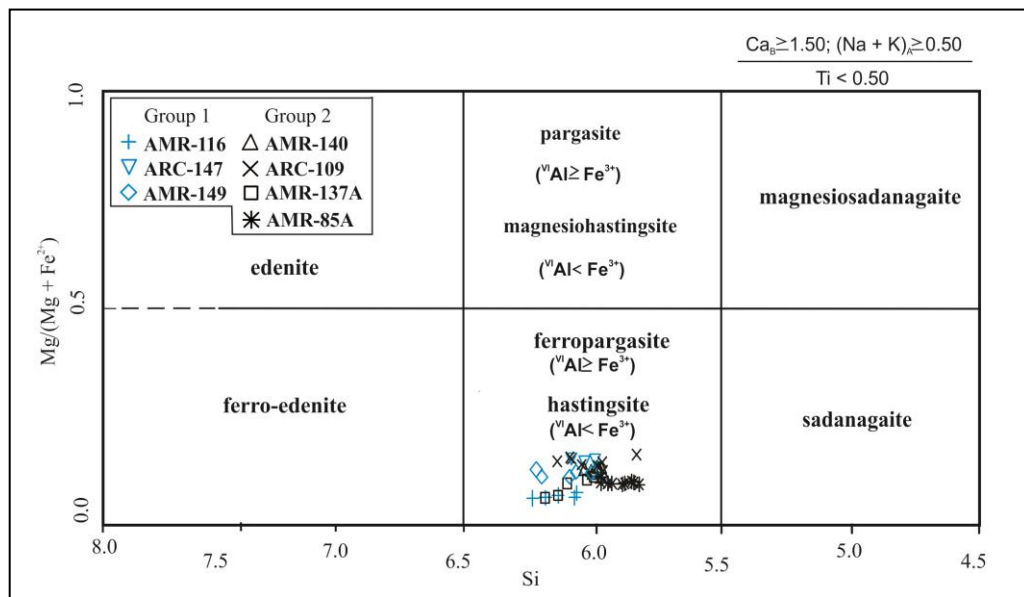


Figure 2.7 - Classification diagram (Leake et al., 1997) for amphiboles (hastingsite) of the Planalto Suite.

2.6.2 Biotite

The analyzed biotite occurs as millimeter-sized platy crystals associated with aggregates of hornblende, titanite, zircon, ilmenite, apatite, and more rarely, allanite and magnetite or as interstitial crystals. Microprobe analyses of the biotite of the Planalto Suite are shown in Table 2.2. The structural formula of biotite was calculated on an anhydrous basis of 22 atoms with positive charge or equivalent to 11 oxygens. It was assumed that all iron is in Fe^{2+} state (Table 2.2). The biotite of the Planalto Suite corresponds to annite (*International Mineralogical Association, IMA, criteria; Rieder et al., 1998*). The Fe/(Fe+Mg) versus Al^{IV} diagram (Figure 2.8a; Deer et al., 1992) shows that the biotite of the Planalto Suite is extremely enriched in Fe. However, they show relatively high contents of total Al in comparison with the annite end-member and their compositions are slightly displaced towards siderophyllite (Figure 2.8). The biotite of the Vila Feitosa pluton is slightly enriched in MgO compared to those of other plutons (Figure 2.8b; Table 2.2). In the Al total x Mg diagram

(Figure 2.8b; fields of Nachit et al., 1985) the biotite displays affinity with biotite of subalkaline rocks which is consistent with the ferroan character and A-type affinity of Planalto granites (Feio et al., 2012).

2.6.3. Plagioclase

The plagioclase of the Planalto Suite granites occurs as medium-grained porphyroclasts or as fine-grained crystals making part of the matrix of the rocks. Unaltered crystals of both plagioclase textural types were analyzed and the obtained compositions (Table 2.3) indicate that in most cases there is no accentuated compositional contrast between associate porphyroclasts and fine grains of the matrix but in some analyzed samples the latter tend to be more sodic. Optical and chemical data indicate that the dominant plagioclase, now forming the porphyroclasts, has calcic oligoclase (An_{25-21}) to sodic oligoclase (An_{17-10}) composition. The recrystallized grains have generally similar oligoclase compositions, but new formed grains of albite (An_{9-2}) were also identified. This suggests that during rock deformation and the partial recrystallization of feldspars, the oligoclase feldspar remained generally in equilibrium but locally albite was formed.

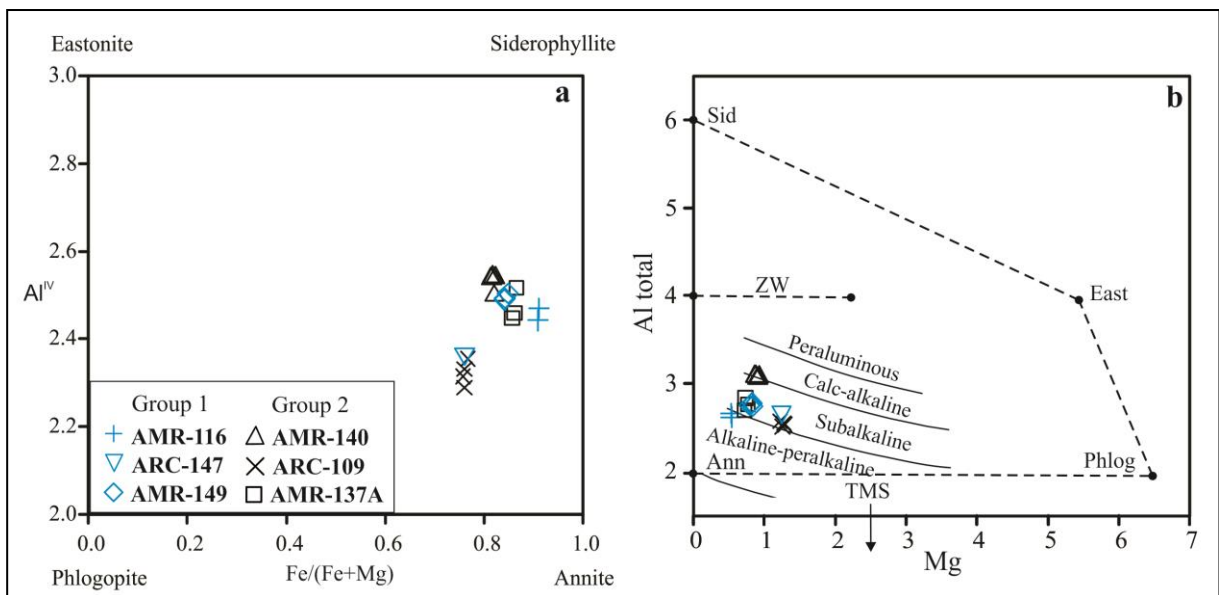


Figure 2.8 - Compositional variation of the biotite of the Planalto Suite. a) IVAl – Fe/(Fe+Mg) diagram (Deer et al., 1992); b) Al total x Mg diagram (fields of Nachit et al., 1985); Abbreviations: Sid - siderophyllite; East - eastonite; phlogopite; Ann -annite; TSM - tetrasilicic mica; Zw – zinnwaldite.

Table 2.1: Representative electron microprobe analyses of amphiboles of the Planalto Suite.

Samples	AMR-116			AMR-137A			AMR-140			AMR-149			AMR-85A				ARC-109			ARC-147			
Facies	BHSg			BHSg			BHMzG			HBMzG			HSG				HBSG			BHMzG			
Analyses	C3_1.1	C3_1.3	C4_2	C2_2	C3_1	C3_2	C4_1.3	C5_1.1	C5_1.2	C1_1.1	C1_2.2	C2_2	C1_1.1	C4_1	C4_2	C5_1.1	C1_2	C2_1.1	C3_1.1	C1_1.1	C1_1.2	C1_1.3	
type	K-Hs	K-Hs	K-Hs	K-Hs	K-Hs	K-Hs	K-Hs	K-Hs	K-Hs	K-Hs	K-Hs	K-Hs	K-Hs	K-Hs	K-Hs	K-Hs	K-Hs	K-Hs	K-Hs	K-Hs	K-Hs	K-Hs	
	rim	core	core	core	core	rim	core	rim	core	rim	core	core	rim	core	rim	rim	rim	core	rim	rim	rim	core	rim
SiO ₂ (Wt.%)	38.17	38.58	37.64	37.60	38.13	38.13	36.52	36.51	37.26	37.24	37.36	36.77	35.83	35.50	36.33	36.25	36.53	37.76	37.99	37.64	37.62	37.07	
TiO ₂	1.01	1.17	0.51	0.54	0.62	1.20	0.51	0.36	0.45	0.79	0.79	0.71	0.33	0.49	0.91	1.14	0.44	1.01	0.89	0.63	0.64	0.52	
Al ₂ O ₃	10.90	10.85	11.57	12.21	11.80	10.85	12.33	12.61	12.53	11.23	11.43	11.85	12.20	12.59	11.59	11.60	12.11	11.18	10.89	12.23	12.62	12.73	
Fe ₂ O ₃	4.96	3.34	7.07	8.23	6.48	5.41	7.25	7.28	8.03	4.84	6.98	7.61	6.48	8.15	6.57	6.31	7.04	6.32	6.44	4.84	5.44	6.90	
FeO	27.41	28.63	25.99	24.01	25.50	27.48	23.06	22.98	23.08	26.06	24.22	24.24	24.97	23.42	24.79	24.99	23.99	24.10	24.17	23.97	23.95	22.43	
MnO	0.40	0.30	0.41	0.48	0.46	0.40	0.59	0.50	0.50	0.40	0.47	0.56	0.31	0.41	0.35	0.42	0.48	0.66	0.59	0.68	0.59	0.78	
MgO	1.00	1.01	1.13	1.66	1.47	1.09	1.87	1.87	1.90	1.80	1.86	1.64	1.44	1.44	1.69	1.47	1.87	2.40	2.31	2.47	2.34	2.26	
CaO	10.67	10.90	10.84	10.75	10.78	10.90	10.46	10.73	10.77	11.06	10.72	10.89	10.69	10.38	10.52	10.52	10.68	10.64	10.55	10.83	10.75	10.55	
Na ₂ O	1.71	1.73	1.51	1.50	1.56	1.67	1.62	1.32	1.34	1.59	1.35	1.34	1.72	1.64	1.82	1.68	1.63	1.97	1.82	1.70	1.71	1.56	
K ₂ O	2.24	2.25	2.40	2.30	2.30	2.22	2.27	2.30	2.26	2.36	2.37	2.44	2.60	2.59	2.41	2.41	2.56	2.07	2.12	2.35	2.55	2.37	
F	0.36	0.30	0.25	0.43	0.36	0.39	0.33	0.34	0.32	0.36	0.30	0.21	0.23	0.03	0.13	0.15	0.59	0.44	0.61	0.46	0.06	0.39	
Cl	2.41	2.18	2.28	1.49	1.45	2.17	0.96	1.12	1.12	1.77	1.96	1.88	3.73	3.72	3.39	3.49	2.18	1.75	1.94	1.65	1.64	1.75	
H ₂ O	1.07	1.16	1.16	1.30	1.34	1.13	1.43	1.39	1.43	1.21	1.21	1.27	0.76	0.86	0.90	0.86	1.00	1.21	1.07	1.22	1.43	1.23	
Subtotal	102.30	102.40	102.77	102.49	102.25	103.04	99.20	99.30	101.00	100.71	101.01	101.41	101.28	101.22	101.39	101.29	101.11	101.50	101.37	100.66	101.32	100.54	
O-F-Cl	0.69	0.62	0.62	0.52	0.48	0.65	0.36	0.39	0.39	0.55	0.57	0.51	0.94	0.85	0.82	0.85	0.74	0.58	0.70	0.57	0.39	0.56	
Total	101.61	101.79	102.15	101.97	101.77	102.38	98.84	98.91	100.61	100.16	100.44	100.90	100.35	100.37	100.57	100.44	100.37	100.92	100.68	100.09	100.93	99.98	
Number of cations per formula unit based on twenty three oxygen atoms																							
Si	6.182	6.232	6.060	5.994	6.098	6.133	5.976	5.967	5.983	6.088	6.063	5.962	5.923	5.848	5.967	5.967	5.959	6.080	6.136	6.082	6.031	5.989	
Al ^{IV}	1.818	1.768	1.940	2.006	1.902	1.867	2.024	2.033	2.017	1.912	1.937	2.038	2.077	2.152	2.033	2.033	2.041	1.920	1.864	1.918	1.969	2.011	
Al ^{VI}	0.263	0.298	0.255	0.287	0.323	0.189	0.354	0.396	0.353	0.252	0.249	0.226	0.301	0.292	0.211	0.218	0.287	0.200	0.209	0.410	0.415	0.414	
Ti	0.123	0.142	0.062	0.064	0.075	0.145	0.062	0.044	0.054	0.097	0.097	0.087	0.041	0.060	0.112	0.141	0.054	0.123	0.108	0.076	0.077	0.064	
Fe ⁺³	0.605	0.407	0.856	0.988	0.779	0.654	0.892	0.895	0.971	0.595	0.853	0.928	0.807	1.010	0.811	0.782	0.864	0.765	0.783	0.588	0.657	0.838	
Fe ⁺²	3.713	3.867	3.499	3.200	3.411	3.696	3.154	3.141	3.099	3.563	3.288	3.287	3.453	3.227	3.404	3.441	3.273	3.246	3.265	3.239	3.212	3.031	
Mn	0.055	0.041	0.056	0.065	0.062	0.055	0.082	0.069	0.068	0.056	0.065	0.077	0.043	0.057	0.048	0.058	0.066	0.090	0.080	0.093	0.080	0.107	
Mg	0.241	0.244	0.272	0.395	0.350	0.261	0.455	0.456	0.455	0.438	0.449	0.396	0.355	0.354	0.413	0.361	0.455	0.576	0.556	0.594	0.559	0.545	
Ca	1.852	1.886	1.870	1.835	1.848	1.878	1.834	1.879	1.852	1.938	1.863	1.892	1.893	1.831	1.850	1.856	1.867	1.835	1.826	1.875	1.846	1.826	
Na	0.537	0.543	0.473	0.464	0.485	0.522	0.512	0.417	0.417	0.504	0.424	0.423	0.553	0.524	0.581	0.535	0.516	0.614	0.569	0.533	0.531	0.490	
K	0.463	0.464	0.492	0.467	0.470	0.455	0.474	0.480	0.463	0.492	0.491	0.504	0.548	0.543	0.505	0.506	0.532	0.425	0.436	0.484	0.521	0.488	
F	0.184	0.151	0.127	0.217	0.180	0.196	0.172	0.173	0.164	0.187	0.156	0.108	0.119	0.018	0.069	0.079	0.305	0.223	0.313	0.237	0.029	0.201	
Cl	0.662	0.596	0.623	0.401	0.392	0.592	0.267	0.310	0.305	0.491	0.538	0.517	1.044	1.039	0.943	0.974	0.604	0.479	0.532	0.451	0.445	0.478	
OH	1.154	1.253	1.250	1.382	1.429	1.211	1.561	1.517	1.531	1.322	1.307	1.375	0.837	0.943	0.988	0.947	1.091	1.299	1.156	1.312	1.527	1.321	
Al total	2.081	2.066	2.196	2.294	2.225	2.056	2.378	2.429	2.370	2.163	2.186	2.264	2.377	2.444	2.244	2.251	2.329	2.121	2.073	2.329	2.384	2.425	
Fe/(Fe+Mg)	0.939	0.941	0.928	0.890	0.907	0.934	0.874	0.873	0.872	0.891	0.880	0.893	0.907	0.901	0.892	0.905	0.878	0.849	0.855	0.845	0.852	0.848	

Total Fe reported as FeO. Structural formulae as 13-CNk. Key to abbreviations: H-hornblende; B-biotite; MzG-monzogranite; SG-syenogranite; Hastingsite-NaCa₂(Fe⁺²₄Fe⁺³)Si₆Al₂O₂₂(OH)₂; Chloro prefix-Cl > OH,F; Potassic prefix-^AK > ^{ANa},^{ACa},^A[]; K-Hs-potassian-hastingsite; Cl-Chloro.

Table 2.2: Electron microprobe analyses of biotite of the Planalto Suite.

Samples	AMR-116		AMR-137A			AMR-140					AMR-149			ARC-109				ARC-147
Facies	BHSg		BHSg			BHMzG					HBMzG			HBSg				BHMzG
Analyses	C3_1.1	C3_1.2	C2_1.2	C3_2	C3_3	C2_1.1	C2_1.2	C2_1.3	C2_1.4	C5_1.1	C1_1	C1_2.2	C2_1	C2_1.1	C2_1.2	C3_1	C3_2	C2_1
SiO ₂ (Wt.%)	33.69	33.79	34.57	34.49	34.03	34.46	34.30	33.86	33.69	33.97	33.63	33.65	33.45	35.66	35.10	35.17	35.72	35.21
TiO ₂	2.62	2.67	2.31	2.23	2.13	1.91	1.90	1.85	2.03	1.67	1.80	1.89	1.78	2.44	2.32	2.49	2.45	2.30
Al ₂ O ₃	13.47	13.70	14.87	14.59	14.96	16.62	16.65	16.39	16.19	16.55	14.77	14.86	14.88	13.29	13.30	13.64	13.64	14.22
FeO	34.75	34.79	32.94	32.99	33.67	29.72	30.10	29.78	29.39	30.15	32.01	32.12	31.71	29.40	29.23	29.62	30.00	29.09
MnO	0.28	0.28	0.40	0.35	0.26	0.30	0.23	0.39	0.37	0.29	0.27	0.39	0.28	0.35	0.30	0.30	0.27	0.45
MgO	1.94	1.91	3.06	3.11	2.95	3.70	3.90	3.81	3.73	3.68	3.44	3.27	3.38	5.33	5.41	5.19	5.45	5.13
CaO	0.03	0.00	0.03	0.00	0.03	0.00	0.00	0.00	0.01	0.00	0.06	0.00	0.01	0.03	0.03	0.01	0.04	0.03
Na ₂ O	0.02	0.06	0.06	0.10	0.04	0.02	0.10	0.05	0.07	0.09	0.05	0.02	0.01	0.07	0.07	0.08	0.06	0.05
K ₂ O	9.02	9.81	9.05	9.03	9.00	9.42	9.44	9.54	9.74	9.50	9.44	9.37	9.31	9.24	9.28	9.17	9.16	9.16
H ₂ O	2.98	2.95	3.38	3.34	3.36	3.49	3.45	3.38	3.41	3.44	3.15	3.24	3.13	2.94	2.88	3.01	2.91	3.01
F	0.14	0.28	0.25	0.31	0.22	0.23	0.28	0.36	0.27	0.28	0.36	0.18	0.30	1.03	1.11	0.90	1.15	1.00
Cl	2.30	2.30	0.97	0.90	1.01	0.63	0.73	0.67	0.65	0.61	1.36	1.34	1.44	1.26	1.17	1.16	1.28	1.01
Subtotal	101.25	102.50	101.86	101.44	101.67	100.49	101.07	100.07	99.53	100.24	100.33	100.32	99.68	101.04	100.18	100.74	102.13	100.66
O=F-Cl	0.58	0.63	0.32	0.33	0.32	0.24	0.28	0.30	0.26	0.26	0.46	0.38	0.45	0.72	0.73	0.64	0.77	0.65
Total	100.67	101.87	101.54	101.11	101.35	100.25	100.79	99.77	99.27	99.98	99.88	99.94	99.23	100.32	99.45	100.10	101.36	100.01
Number of cations per formula unit based on twenty two oxygen atoms																		
Si	22.266	22.142	22.173	22.235	21.968	22.001	21.841	21.826	21.833	21.850	22.030	22.021	22.028	22.854	22.717	22.608	22.674	22.566
Al ^{IV}	9.734	9.858	9.827	9.765	10.032	9.999	10.159	10.174	10.167	10.150	9.970	9.979	9.972	9.146	9.283	9.392	9.326	9.434
Al ^{VI}	0.761	0.726	1.415	1.319	1.353	2.506	2.336	2.278	2.200	2.397	1.434	1.484	1.578	0.893	0.862	0.943	0.880	1.309
Ti	1.302	1.314	1.114	1.080	1.036	0.918	0.908	0.899	0.988	0.808	0.887	0.930	0.879	1.177	1.130	1.205	1.170	1.109
Fe	19.207	19.063	17.670	17.787	18.177	15.871	16.033	16.052	15.929	16.220	17.537	17.579	17.465	15.759	15.820	15.921	15.924	15.595
Mn	0.159	0.153	0.216	0.191	0.144	0.161	0.126	0.212	0.205	0.156	0.151	0.217	0.156	0.189	0.162	0.164	0.147	0.244
Mg	1.914	1.862	2.923	2.990	2.840	3.526	3.705	3.658	3.603	3.532	3.355	3.187	3.314	5.090	5.217	4.969	5.156	4.904
Ca	0.023	0.000	0.018	0.000	0.024	0.000	0.000	0.001	0.005	0.000	0.043	0.000	0.008	0.019	0.018	0.010	0.030	0.019
Na	0.029	0.071	0.068	0.128	0.051	0.021	0.121	0.056	0.082	0.113	0.066	0.022	0.015	0.086	0.082	0.093	0.075	0.056
K	7.604	8.196	7.401	7.428	7.411	7.672	7.671	7.844	8.047	7.797	7.883	7.821	7.823	7.556	7.661	7.522	7.419	7.491
OH	13.136	12.880	14.446	14.378	14.454	14.857	14.651	14.538	14.747	14.760	13.745	14.146	13.770	12.551	12.452	12.913	12.321	12.885
F	0.291	0.570	0.503	0.636	0.443	0.456	0.562	0.726	0.543	0.578	0.742	0.370	0.627	2.080	2.268	1.820	2.305	2.019
Cl	2.573	2.550	1.051	0.986	1.103	0.686	0.787	0.736	0.710	0.662	1.513	1.483	1.603	1.370	1.280	1.267	1.374	1.096
Al total	10.495	10.585	11.242	11.083	11.385	12.506	12.494	12.453	12.367	12.547	11.404	11.462	11.550	10.039	10.146	10.335	10.206	10.743
Fe/Fe+Mg	0.909	0.911	0.858	0.856	0.865	0.818	0.812	0.814	0.816	0.821	0.839	0.847	0.841	0.756	0.752	0.762	0.755	0.761

Total Fe reported as FeO. Structural formulae on the bases of 22 oxygens. Key to abbreviations: Bt-biotite; H-hornblende; B-biotite; MzG-monzogranite; SG-syenogranite.

Table 2.3: Representative electron microprobe analyses of plagioclase of the Planalto Suite.

Sample	AMR-140		AMR-149		ARC-109		AMR-85A		ARC-147		AMR-137A		
Facies	BHMzG		HBMzG		HBSG		HSG		BHMzG		BHSG		
Analyses	C6_1.2	C3_2	C5_2.1	C5_3	C5_1.2	C4_1.1	C6_1.4	C6_3	C3_1.3	C4_1.3	C5_1.1	C4_1.3	C4_1.4
type	olig	olig	alb	alb	olig	olig	olig	olig	olig	olig	olig	alb	alb
		R		R		R		R		R		R	R
SiO ₂ (wt%)	63.83	64.45	64.24	65.25	62.26	61.59	63.15	64.64	64.12	62.96	64.20	65.92	67.65
Al ₂ O ₃	22.02	21.54	21.16	20.05	23.15	23.67	22.77	22.00	22.18	22.73	22.26	21.51	20.22
FeO	0.08	0.04	0.20	0.04	0.02	0.04	0.00	0.00	0.00	0.05	0.00	0.00	0.01
CaO	2.55	2.34	1.37	0.79	4.17	4.89	3.66	2.90	2.85	3.58	2.81	1.89	0.37
Na ₂ O	10.70	10.76	10.86	11.29	9.58	9.09	10.04	10.17	9.83	10.13	10.49	10.66	11.72
K ₂ O	0.21	0.11	0.35	0.10	0.20	0.30	0.13	0.14	0.19	0.11	0.13	0.18	0.10
Total	99.38	99.25	98.18	97.52	99.39	99.58	99.75	99.85	99.17	99.57	99.88	100.16	100.08
Number of cations per formula unit based on eight oxygen atoms													
Si	2.810	2.842	2.860	2.919	2.758	2.731	2.781	2.846	2.847	2.776	2.817	2.886	2.948
Al	1.142	1.120	1.110	1.057	1.209	1.237	1.182	1.142	1.161	1.181	1.151	1.110	1.039
Fe	0.003	0.002	0.007	0.002	0.001	0.001	0.000	0.000	0.000	0.002	0.000	0.000	0.000
Ca	0.120	0.111	0.066	0.038	0.198	0.232	0.173	0.137	0.136	0.169	0.132	0.089	0.017
Na	0.913	0.920	0.937	0.979	0.823	0.781	0.857	0.868	0.846	0.866	0.892	0.905	0.990
K	0.012	0.006	0.020	0.006	0.012	0.017	0.007	0.008	0.011	0.006	0.007	0.010	0.006
Cations	5	5	5	5	5	5	5	5	5	5	5	5	5
Albite	87	89	92	96	78	76	83	86	85	83	87	90	98
Anortite	11	11	6	4	21	23	17	13	14	16	13	9	2
orthoclase	1	1	2	1	1	2	1	1	1	1	1	1	1

R - Recrystallized; olig – oligoclase; alb – albite; H-hornblende; B-biotite; MzG-monzogranite; SG-syenogranite.

2.6.4 Titanite

Titanite (CaTiSiO_5) is a common accessory mineral in intermediate and granitoid metaluminous plutonic rocks (Cuney and Friederich, 1987; Robinson and Miller, 1999). According to Frost et al. (2000), titanite can occur in three different ways; (1) primary igneous mineral; (2) mineral formed during cooling of igneous rocks (subsolidus); and (3) metamorphic mineral in many rock types. Commonly, titanite is present in metaluminous I-type granites, with an intermediate silica content and high calcium content. In addition, it may be absent in many high-silica, evolved granites due to the fact that the CaO content decreases with the increase of SiO_2 . The stable Ti phases in many igneous rocks are titanomagnetite and ilmenite instead of titanite. This can indicate that crystallization occurred at relatively low oxygen fugacity that is inadequate to stabilize titanite. Titanite is found in relatively oxidized rocks and typically occurs with hornblende (Frost and Lindsley, 1991; Wones, 1989; Frost et al., 2000).

Frost et al. (2000) argue that during the cooling of plutonic rocks, titanite can be formed by two processes: (1) in association with peritectic reactions involving hydration of pyroxene and its replacement by hornblende. This hydration can occur in the magmatic stage or in the subsolidus associated to deuteric change, depending on the water activity in the magma; (2) oxidation during post-magmatic reequilibration in calc-alkaline rocks that followed initially a cooling trend under reduced conditions with ilmenite formation. Dall'Agnol et al. (1999) consider that in the oxidized A-type Jamon granite, titanite formation is related to a peritectic late magmatic reaction leading the replacement of hornblende by biotite.

Petrographic studies indicate that there are no significant textural differences between the titanites of the Group 1 and Group 2 granites of the Planalto Suite. In both groups, titanite occurs as anhedral irregular grains surrounding ilmenite crystals (corona-type texture; Figure 2.6a, b) or as anhedral to subhedral crystals associated with mafic clots. Locally in the Group 2, it is associated with amphibole, ilmenite and magnetite (Figure 2.6c, d). Besides, there is no positive correlation between modal contents of opaque minerals and titanite and several samples of Group 2 granites with high MS values have no significant modal titanite.

The chemical composition of titanite of 5 samples, two of the Group 1 and three of the Group 2 were analyzed (Table 2.4). The compositions of the titanite of both groups are similar and all of them show low Fe/Al ratios (0.1 to 0.4; Figure 2.9; Table 2.4). Kowallis et al. (1997) argue that low Fe/Al ratios in titanite are an evidence of its formation in hydrothermal and/or metamorphic environments. In the Fe vs Al diagram (Figure 2.9), the Planalto titanite

compositions plot near the field of titanite formed in metamorphic conditions which indicates that its origin may be related to secondary processes. Nevertheless, it is noteworthy that the distribution of Planalto titanites in that diagram does not coincide exactly with the field of metamorphic titanite because the former are enriched in Fe compared to the titanites representative of metamorphic settings. Another restriction is that we do not dispose of information about the titanites considered by Kowallis et al. (1997) and Aleinikoff et al. (2002) in their works nor on the exact nature of the rocks that contain those titanites. For these reasons and the lack of experimental support, it is unclear whether the interpretation of the mentioned authors can be extrapolated for the studied granites. However, the sum of petrographic and mineralogical evidence suggest that titanite can be a secondary phase in the Planalto granite and possibly related to subsolidus processes that affected the Planalto granites or to superimposed metamorphic processes.

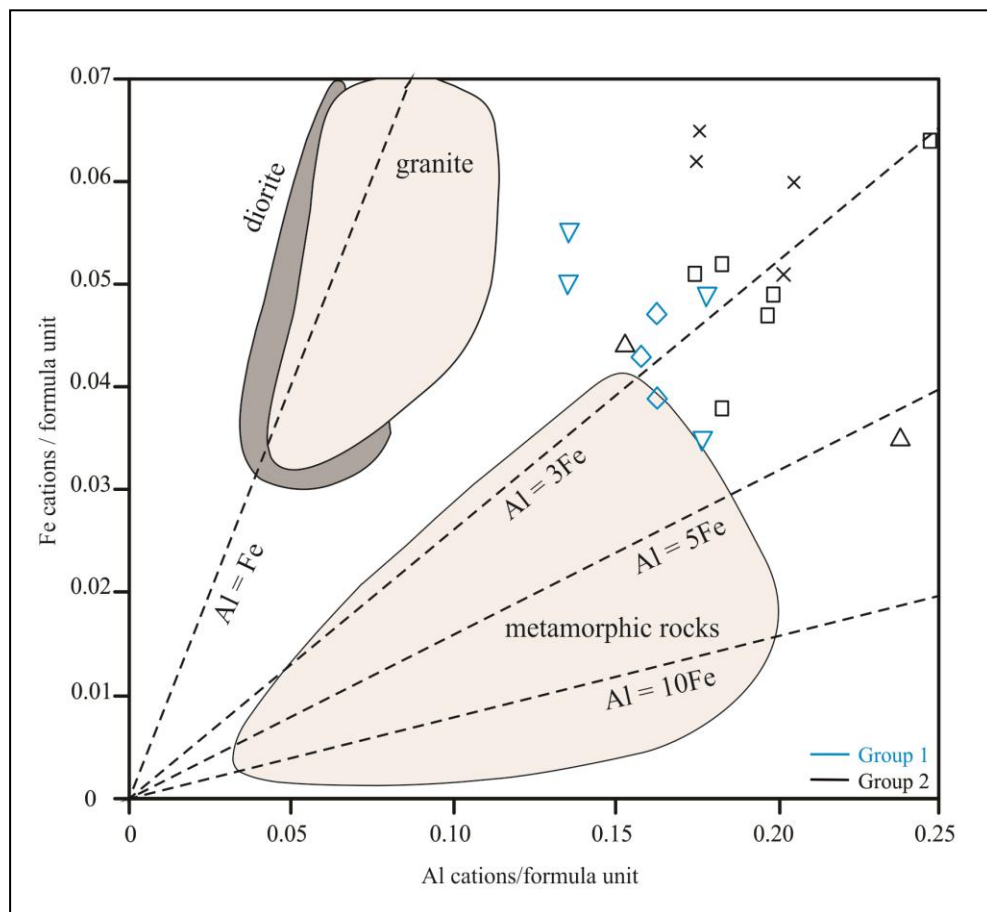


Figure 2.9 - Fe vs Al diagram for the titanite of the Planalto Suite. Based on Aleinikoff et al. (2002, modified). Fields for magmatic and metamorphic titanite compositions from Kowallis et al. (1997). Symbols for the Planalto granites as in Figure 2.8.

Table 2.4: Representative electron microprobe analyses of titanite of the Planalto Suite.

Sample	AMR-137A						AMR-140		AMR-149			ARC-109				ARC-147			
Facies	BHSg						BHMzG		HBMzG			HBSG				BHMzG			
Analyses	C2_1	C2_2	C3_1	C3_3	C3_4	C4_2	C3_1	C7_1.1	C1_1	C3_1	C3_2	C2_1	C2_2	C2_3	C3_1	C1_1.1	C1_1.2	C2_1.1	C2_1.2
SiO ₂	30.31	30.09	30.15	30.24	30.54	31.01	30.44	29.04	29.47	29.70	29.82	29.97	30.06	30.48	30.18	30.08	30.50	29.97	30.57
TiO ₂	31.99	31.27	31.10	32.26	32.65	29.85	30.47	32.47	32.88	33.18	33.03	31.36	30.36	31.21	31.15	33.01	32.25	33.27	32.55
Al ₂ O ₃	4.61	4.94	4.99	4.43	4.66	6.21	6.03	3.76	4.06	3.96	4.10	4.38	5.10	5.09	4.33	3.42	4.53	3.38	4.49
Cr ₂ O ₃	0.06	0.01	0.00	0.04	0.02	0.00	0.03	0.00	0.00	0.00	0.03	0.00	0.00	0.03	0.00	0.00	0.00	0.00	0.00
FeO	1.85	1.66	1.73	1.81	1.36	2.26	1.24	1.52	1.66	1.52	1.38	2.28	2.10	1.82	2.15	1.93	1.74	1.75	1.24
MnO	0.03	0.12	0.11	0.06	0.11	0.07	0.03	0.15	0.10	0.00	0.12	0.03	0.13	0.11	0.05	0.18	0.16	0.18	0.20
MgO	0.04	0.04	0.03	0.03	0.05	0.05	0.03	0.00	0.06	0.02	0.05	0.09	0.05	0.04	0.09	0.03	0.00	0.04	0.03
CaO	27.66	27.81	28.14	28.13	28.51	26.20	28.38	27.66	27.32	27.85	27.67	27.21	27.33	28.00	27.19	27.58	28.22	27.48	27.88
Na ₂ O	0.04	0.01	0.02	0.00	0.06	0.07	0.06	0.07	0.04	0.06	0.04	0.00	0.05	0.09	0.06	0.10	0.03	0.08	0.07
K ₂ O	0.00	0.09	0.00	0.02	0.00	0.09	0.02	0.01	0.00	0.02	0.04	0.02	0.01	0.02	0.00	0.00	0.00	0.01	0.01
Total	96.60	96.02	96.27	97.01	97.96	95.80	96.73	94.66	95.58	96.31	96.27	95.33	95.20	96.87	95.21	96.32	97.42	96.16	97.04
Number of cations per formula unit based on five oxygen atoms																			
Si	1.022	1.021	1.021	1.017	1.015	1.047	1.022	1.004	1.006	1.006	1.010	1.026	1.029	1.025	1.033	1.021	1.021	1.018	1.024
Ti	0.811	0.798	0.792	0.816	0.817	0.758	0.769	0.844	0.844	0.846	0.841	0.807	0.782	0.789	0.802	0.843	0.812	0.850	0.820
Al	0.183	0.197	0.199	0.175	0.183	0.247	0.238	0.153	0.163	0.158	0.163	0.176	0.205	0.202	0.175	0.136	0.178	0.135	0.177
Cr	0.002	0.000	0.000	0.001	0.001	0.000	0.001	0.000	0.000	0.000	0.001	0.000	0.000	0.001	0.000	0.000	0.000	0.000	0.000
Fe	0.052	0.047	0.049	0.051	0.038	0.064	0.035	0.044	0.047	0.043	0.039	0.065	0.060	0.051	0.062	0.055	0.049	0.050	0.035
Mn	0.001	0.004	0.003	0.002	0.003	0.002	0.001	0.004	0.003	0.000	0.003	0.001	0.004	0.003	0.002	0.005	0.004	0.005	0.006
Mg	0.002	0.002	0.002	0.001	0.002	0.003	0.002	0.000	0.003	0.001	0.002	0.005	0.003	0.002	0.004	0.002	0.000	0.002	0.001
Ca	0.999	1.011	1.021	1.014	1.016	0.948	1.020	1.024	0.999	1.011	1.004	0.998	1.002	1.009	0.997	1.003	1.012	1.000	1.001
Na	0.002	0.001	0.001	0.000	0.004	0.005	0.004	0.005	0.003	0.004	0.003	0.000	0.003	0.006	0.004	0.007	0.002	0.005	0.004
K	0.000	0.004	0.000	0.001	0.000	0.004	0.001	0.000	0.000	0.001	0.002	0.001	0.000	0.001	0.000	0.000	0.000	0.000	0.001
Fe/Al	0.284	0.239	0.246	0.291	0.208	0.259	0.147	0.288	0.288	0.272	0.239	0.369	0.293	0.252	0.354	0.404	0.275	0.370	0.198

H-hornblende; B-biotite; MzG-monzogranite; SG-syenogranite.

2.6.5 Ilmenite

Ilmenite (FeTiO_3) is a common mineral both in igneous and metamorphic rocks. The formula of ilmenite is $(\text{Fe, Mg, Mn})\text{TiO}_3$ and it forms a solid solution series with geikielite (MgTiO_3) and pyrophanite (MnTiO_3). Identifying the primary compositional variation of ilmenite in plutonic rocks is difficult because this mineral can have a complex evolution and is formed in different ways: It can be product of direct crystallization from the magma, product of oxy-exsolution of the titanomagnetite (Buddington and Lindsley, 1964; Haggerty, 1991; Dall'Agnol et al., 1997) or it can be related to secondary processes. The processes of oxy-exsolution and exsolution are generally effective during the late- and post-magmatic evolution of plutonic igneous rocks and primary ilmenite and titanomagnetite compositions (respectively, ilmenite – hematite and magnetite-ulvospinel solid solutions) are only occasionally preserved.

Ilmenite of seven samples from Planalto Suite, (Table 2.5) and the ilmenite of different granite groups or distinct textural varieties do not show outstanding contrasts. The Ilmenite shows variable proportions of pyrophanite, but MnO contents are moderate (2.0 to 6.8 %; Table 2.5).

2.6.6 Magnetite

Magnetite is the main ferromagnetic mineral and may be present in various rock types. In igneous rocks, it crystallize generally as titanomagnetite, term employed to designate all members of the magnetite – ulvospinel solid solution series. However, in plutonic rocks, due to slow cooling of the magma, the primary titanomagnetite is submitted to an extensive reequilibration during the subsolidus stage and affected by oxy-exsolution processes that transform it in intergrowths of pure magnetite with different textural varieties of ilmenite or even in texturally homogeneous magnetite crystals (Haggerty, 1991; Dall'Agnol et al., 1997). As a consequence, in granitoid rocks, the magnetite commonly approaches the pure end term composition (Fe_3O_4).

Magnetite occurs only in Group 2 of the Planalto Suite and its composition is similar to that of the pure magnetite (Table 2.5) which suggests that it was strongly re-equilibrated or, alternatively, that it crystallized in subsolidus conditions at relatively low temperatures compared to those prevalent during the magmatic stage.

Table 2.5: Representative electron microprobe analyses of ilmenite and magnetite of the Planalto Suite.

Sample	GROUP 1						GROUP 2										
	AMR-116		AMR-149	ARC-147	AMR-137A		AMR-140	AMR-85A		ARC-109		AMR-137A	AMR-140		AMR-85A		
	BHSg		HBMzG	BHMzG	BHSg		BHMzG	HSG		HBSG		BHSg	BHMzG		HSG		
Mineral	Ilm	Ilm	Ilm	Ilm	Ilm	Ilm	Ilm	Ilm	Ilm	Ilm	Ilm	Mgt	Mgt	Mgt	Mgt	Mgt	
SiO ₂ (wt%)	0.03	0.03	0.03	0.02	0.02	0.01	0.04	0.04	0.11	0.00	0.02	0.15	0.08	0.18	0.04	0.06	
TiO ₂	52.82	53.16	53.17	51.52	52.95	53.48	52.35	51.37	52.95	51.71	51.20	0.00	0.00	0.00	0.11	0.00	
Al ₂ O ₃	0.02	0.00	0.00	0.00	0.03	0.00	0.01	0.00	0.00	0.00	0.00	0.06	0.03	0.02	0.09	0.05	
Fe ₂ O ₃	0.00	0.00	0.00	1.22	0.00	0.00	0.00	1.15	0.00	1.35	2.14	70.46	67.30	66.74	67.77	68.40	
FeO	43.00	42.16	40.88	39.34	41.94	41.37	40.85	43.38	42.77	42.47	42.14	32.08	30.40	30.41	30.70	30.88	
MnO	3.78	4.14	5.96	6.80	4.59	4.67	4.94	2.80	3.03	3.91	3.79	0.00	0.04	0.00	0.04	0.00	
MgO	0.00	0.00	0.01	0.00	0.01	0.00	0.00	0.02	0.00	0.04	0.03	0.00	0.00	0.00	0.01	0.00	
CaO	0.02	0.03	0.11	0.11	0.02	0.04	0.15	0.00	0.08	0.01	0.04	0.05	0.04	0.03	0.08	0.06	
Cr ₂ O ₃	0.00	0.05	0.00	0.00	0.00	0.05	0.00	0.04	0.03	0.02	0.07	0.00	0.00	0.00	0.01	0.01	
V ₂ O ₃	0.53	0.46	0.43	0.65	0.50	0.42	0.41	0.65	0.61	0.50	0.53	0.00	0.03	0.01	0.00	0.00	
Total	100.20	100.04	100.59	99.66	100.06	100.04	98.75	99.45	99.58	100.03	99.96	102.80	97.88	97.39	98.84	99.47	
Ilmenite: number of cations per formula unit based on three oxygen atoms; Magnetite: number of cations per formula unit based on four oxygen atoms																	
Si	0.001	0.001	0.001	0.000	0.001	0.000	0.001	0.001	0.003	0.000	0.001	0.006	0.003	0.007	0.002	0.002	
Al	0.000	0.000	0.000	0.000	0.001	0.000	0.000	0.000	0.000	0.000	0.000	0.002	0.001	0.001	0.004	0.002	
Ti	1.001	1.009	1.003	0.981	1.005	1.016	1.006	0.981	1.010	0.982	0.973	0.000	0.000	0.000	0.003	0.000	
Fe ⁺³	0.000	0.000	0.000	0.023	0.000	0.000	0.000	0.022	0.000	0.026	0.041	1.986	1.993	1.985	1.986	1.993	
Fe ⁺²	0.906	0.890	0.858	0.833	0.885	0.874	0.873	0.921	0.907	0.897	0.890	1.004	1.000	1.005	1.000	1.000	
Mn	0.081	0.089	0.127	0.146	0.098	0.100	0.107	0.060	0.065	0.084	0.081	0.000	0.001	0.000	0.001	0.000	
Mg	0.000	0.000	0.000	0.000	0.001	0.000	0.000	0.001	0.000	0.001	0.001	0.000	0.000	0.000	0.001	0.000	
Ca	0.001	0.001	0.003	0.003	0.000	0.001	0.004	0.000	0.002	0.000	0.001	0.002	0.002	0.001	0.003	0.003	
Cr	0.000	0.001	0.000	0.000	0.000	0.001	0.000	0.001	0.001	0.000	0.001	0.000	0.000	0.000	0.000	0.000	
V	0.011	0.009	0.009	0.013	0.010	0.009	0.008	0.013	0.012	0.010	0.011	0.000	0.001	0.000	0.000	0.000	
Total	2.000	1.999	2.000	2.000	2.000	2.000	2.000	2.000	2.000	2.000	2.000	3.000	3.000	3.000	3.000	3.000	
												% Usp	2.248	2.363	2.375	2.34	2.33
% Ilm	90.319	88.448	85.518	83.399	88.051	86.537	86.933	92.144	90.093	89.688	89.150						
% Pir	8.030	8.795	12.630	14.587	9.758	9.883	10.652	6.031	6.453	8.359	8.125						
% Hem	0.000	0.000	0.000	1.164	0.000	0.000	0.000	1.103	0.000	1.283	2.041						

Ilm – Ilmenite; Mgt - Magnetite; H-hornblende; B-biotite; MzG-monzogranite; SG-syenogranite; Ilm – ilmenita; Pir – pyrophanite; Hem – hematite; Usp - Ulvöspinel

2.7 DISCUSSION

2.7.1 Estimation of crystallization parameters of the Planalto Suite

The main factors responsible for crystallization and mineralogy of a rock are: chemical composition of the magma, pressure, temperature, oxygen fugacity, and nature and content of volatiles (e.g., Martin, 2007; Papoutsas and Pe-Piper, 2014; Erdmann et al., 2014). Thus, the definition or evaluation of these factors is relevant to understand the geological processes responsible for the Planalto Suite formation. However, in igneous rocks, the estimation of these factors is generally based in the original magmatic compositions of the main mineral phases and, as discussed before, we have textural and chemical evidences that the main rock-forming minerals of the Planalto Suite were re-equilibrated during their subsolidus evolution, possibly due to deformational processes or eventually metamorphic imprint. Nevertheless, we believe that the whole rock and mineral compositions of the studied granites were not submitted to intense changes and is always valid to evaluate if the mentioned parameters can be better constrained using mineralogical data.

2.7.1.1 Temperature

Watson and Harrison (1983) and Harrison and Watson (1984) demonstrated that the activity in the magma of Zr and P₂O₅ required for the zircon and apatite saturation depends mainly on temperature and SiO₂ content in melt. Zircon saturation temperature (T_{Zr}) calculated from the whole rock composition provides minimum temperature estimates if magma is subsaturated and maximum if saturated (Miller et al., 2003). This mineral is used because it is ubiquitous in intermediate to felsic plutonic rocks. For plutons with great amount of inherited zircon, The T_{Zr} provides a useful estimate of magma initial temperature at source, an important parameter that is inaccessible from other methods (Miller et al., 2003). The initial relationship among zircon solubility, temperature, and major element composition of melt defined by Watson and Harrison (1983) based on experiments, can be expressed as:

$$T_{Zr} = 12,900 / [2.95 + 0.85M + \ln(496,000/Zr_{melt})], \text{ where } M = (Na+K+2Ca)/(Al \cdot Si)$$

On the other hand, Harrison and Watson (1984) demonstrated that in felsic magmas the apatite saturation temperature (T_{Ap}) is dependent primarily on temperature, SiO₂ content and it is independent of pressure (in crustal pressures range) or H₂O content in a range from 0 to 10 wt%. Their original equation can be expressed as:

$$T_{Ap} = [8400 + ((SiO_2 - 0.5)2.64 \times 10^4) / (\ln (0.426/P_2O_{5melt}) + [3.1 \times (12.4(SiO_2 - 0.5))])]$$

The proposed equations for initial calculation of crystallization temperatures by geothermometers of Zr and apatite saturation were applied for the Planalto Suite samples submitted to mineral chemistry studies and the results are given in Table 2.6. According to the equation proposed by Watson and Harrison (1983), the zircon saturation thermometer provided initial temperatures variable between 897–854 °C (Table 2.6), petrologically consistent with near liquidus expected temperatures for A-type granites and charnockitic rocks. Moreover, there is clear petrographic evidence that zircon is an early crystallized phase in the Planalto granites, because euhedral zircon grains are included in amphibole, biotite, plagioclase, and iron-titanium oxides. Besides, it is highly improbable that the temperatures attained during the deformation of the studied rocks or during a hypothetical metamorphic imprint have been high enough to affect zircon equilibrium. Finally, there is no evidence of inherited zircon in the Planalto granites (Feio et al., 2012, 2013). Hence, it is reasonable to admit that the whole rock zirconium content obtained in the Planalto samples is representative of the zirconium content of the Planalto magma. This suggests that the near liquidus magma temperatures indicated for the Planalto granites by the zircon saturation thermometer are consistent.

On the other hand, the apatite saturation thermometer provided much lower temperatures (704–620 °C). Most of these temperatures are below the solidus temperature admitted for granitic systems with moderate water and not enriched in fluorine, boron and lithium (approximately 700° C; Naney, 1983; Dall’Agnol et al., 1999). Another restrictive aspect is that, as commonly happens in metaluminous granites, apatite is like zircon an early crystallized accessory mineral in the Planalto granites and the apatite saturation temperatures should approach that of liquidus better than those of the solidus. The apparent inconsistency of the temperatures obtained using the apatite geothermometer suggests that P could had a mobile behavior during deformation and the actual P content of the whole rock do not correspond to the P content of the magma. Anyway, the temperatures suggested by the apatite thermometer will not be further considered in this paper.

More recently, Ridolfi et al. (2010) and Ridolfi and Rezzulli (2012) reviewed thermobarometric equations available in the literature and presented calibration models to estimate temperature using concentrations of main oxides in amphibole. These equations are recommended for amphiboles crystallized from H₂O-poor to H₂O-rich, calc-alkaline to alkaline magmas, which evolved at moderately reduced to moderately oxidized conditions (Erdmann et al, 2014). However, Erdmann et al. (2014) state that the equation of Ridolfi et al. (2010), given below, is more accurate for temperature calculations.

$$T(^{\circ}\text{C}) = -151.487\text{Si}^* + 2041; \text{Si}^* = \text{Si} + (\text{Al}^{\text{IV}}/15) - (2\text{Ti}^{\text{IV}}) - (\text{Al}^{\text{VI}}/2) - (\text{Ti}^{\text{VI}}/1.8) + (\text{Fe}^{3+}/9) + (\text{Fe}^{2+}/3.3) + (\text{Mg}/26) + (\text{Ca}^{\text{B}}/5) + (\text{Na}^{\text{B}}/1.3) - (\text{Na}^{\text{A}}/15) + ([\text{A}]/2.3)$$

The geothermometer of Ridolfi et al. (2010) provided temperatures between 910–831 °C (Table 2.6) for the Planalto Suite, largely superposed with those obtained with the zircon saturation thermometer (897–854 °C). These data are indicative of the liquidus temperature and suggest an interval from 910–850° C for the initial crystallization temperatures of the Planalto Suite. These probable near liquidus temperature are relatively high and reinforce the need of high melt temperatures which is consistent with a granulitic source admitted for the Planalto magmas (Feio et al., 2012).

The solidus temperature is not easy to establish. The lack in most samples of strong hydrothermal alteration indicated by the common preserved aspect of amphibole, biotite and plagioclase and the relatively low contents of fluorine in amphibole and biotite (Tables 2.1 and 2) suggest that it should be near 700 °C as pointed out by experimental studies of granitic systems with low fluorine contents (Naney, 1983; Dall’Agnol et al., 1999; Klimm et al., 2003). Hence, a maximum temperature crystallization range of 910-700 °C can be estimated for the Planalto granites.

Table 2.6 – Estimate of pressure and temperature of crystallization for the granites of the Planalto Suite.

PLANALTO SUITE Samples	Type-area			Eastern of Canaã dos Carajás		Vila Feitosa	
	AMR-137A	AMR-140	AMR-149	AMR-116	AMR-85A	ARC-109	ARC-147
Facies	BHSG	BHMzG	HBMzG	BHSG	HSG	HBSG	BHMzG
Group	2	2	1	1	2	C	1
Pressures (MPa)							
Al Total	2.1	2.4 - 2.6	2.0 - 2.1	2.1	2.3 - 2.5	2.1 - 2.3	2.3 - 2.4
Johnson and Rutherford (1989)	530	670 - 750	500 - 540	540,0	630 - 710	540 - 630	630 - 670
Blundy and Holland (1990)	698	870 - 950	680 - 740	698	780 - 900	700 - 780	802 - 870
Schmidt (1992)	694	860 - 930	670 - 730	694	770 - 890	690 - 780	810 - 860
Anderson and Smith (1995)	660	800 - 890	620 - 660	660	750 - 850	660 - 750	750 - 800
Ridolfi et al. (2010)	394	606-808	341- 394	394	525 - 700	394-525	525 - 606
Temperature (°C)							
Zr in ppm (Feio et al, 2012)	502	387	462	393	499	487	356
P ₂ O ₅ %w.t (Feio et al, 2012)	0.04	0.04	0.05	0.03	0.04	0.09	0.09
Zircon (Watson and Harrison, 1983)	897	870	890	868	893	886	854
Apatite (Harrison and Watson 1984)	643	640	654	620	641	702	704
Ridolfi et al. (2010)	841 - 872	882 - 898	843 - 883	831 - 855	867 - 910	851 - 878	877 - 889

Blundy and Holland (1990): P (kbar) = 5.03 Al_t - 3.53; Schmidt (1992): P (± 0,6 kbar) = 4.76 Al_t - 3.01; Johnson and Rutherford (1989): P (±0,5 kbar) = 4.23 Al_t - 3.46. BHSG = Biotite-hornblende-syenogranite; BHMzG = Biotite-hornblende-monzogranite; HSG = hornblende-syenogranite; HBSG = hornblende-biotite-syenogranite.

2.7.1.2 Pressure

According to Hammarstron and Zen (1986), the total aluminum content of hornblendes from calc-alkaline rocks increases with pressure, if the paragenesis is constituted by amphibole, biotite, plagioclase, alkali feldspar, quartz, titanite, and Fe-Ti oxides (Hollister et al., 1987; Johnson and Rutherford 1989; Thomas and Ernst 1990; Schmidt, 1992; Anderson and Smith, 1995). The Al-in hornblende geobarometer was proposed to estimate the pressure at the end of crystallization of intermediate and silicic plutons, which should correspond to the pressure of their emplacement or approach it (Anderson and Smith, 1995; Anderson et al., 2008). The geobarometer is based on the assumption that the mentioned solid phases are in equilibrium at the end of the magma crystallization with residual liquid and possibly a volatile phase.

Despite its subalkaline character, the Planalto Suite has the paragenesis considered ideal for the application of geobarometer models (Hammarstrom & Zen 1986; Hollister et al 1987), except that its plagioclase ($An < 25$) is more sodic than those found in the typical calc-alkaline granitoids for which the geobarometer was initially proposed ($\sim An_{25-35}$; Anderson and Smith, 1995). According to Anderson and Smith (1995, p. 556), the more sodic composition of the plagioclase should cause lowering of Al in hornblende and derived pressures.

Among several models, the geobarometers of Johnson and Rutherford (1989), Blundy and Holland (1990) and Schmidt (1992) will be considered here because their models resulted of experimental calibration. According to Blundy and Holland (1990), Al change in the amphibole occurs through pressure and temperature changes, whereas Johnson and Rutherford (1989) and Schmidt (1992) considered only pressure as responsible for changes in Al content in amphibole. Employing the geobarometer equations proposed by Blundy and Holland (1990) and Smith (1992), the pressures for the emplacement of the Planalto Suite are similar and range from 950 to 650 MPa. Using that of Johnson and Rutherford (1989), the pressures vary from 750 to 530 MPa and tend to be lower than those indicated by the two other mentioned geobarometers (Table 2.6). Besides, all three employed geobarometers provided very similar pressures for the studied plutons either for that of the type area, as for those of Vila Feitosa and eastern of Canaã dos Carajás suggesting that pressures imposed during the crystallization of the plutons of the Planalto Suite were similar, regardless of pluton location.

Anderson and Smith (1995), Anderson et al. (2008), and Erdmann et al. (2014) have also emphasized the significant effect of temperature in the Al in amphibole geobarometer and the need to introduce this variable in the equation for pressure calculation. Accordingly, Anderson and Smith (1995) have proposed the equation below to calculate the pressure:

$$P \text{ (kbar)} = 4.76Al - 3.01 - \{[(T^{\circ}\text{C} - 675)/85] * [0.530Al + 0.005294 (T^{\circ}\text{C} - 675)]\}$$

Although the core and rim of hornblende crystals of the Planalto Suite have similar compositions (Figure 2.10; Table 2.1), the pressure was estimated using only the composition of hornblende rims. If the temperature effect is not considered, the plot $^{IV}\text{Al} + ^{VI}\text{Al}$ vs. $(\text{Fe}/(\text{Fe} + \text{Mg}))$ in hornblende, based in Anderson and Smith (1995, their Figure 10), indicate that the Planalto granites crystallized at pressures ≥ 700 MPa. However, these pressure estimates do not consider the temperature effect that could be evaluated employing the equation proposed by Anderson and Smith (1995) on the condition that the temperature could be determined or at least estimated. As discussed in the previous section, the zircon geothermometer and the equation proposed by Ridolfi et al. (2010) indicate elevated temperatures (around 910-850 °C) for the liquidus of the Planalto granites. However, those temperatures should not be employed for the pressure calculation, because in near liquidus temperatures the equilibrium assemblage necessary for the use of the geobarometer was certainly not present. Another restriction is related to the inadequacy of the available geobarometers for temperatures higher than 800 °C because those temperatures are far outside the experimental calibration (Anderson and Smith, 1995, p. 554). Finally, it is not sure that the amphibole compositions of the Planalto granites at the end of their crystallization were not modified by deformational processes.

Leaving behind these important drawbacks and accepting a temperature of 700 °C for the near solidus of the Planalto granites, the equation with temperature effect correction of Anderson and Smith (1995) indicates a pressure range of 890-620 MPa for the magma emplacement. If these estimates are consistent, the pressures for the Planalto magma emplacement would be relatively high and would superpose with the lower values indicated by the geobarometers without temperature correction.

Taking in account the fact that the use of the Al-in hornblende geobarometers for pressure calculation in the case of low- $f\text{O}_2$ granites, such as those of the Planalto Suite, is not recommended by Anderson and Smith (1995), because none of the calibrations have employed hornblendes with $\text{Fe}/(\text{Fe} + \text{Mg})$ above 0.65 or have been conducted at $f\text{O}_2$ near or below FMQ, and the possibility of re-equilibration of amphibole, we can try to estimate the pressure for the Planalto Suite using independent field, petrological and geochemical

evidence. Previous works indicate that the Planalto magmas derived from deep-seated granulitic or charnockitic sources (Feio et al., 2012) and the pressure at the source can be estimated in 700 to 900 MPa. On the other hand, the Planalto granites were affected by ductile deformation and show penetrative foliation and local lineation, as well as strong recrystallization. The granite magmas should be largely crystallized at their emplacement to be able to register the deformational stress. These features are indicative of the emplacement of the plutons in crustal depths equivalents at least to those of the mesozone corresponding possibly to a pressure of 300 to 500 MPa. We can admit also that hornblende was largely crystallized at the moment of the granite emplacement, as suggested by the absence of zoning and similar compositions of crystals core and rim (Figure 2.10). It can be concluded that pressures of 700 to 900 MPa at the magma source and of 300 to 500 MPa at the emplacement level are suitable for the Planalto Suite. We admit that the estimated pressures are not demonstrated but we believe that they are consistent with the general characteristics of the Planalto Suite.

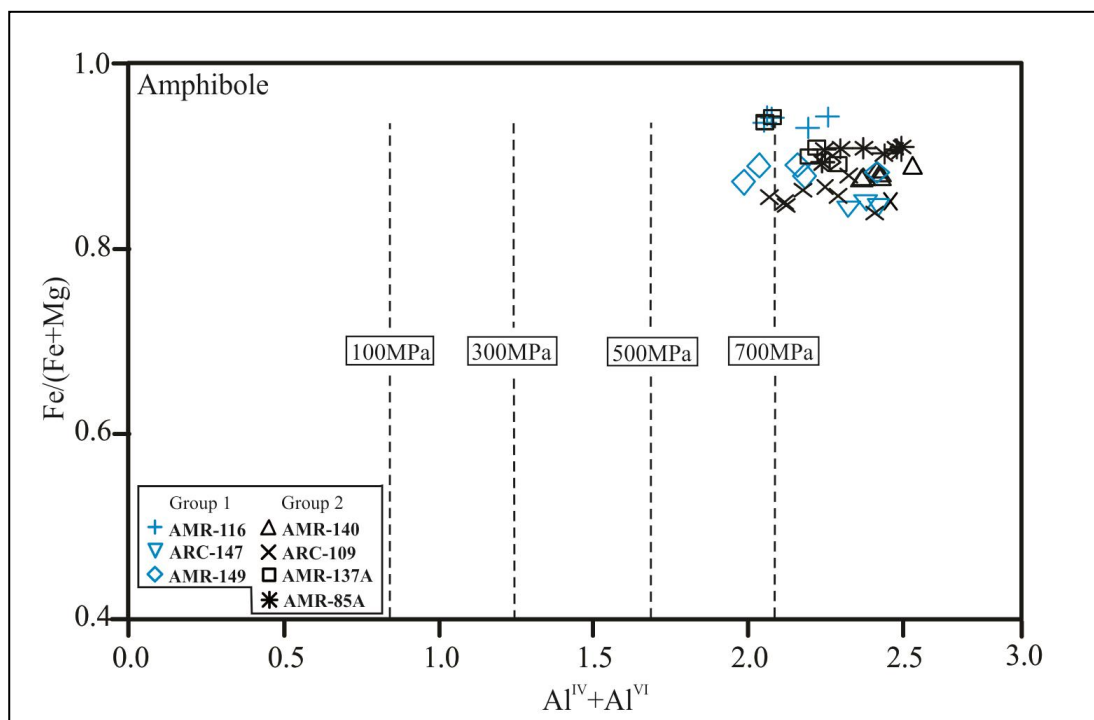


Figure 2.10 - Fe/(Fe+Mg) x Al diagram for amphiboles of the Planalto Suite (isobars from Anderson and Smith, 1995, based on Schmidt, 1992) showing possible crystallization pressure ranges of amphibole without temperature correction (see text).

2.7.1.3 Oxygen fugacity (fO_2)

Oxygen fugacity is the main physical parameter that controls the formation of iron-titanium oxide minerals. Experimental studies show that the oxygen fugacity is strongly

dependent of temperature, but can be also modified through variations of pressure, presence of water and volatiles (Clowe et al., 1988; Carmichael 1991; Frost, 1991; Frost and Lindsley, 1991; Moore et al. 1995; Anderson and Smith 1995; Baker and Rutherford 1996; Gaillard et al., 2001).

The Planalto Suite has high $\text{FeOt}/(\text{FeOt}+\text{MgO})$ ratios in whole rock (generally between 0.88 and 0.99; Feio et al., 2012, their Table 1; cf. Supplementary data, Table S3). A similar picture is observed in amphibole and biotite which show high $\text{Fe}/(\text{Fe}+\text{Mg})$ values, varying respectively from 0.84 and 0.94 and 0.75 and 0.91 (Tables 2.1 and 2.2). When the compositions of Planalto amphibole and biotite are plotted respectively in the diagrams $^{\text{IV}}\text{Al} - \text{Fe}/(\text{Fe}+\text{Mg})$ and $^{\text{IV}}\text{Al} + ^{\text{VI}}\text{Al} - \text{Fe}/(\text{Fe}+\text{Mg})$ (Figures 2.11a, b) that show the fields defined for the Proterozoic anorogenic granites of Laurentia (Anderson and Bender, 1989; Anderson et al., 2008), it is indicated that the Planalto granites crystallized under low $f\text{O}_2$ conditions, generally compatible with those prevalent for granites of the ilmenite series (Ishihara, 1981).

Wones and Eugster (1965) studied experimentally the stability of biotite at different oxygen fugacity conditions. A direct comparison between the data obtained by Wones and Eugster (1965) and the biotite composition in the Planalto granites is limited because we do not have control of the $\text{Fe}^{+3}/\text{Fe}^{+2}$ ratios in our analyzed biotites and the experimental pressures (100 to 200 MPa) are significantly lower than those assumed for the studied granites. However, if we forget the mentioned handicaps and admit that biotite crystallized in a temperature interval of 800 to 700 °C in the Planalto granites, the $f\text{O}_2$ conditions indicated by the $\text{Fe}/\text{Fe}+\text{Mg}$ ratios in their biotites should be situated around the FMQ buffer (Wones and Eugster, 1965, their Figure 5). The evidence given by mineral chemistry data is entirely consistent with the low MS values and the presence of ilmenite as the sole significant iron-titanium oxide mineral in the Planalto Group 1. However, there is some ambiguity in the Group 2 granites, which rocks have relatively high MS values and contain magnetite associated with ilmenite. This characteristic is consistent with magnetite series granites (Ishihara, 1981) and suggests a possible oxidized character. However, the high $\text{Fe}/(\text{Fe}+\text{Mg})$ in whole rock, amphibole, and biotite, is indicative of crystallization under low $f\text{O}_2$. It is implicit in this reasoning the assumption that magnetite was a magmatic phase re-equilibrated during cooling as indicated by textural evidence (Figures 2.6c, d).

With respect to the $f\text{O}_2$ behavior along the crystallization of the granites of the Planalto Suite, it looks clear that the Group 1 granites evolved in the ilmenite stability field and out of the equilibrium field of magnetite, thus below the FMQ buffer (Figure 2.12). Contrarily, two

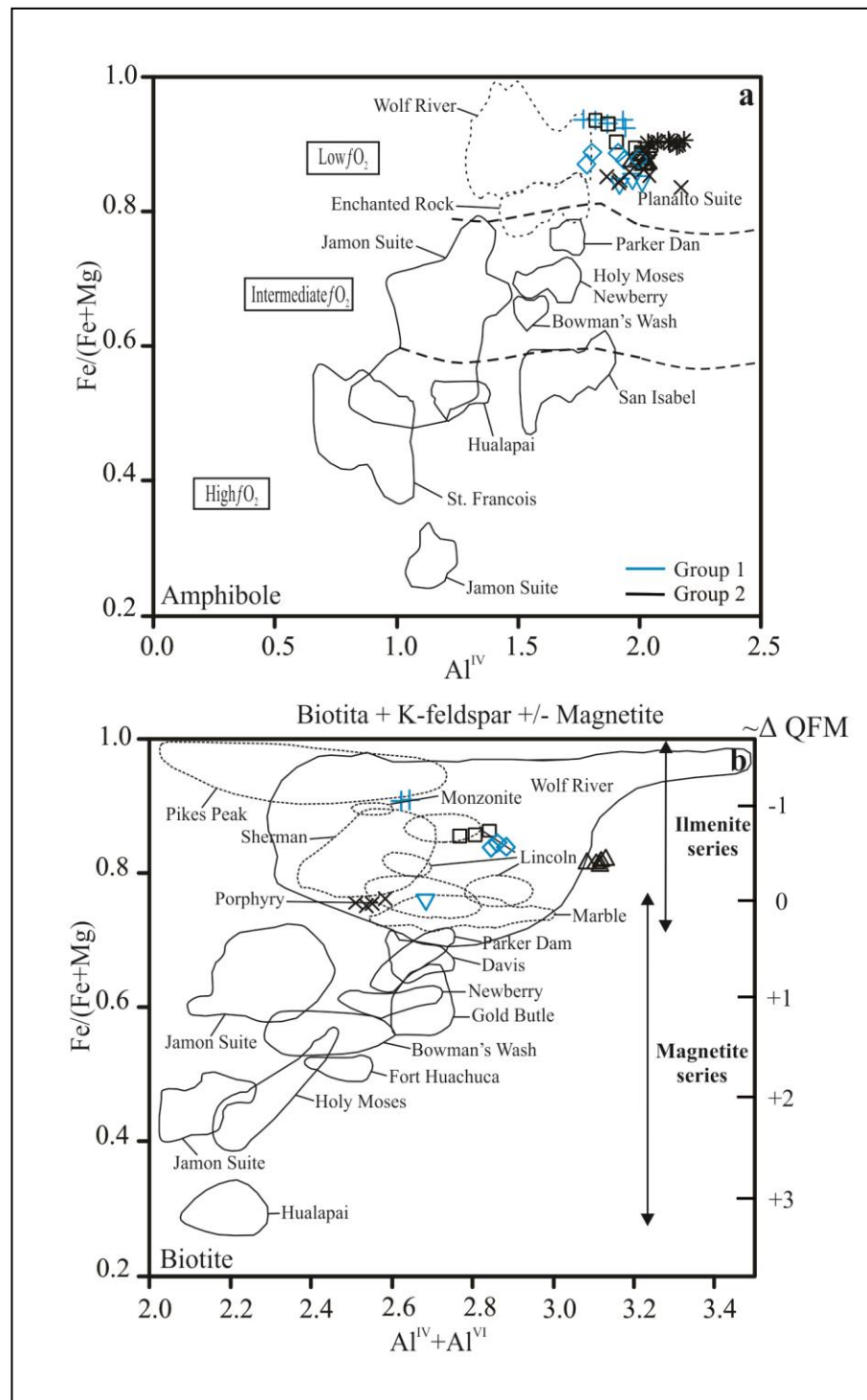


Figure 2.11 - Compositional variation of amphibole and biotite of the Planalto Suite; a) Fe/(Fe+Mg) ratio versus Al^{IV} diagram showing the low fO_2 character of Planalto amphibole (Low, Intermediate and High fO_2 fields according to Anderson and Smith, 1995); amphiboles of A-type granites of Carajás (Jamon Suite; Dall'Agnol et al., 2005; Rämö et al., 2002) and mid-Proterozoic granites of the United States (Anderson and Smith, 1995; Frost et al., 1999) are shown for comparison; b) Fe/(Fe+Mg) versus Al^{IV} + Al^{VI} diagram showing the biotite composition of Planalto granites and those from A-type granites of Carajás (Jamon Suite; Dall'Agnol et al., 2005) and United States (Anderson and Bender, 1989; Barker et al., 1975; Pikes Peak; Anderson et al., 2008; Wolf River and the ranges of ilmenite series and magnetite series granites; Frost et al., 1999; Sherman batholith).

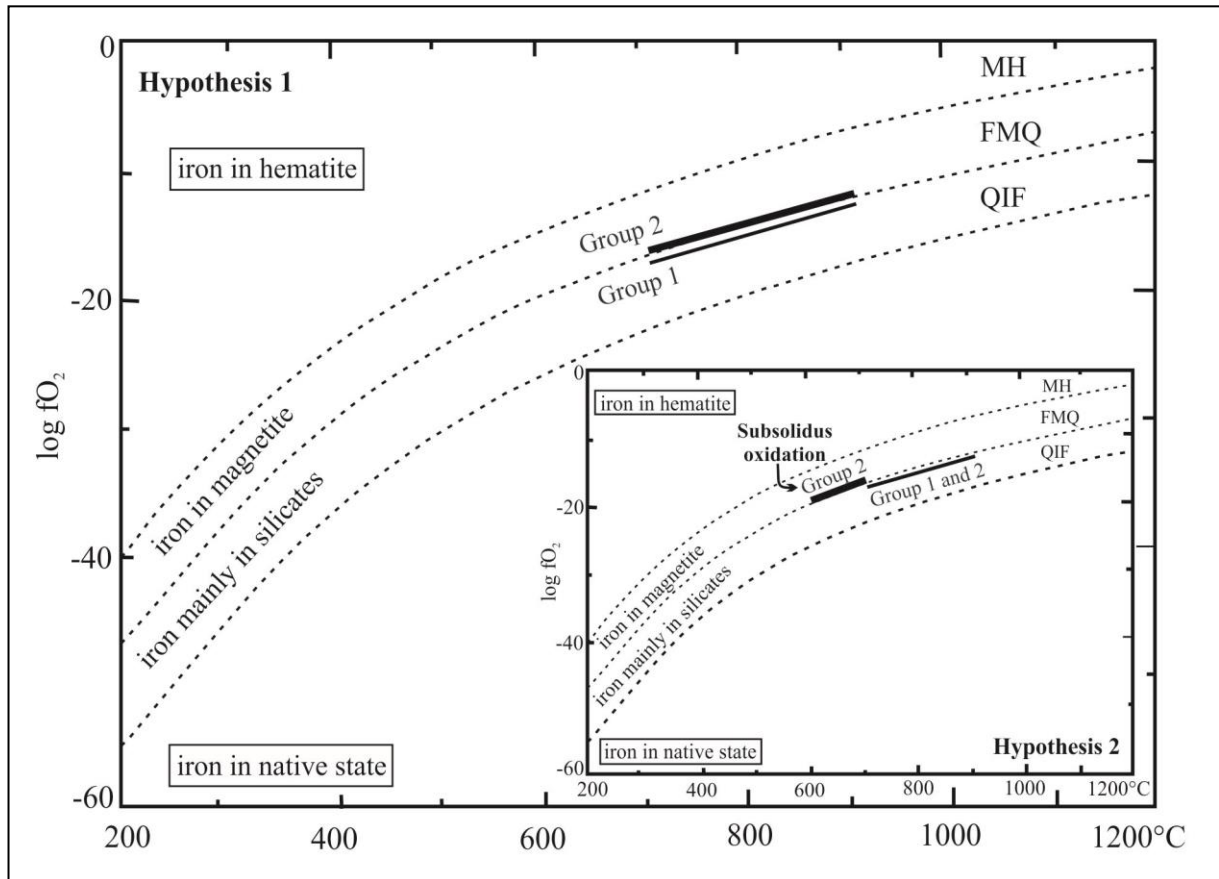


Figure 2.12 - Diagram T vs $\log fO_2$ showing possible temperature intervals of formation and estimated fO_2 conditions for the Planalto Suite granites. Curves of the main stability buffers and different Fe phases in function of the oxidation stage in the Fe-Si-O system based on Frost (1991). Grayish lines illustrate the evolution of the Planalto granites of Groups 1 and 2 in two different hypotheses (see text). QIF = quartz-ilmenite-fayalite; FMQ = fayalite-magnetite-quartz; MH = magnetite-hematite.

hypotheses can be envisaged to explain the behavior of the Group 2 granites that contain magnetite. First, assuming that magnetite was a primary magmatic phase, its occurrence can be due to the fact that the Group 2 granites would evolve in relatively more oxidizing conditions than those of the Group 1, on or slightly above FMQ buffer, making possible magnetite crystallization (Figure 2.12; A similar picture was envisaged for the Mesoproterozoic Sherman and Lincoln A-type granites; Frost et al., 2000, their Fig. 16).

Despite the occurrence of magnetite, the overall reducing conditions remain in the magma and this could explain the elevated $Fe/(Fe+Mg)$ found in amphibole and biotite and the high $FeOt/(FeOt+MgO)$ in whole rock. Contrarily to the common sense that magnetite-bearing granites are necessarily oxidized, as suggested by the classical classification of Ishihara (1981), the presence of magnetite in granites is not incompatible with reduced character (cf. Anderson and Smith, 1995; Anderson et al., 2008; Dall'Agnol and Oliveira,

2007). The second hypothesis is based on the assumption that magnetite was formed in the post-magmatic stage. In this case, it could be supposed that the original Planalto magma evolved in reducing conditions below FMQ, but during the hydrothermal stage, the Group 2 granites would be submitted to more oxidizing conditions, passing to evolve on conditions coincident with FMQ or slightly above it (Figure 2.12). The first proposed hypothesis for the fO_2 evolution in the Planalto granites is preferred by the authors.

2.7.1.4 Water content

Petrographic data shows that calcic amphibole is one of the main mafic phase found in the Planalto granites. It is possible that amphibole was re-equilibrated during the evolution of the Planalto Suite, but there is no evidence that it could be formed in subsolidus conditions. On the other hand, experimental data in granitic systems show that calcic amphibole crystallization is extremely dependent on the H_2O content in magma, as well as of the CaO content in the system. A minimum water content of 4 wt% at 200 to 400 MPa is needed to stabilize amphibole in magmatic temperatures (Naney, 1983; Dall'Agnol et al., 1999; Klimm et al., 2003; Bogaerts et al., 2006) and 5 wt% of water at 400 MPa or 7 to 9 wt% of water at 960 MPa are required for the amphibole to be the silicic liquidus phase and to prevent pyroxene formation (Naney, 1983; Prouteau and Scaillet, 2003; Oliveira et al., 2010). Clinopyroxene relicts included in amphibole are locally present in the Planalto granites (Feio et al., 2012), but clinopyroxene is extremely rare as demonstrated by its absence in all samples submitted to modal analyses (Table S1). This suggests that the stability field of clinopyroxene was rarely reached and, if it was stable in the early magmatic stage, it should have reacted completely during cooling (Naney, 1983; Dall'Agnol et al., 1999).

Ridolfi et al. (2010) and Ridolfi and Renzulli (2012) published chemometric equations to estimate, between other crystallization parameters, the melt H_2O contents. Erdmann et al. (2014) have made an evaluation of the reliability of the calibrations proposed by those authors and have concluded that: “*Calculated melt H_2O contents are incorrect estimates, increasing from felsic to mafic magmas and for amphibole crystallized at low to high temperature*” (Erdmann et al., 2014, p. 1016).

According to Frost and Frost (2008), hornblende-biotite granites can be produced from hydrated residual melt enriched in fluids derived from charnockitic evolved magmas. The structural features of the Planalto Suite granites and their close association with charnockitic rocks were emphasized by Feio et al. (2012). They argued that the Planalto Suite could

correspond to hydrated granites of a reduced charnockitic series derived from tholeiitic sources.

It is concluded that the Planalto granites derived from magmas with more than 4 wt % of H₂O and, depending of the assumed pressure of crystallization, possibly even more than 7 wt % of H₂O as indicated by the rarity or absence of pyroxene in the granite. Notwithstanding, some contrast in composition between the Paleoproterozoic Jamon granite and the Planalto Suite, the experimental studies in the Jamon granite (Dall'Agnol et al., 1999) suggest that, in reduced conditions such those prevalent during the crystallization of the Planalto Suite, the amphibole will remain stable in the magma until the end of the crystallization and will not react with the residual liquid. The textures of the Planalto granites indicate that effectively the amphibole was preserved of peritectic reactions during the magma evolution.

2.7.2 Comparison between the Planalto Suite and similar granites

A-type or ferroan (*sensu* Frost and Frost, 2008) granites are formed mostly in non-compressional tectonic settings and were originally defined as anorogenic granites (Loiselle and Wones, 1979) but their occurrence in post-collisional or post-orogenic settings was also demonstrated (Sylvester, 1989; Whalen et al., 1987; Eby, 1992; Nardi and Bittencourt, 2009) and it is nowadays admitted without restrictions (*cf.* Dall'Agnol et al., 2012). A-type granites are more abundant in the late Paleoproterozoic and Mesoproterozoic and rare in the early Proterozoic and Archean (*cf.* Emslie, 1991; Rämö and Haapala, 1995; Dall'Agnol et al., 2012 and references therein; see Moore et al., 1993, for an example of Neoproterozoic rapakivi, A-type granites).

2.7.2.1 Comparison between the Planalto Suite and similar granites of the Carajás Province

On the basis of the affinity of the Planalto Suite with A-type granites and its relationship with charnockitic assemblages, it is interesting to compare the mineralogical characteristics and crystallization parameters defined in the present study for that suite with those observed in similar granites. Some of the few examples in the literature of Archean ferroan granites are found in the Carajás Province and correspond to the Planalto and Vila Jussara suites, the Estrela Granitic Complex, and the Serra do Rabo and Igarapé Gelado granites (Feio et al., 2012; Silva et al., 2014; Barros et al., 2009; Sardinha et al., 2006). Besides their Archean age, these granites differ of most A-type granites by the fact that they are intensely deformed, foliated granites (*cf.* Barros et al., 1997, 2009, and Tavares, 2015, for different hypothesis to

explain this feature). Paleoproterozoic, A-type granites are also abundant in the Carajás Province and their comparison with the Planalto Suite is also relevant. For this reason, among the granites of the Carajás Province, we have taken for comparison: the Archean Estrela Granitic Complex and Serra do Rabo Granite (Barros et al., 2009; Sardinha et al., 2006) and the Paleoproterozoic Jamon and Cigano A-type granites (Dall'Agnol et al., 1999, 2005).

The Planalto Suite and the Estrela Granitic Complex are similar in geochemistry and mineralogy (despite its modal composition enriched in alkali feldspar compared to the Planalto and Estrela granites, the same is true for the Serra do Rabo granite, not shown in the figures; Sardinha et al., 2006; Barros et al., 2009). Both have hastingsite associated with annitic biotite as the main mafic minerals (Figure 2.13). The amphibole and the mica have high total Al content and very low $Mg/(Mg+Fe^{2+})$ ratio. In the Planalto granites, pyroxenes are generally absent but relicts of clinopyroxene occur in some varieties (Feio et al., 2012). In the Estrela complex, the general picture is similar but a subordinated clinopyroxene-amphibole monzogranite was described (Barros et al., 1997, 2009). The main iron oxide mineral is ilmenite. Magnetite is found only in some facies as exemplified by the Group 2 granites of the Planalto Suite. The petrogenetic model proposed for the Planalto (Feio et al., 2012) and Estrela (Barros et al., 2009) granites involves high temperature partial melting of granulitic sources of tholeiitic character (Feio et al., 2012). Their magmas should be generated at pressures of 700 to 900 MPa, have high liquidus temperatures (near 900 °C), evolved in reduced conditions (below FMQ or on to slightly above FMQ) and were probably emplaced at pressures of 300 to 500 MPa (in the case of the Estrela Complex pressures < 380 MPa were assumed by Barros et al., 2001).

On the other hand, the Paleoproterozoic anorogenic A-type granites of the Carajás Province display some contrasts in mineralogy when compared with the Planalto granites. The former are represented by the oxidized Jamon Suite which amphiboles are ferro-edenite and edenite and by the reduced Cigano Granite of the Serra dos Carajás Suite, which amphibole is hastingsite (Dall'Agnol et al., 2005). In the dominant monzogranite varieties of the Jamon Granite, $Fe/(Fe+Mg)$ ratios vary between 0.47 and 0.73 in the amphiboles, and between 0.6 and 0.7 in the biotites (Figures 2.13a, b). A different picture is observed in the Cigano Granite where amphibole and biotite $Fe/(Fe+Mg)$ ratios range respectively from 0.85 to 0.94, and from 0.78 to 0.88. For the Jamon pluton, a pressure of 320 ± 70 MPa for the emplacement, a liquidus temperature of ca. 870 °C and an oxygen fugacity near NNO were assumed (Dall'Agnol et al., 1999). The liquidus temperature of the magma is not substantially distinct of that estimated for the Planalto Suite, but the pressure of emplacement is

comparatively lower and there is a strong contrast in the oxygen fugacity during magma evolution. On contrast, the Cigano Granite evolved in reducing conditions and approaches the Planalto Suite in this respect and also in other crystallization parameters. However, the Al^{IV} contents in its amphibole tend to be lower and total Al in its biotite is lower compared to the Planalto granites, which possibly implies lower pressure of emplacement.

2.7.2.2 Comparison between the Planalto Suite and similar granites of other provinces in the world

In the international scenario, we have chosen for comparison the Neoproterozoic, post-collisional magmatism of the hornblende-biotite granite (HBG) event and the spatially associated Anorthosite – Mangerite – Charnockite (AMC) Suite of the Rogaland Anorthosite Province in southern Norway (Bogaerts et al., 2003, 2006; Vander Auwera et al., 2014); the Mesoproterozoic Wolf River batholith of USA (Anderson, 1980; Anderson and Smith, 1995) and Finnish rapakivi granites (Rämö and Haapala, 1995; Elliot, 2001; Kosunen, 2004); and the Matok pluton of the Limpopo Belt, South Africa (Rapopo, 2010; Laurent et al., 2014; Rajesh et al., 2014).

The HBG suite is represented in our comparison by the Lyngdal granodiorite and associated granitoids (Tranevåg massif). The HBG granitoids commonly display a syn-magmatic foliation and its amphibole is classified as magnesio-hastingsite, hastingsite, edenite and Fe-edenite with Fe/(Fe+Mg) varying between 0.58 and 0.44. Biotite is dominantly magnesian with Fe/(Fe+Mg) between 0.36 and 0.51. Al-in amphibole geobarometers indicate pressures of emplacement between 530 and 400 MPa for the Lingdal massif and $P < 360$ MPa for the Tranevåg one. The magmas evolved at fO_2 conditions near or above NNO (Bogaerts et al., 2003).

The estimated pressures for HBG emplacement are similar to those of the Planalto granites but they differ markedly in the fO_2 conditions during magmatic evolution, oxidizing in the HBG, reduced in the studied granites. On the other hand, the AMC Suite of the same province is reduced and in this respect similar to the Planalto granite (Vander Auwera et al., 2014). The Farsund pluton is a peculiar intrusion of the Rogaland Province because it is composed of granitic rocks similar to HBG and charnockites akin to the AMC suite (Vander Auwera et al., 2014). The Fe/(Fe+Mg) of the amphibole and biotite found in these two kind of rocks show significant differences. Besides, the amphiboles and biotite of the granitoids of the Rogaland Province have lower Al total contents when compared with those of Planalto Suite and Estrela Complex (Figures 2.13a, b).

The amphibole and biotite of Wolf River batholith show high Fe/(Fe+Mg) (Figure 2.13a, b) indicating its crystallization at low fO_2 (Anderson and Smith, 1995; Anderson et al., 2008). The Mesoproterozoic rapakivi granites of Finland (not represented in Figure 2.13) also derived from reduced to moderately reduced magmas (Rämö and Haapala, 1995), as exemplified by the Wiborg batholith (Elliot, 2001) and Bodom and Obbnäs plutons (Kosunen, 2004). The Al-in-amphibole geobarometer without temperature correction indicated pressures around 500 MPa for the Wolf River batholith emplacement (Anderson and Smith, 1995) and in the range between 250-540 MPa for the Wiborg batholith (Elliott, 2001). However, geological evidence suggests a lower pressure for the emplacement of Finnish rapakivi granites (Rämö and Haapala, 1995) and Anderson and Smith (1995) argued that the Wolf River pressure was overestimated by a factor of two or three times. They inferred that the low Mg content and the low Fe³⁺ relative to total Fe in hornblende are the cause of the high Al content in amphibole. The amphiboles of Planalto and Estrela granites are enriched in Al compared to Wolf River but the significance of this compositional aspect is still open to discussion.

The Neoproterozoic (ca. 2.67 Ga) Matok pluton was emplaced in the Southern Marginal Zone of the Limpopo Belt, near its border with the Kaapvaal Craton (Pietersburg Block). The Limpopo Belt is generally admitted to result from the tectonic collision between the Zimbabwe and Kaapvaal cratons (Rapopo, 2010; Laurent et al., 2014). However, a subduction related setting was also proposed for its southern margin (Rajesh, 2014). The age and the tectonic setting of the Matok intrusion are similar to those of the Planalto Suite. That pluton is an interesting example of intrusion composed of two large groups of rocks, hypersthene- and hypersthene-clinopyroxene-bearing granitoids (s.l. charnockites) and pyroxene-free granitoids, both groups ranging from diorites through granodiorites to granites (Rapopo, 2010; Laurent et al., 2014, and references therein). Both groups were emplaced contemporaneously and have calc-alkaline geochemical signature. The charnockitic group crystallized from a magma that was relatively depleted in water compared to that of the pyroxene-free granitoids for which a water content > 5% was estimated (Laurent et al., 2014). There are field and geochemical evidence of mingling between these magmas. Besides pyroxenes, the charnockitic rocks contain late-crystallized amphibole and biotite; magnetite (1-3 % modal), apatite, ilmenite, and zircon are the main accessory minerals.

The pyroxene-free granitoids have similar mineral assemblages but the modal abundances are different. Biotite is the main mafic mineral, associated with variable modal proportions of amphibole, magmatic epidote, titanite, zircon, ilmenite, and apatite. Magnetite

is also present but its modal contents are lower than in the charnockitic rocks. Fe/(Fe+Mg) ratios vary generally in the ranges 0.7 - 0.4 (in the amphiboles) and 0.6-0.2 (in the biotites) in the pyroxene-free granitoids and charnockitic rocks. The pistacite molecule (26-33 %) content in analysed crystals of magmatic epidote is compatible with an igneous origin (Rapopo, 2010). According to Rapopo (2010), both groups of rocks from the Matok pluton crystallized initially in similar and oxidizing condition but the pyroxene-free granitoids magma ended its crystallization under relatively more oxidizing conditions. On the other hand, Laurent et al. (2014) suggested that the pyroxene-bearing granitoids crystallized at reduced conditions, an interpretation that is difficult to reconcile with the amphibole and biotite compositions observed in the pluton (cf. Figures 2.13a, b). The latter authors have also estimated that fO_2 was above NNO during the crystallization of the pyroxene-free granitoids. The pressure of emplacement was estimated using the Al-in-amphibole geobarometer modified by Anderson and Smith (1995) resulting in pressures between 860 and 330 MPa for a temperature range of 680-757 °C (Rapopo, 2010). The pyroxene-free granitoids have lower Al_t in amphibole compared to the charnockitic rocks and this implies slightly lower pressure estimates.

Of all examples selected for comparison with the Planalto granites, the Matok pluton is the one that most approaches the studied granites in tectonic setting and age. It has also in common with the Planalto granites the Al-enriched composition of its amphibole and biotite (Figures 2.13a, b). Both magmas were formed at high temperatures and could result from crustal melting of the deep crust (Rapopo, 2010; Feio et al., 2012) or, alternatively, in the case of Matok, from mixing between two distinct magmas derived from mantle sources (Laurent et al., 2014) or from subduction-related magmas (Rajesh, 2014). However, the pressures of emplacement estimated for the Matok pluton tend to be a little higher than those for the Planalto plutons and there is a strong contrast in the oxygen fugacity conditions during magma evolution: intermediate to high in the case of Matok, low for Planalto. Another contrast is related to the water content in the magma, relatively low in the charnockitic rocks of Matok, increasing in the pyroxene-free granitoids of the same pluton and comparatively higher in the Planalto Suite in order to explain the presence of hornblende and the scarcity or absence of pyroxenes in it. The contrasts in fO_2 between these granitoids can be probably explained by the geochemical signature and sources admitted for the Matok pluton and Planalto Suite. In fact, independent of the nature of the Matok sources, it is composed of oxidized calc-alkaline granitoids, transitional from ferroan to magnesian (Laurent et al., 2014; Rajesh, 2014), whereas the Planalto granites are reduced ferroan granites and their magmas possibly derived from Mesoproterozoic granulitic rocks of tholeiitic nature (Feio et al., 2012).

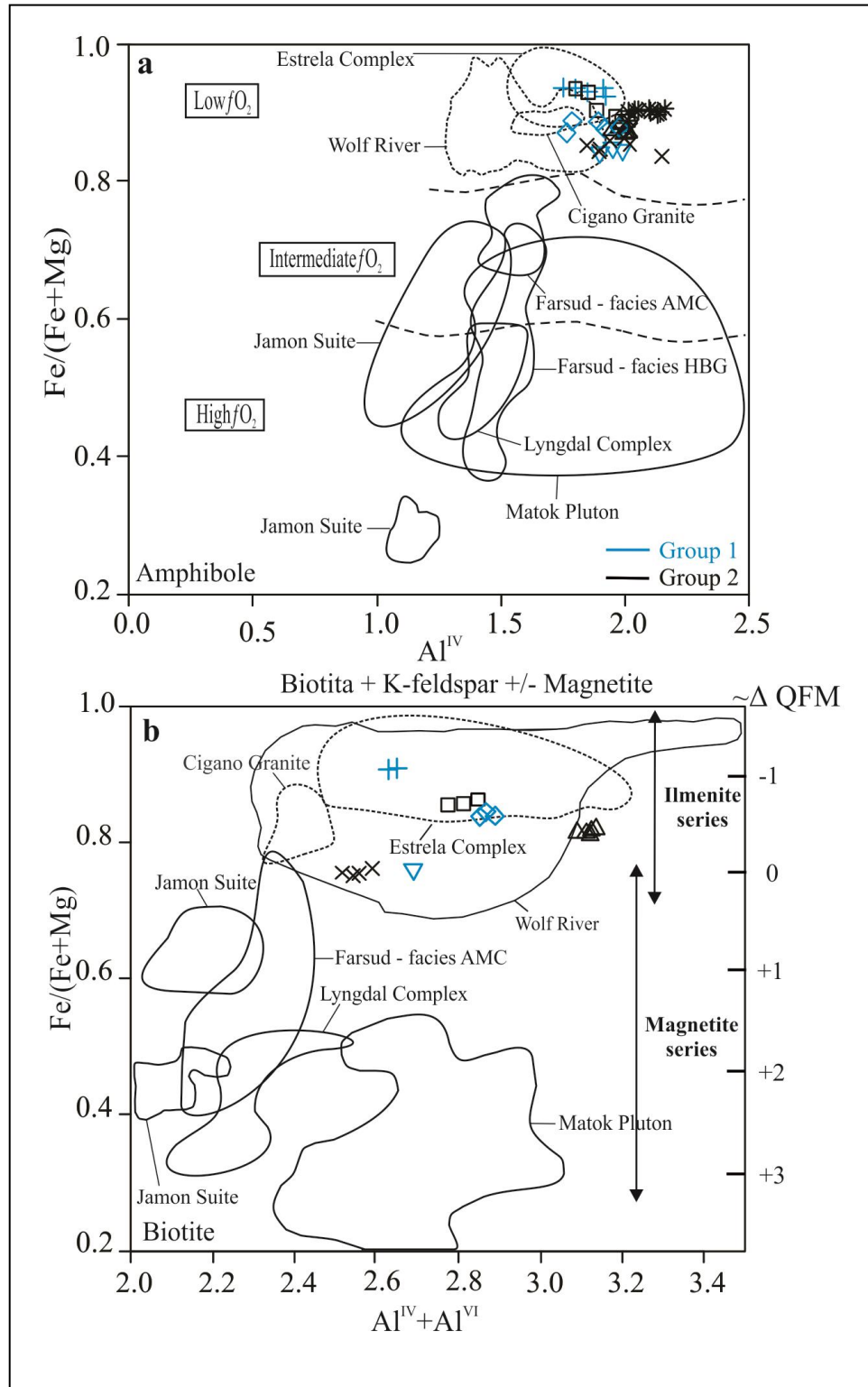


Figure 2.13 - Comparison between amphibole and biotite from the Planalto granites and similar granites. a) $\text{Fe}/(\text{Fe}+\text{Mg}) \times \text{Al}^{\text{IV}}$ diagram showing the distribution of Planalto amphibole and the fields of amphibole composition of granites selected for comparison; b) $\text{Fe}/(\text{Fe}+\text{Mg})$ vs $\text{Al}^{\text{IV}} + \text{Al}^{\text{VI}}$ diagram comparing the distribution of Planalto biotite with that of similar ferroan or A-type granites. In Figure 13a, Low, Intermediate and High $f\text{O}_2$ fields according to Anderson and Smith (1995); in Figure 13b, ilmenite series and magnetite series granites according to Anderson et al. (2008). The sources of the data employed in the comparison are given in the text.

The higher pressure of emplacement suggested for the Matok pluton compared to the Planalto plutons and Estrela Complex is consistent with the large volume of charnockitic rocks in the former, a feature that is only observed in the Planalto Suite in the domain of the Pium charnockites. Charnockitic rocks are absent in most of the Planalto plutons and in the similar Neoproterozoic granites of Carajás charnockitic. This can be interpreted as evidence that the Planalto granites are hydrated varieties of a charnockitic assemblage that were emplaced at higher crustal levels currently exposed by the erosion. In the Limpopo Belt compared to the Carajás Province, a deeper erosion level would be attained exposing the charnockitic assemblages.

It is concluded that the Planalto Suite and similar Neoproterozoic granites of the Carajás Province differ in mineralogical characteristics and crystallization parameters of some classic examples of A-type granites, e.g. the Paleoproterozoic anorogenic granites of Carajás, the Mesoproterozoic rapakivi granites of Central USA and Finland, the HBG Suite and AMC Suite of Southern Norway. On the other hand, despite some contrasts, the Planalto granites are akin to the Fe-K and Mg-K granitoids of the Limpopo Belt, as exemplified by the Matok granitoids. This can be seen as evidence that the tectonic setting of Carajás and Limpopo exerted strong influence in the nature of the granitoid magmas formed during the Neoproterozoic. The differences between Planalto and Matok can be ascribed to the differences in their magma sources.

2.8 CONCLUSIONS

The Neoproterozoic Planalto Suite is composed of monzogranite, syenogranite, and alkali feldspar granite with variable modal contents of biotite and amphibole. Clinopyroxene is absent or occur locally as relic crystals enveloped by amphibole.

Two groups have been distinguished on the basis of the magnetic behavior and iron-titanium oxide minerals: the Group 1 display low magnetic susceptibility values ($MS \leq 0.6247 \times 10^{-3}$ SI), and ilmenite is the only significant iron-oxide mineral; in the Group 2, MS values are moderate ($MS \geq 0.8036 \times 10^{-3}$), and magnetite is associated with ilmenite.

The mineral chemistry data reveal that amphibole varies from potassian-hastingsite to chloro-potassian-hastingsite and biotite approaches annite in composition. Amphibole and mica show high Fe/(Fe+Mg) (0.84 to 0.94 and 0.75 to 0.91, respectively) and are relatively enriched in Al compared to the same minerals of other ferroan granites. Plagioclase composition is generally oligoclase ($An_{23}-An_{11}$) and similar in the porphyroclasts and fine

crystals of the recrystallized matrix. Neoformed grains of albitic composition were also observed.

Magnetic petrology studies indicate that the Planalto Group 1 derived from a reduced magma that evolved in oxygen fugacity below FMQ, whereas the Group 2 crystallized in a little more oxidizing conditions coincident with those of FMQ or slightly above it. Alternatively, the Group 2 granites could also have formed in conditions below FMQ and were oxidized during subsolidus or metamorphic stage. Nevertheless, the overall conditions were reducing for both groups in order to explain the high Fe/(Fe+Mg) in amphibole, mica, and whole rock.

The pressures given by Al-in-amphibole geobarometers are not conclusive in function of the strongly reduced character of the Planalto granites and the uncertainty about their amphibole re-equilibration. However, geological and petrologic evidence indicate pressures of 900-700 MPa for the origin of their magmas and pressures of 500-300 MPa for their emplacement.

The Zircon saturation thermometer provided initial temperatures between 897 and 854 °C and the geothermometer of Ridolfi et al. (2010) temperatures between 910 – 831 °C, whereas the apatite saturation thermometer indicated much lower temperatures (704 – 620 °C) for the Planalto Suite. The apatite temperatures were discarded because they are lower than those generally admitted for the solidus of granite systems and they should probably reflect P mobility during the subsolidus stage. A temperature interval of 910 – 850 °C (Table 2.6) was admitted for the initial crystallization of the Planalto Suite.

The dominance of amphibole and biotite among the mafic minerals of the Planalto Suite and the common absence of pyroxene indicate that the water content in the magma was higher than 4 wt % and could attain even more than 7 % in weight.

The Planalto Suite show strong mineralogical and petrological analogies with other ferroan Neoproterozoic granites of the Carajás Province (Estrela Granitic Complex and Serra do Rabo) and it is concluded that they were probably formed under similar conditions. The amphibole and biotite compositions of Planalto and Estrela are quite enriched in Al and similar in this respect to those of the Neoproterozoic Matok Pluton of the Limpopo Belt. This characteristic was not observed in the Proterozoic A-type granites taken for comparison. On the other hand, in terms of oxygen fugacity conditions, the Planalto granites approach the reduced Mesoproterozoic Wolf River batholith and the Finnish rapakivi granites and the Paleoproterozoic reduced to moderately oxidized granites of, respectively, the Velho Guilherme and Serra dos Carajás suites and differ from the oxidized granites (Jamon Suite) of

the Carajás province and also of Matok. Taking in account the different crystallization parameters and geological setting, the Planalto granites differ significantly of some classical examples of Paleoproterozoic and Mesoproterozoic A-type granites. On the other hand, even if formed in different oxygen fugacity, they approach in many characteristics the Neoproterozoic Fe-K and Mg-K granitoids of the Limpopo Belt, as exemplified by the Matok granitoids. The facts that Planalto and similar granites of Carajás were possibly formed in a collisional setting similar to that generally admitted for the Limpopo Belt and the intimate association in both provinces between those granites and charnockitic rocks indicate that the geological setting could have a strong influence in the nature of the Neoproterozoic granitoid magmas.

Acknowledgments

A. K. B. Gomes, M.A. Oliveira, A.S. Sardinha, and J.E.B. Soares, are acknowledged for previous work in the Planalto Suite. The authors thank: N.F. Botelho for his assistance in the microprobe mineral chemical analyses at the Laboratório de Microsonda Eletrônica of Universidade de Brasília (UNB) and contributions for the manuscript improvement; C. N. Lamarão and A. P. Rodrigues for support in the scanning electron microscope studies and review of the manuscript (CNL); J. E. Scandola, B. R. Frost and an anonymous reviewer for their critical review that significantly improved our manuscript. R. E. Leal for assistance in the elaboration of geological maps and manuscript translation into English; CNPq for research (R. Dall'Agnol; Proc. 306108/2014-3) and CAPES for master and CNPq for DTI scholarships (I. R. V. Cunha). This research received financial support from INCT program (CNPq/FAPESPA/CAPES/PETROBRAS; Proc. 573733/2008-2) and CNPq/Universal; proc. 483330/2012-4 and Federal University of Pará (UFPA). This paper is a contribution to the Brazilian Institute of Amazonian Geosciences (INCT GEOCIAM) and to the IGCP-SIDA 599 project (The Changing Early Earth).

References

- Aleinikoff, N.J., Wintsch, R.P., Fanning, C.M., Dorais, M.J., 2002. U–Pb geochronology of zircon and polygenetic titanite from the Glastonbury Complex, Connecticut, USA: an integrated SEM, EMPA, TIMS, and SHRIMP study. *Chemical Geology* 188, 125-147.
- Almeida, J.A.C., Dall'Agnol, R., Oliveira, M.A., Macambira, M.J.B., Pimentel, M.M., Rämö, O.T., Guimarães, F.V., Leite, A.A.S., 2011. Zircon geochronology and geochemistry of the TTG suites of the Rio Maria granite-greenstone terrane: Implications for the growth of the Archean crust of Carajás Province, Brazil. *Precambrian Research* 187, 201-221.

- Almeida, J.A.C., Dall'Agnol R., Leite A.A.S., 2013. Geochemistry and zircon geochronology of the Archean granite suites of the Rio Maria granite-greenstone terrane, Carajás Province, Brazil. *Journal of South American Earth Sciences* 42, 103-126.
- Althoff, F.J., Barbey, P., Boullier, A.M., 2000. 2.8-3.0 Ga plutonism and deformation in the SE Amazonian craton: the Archean granitoids of Marajoara (Carajás Mineral province, Brazil). *Precambrian Research* 104, 187-206.
- Anderson, J.L., Barth, A.P., Mazdab, J.L.W.F., 2008. Thermometers and Thermobarometers in Granitic Systems. *Reviews in Mineralogy and Geochemistry* 69, 121-142.
- Anderson, J.L., Bender, E.E., 1989. Nature and origin of Proterozoic A-Type granitic magmatismo in the southwestern United States of America. In: R. Gorbatshev (Editor), *Proterozoic Geochemistry*. *Lithos* 23, 19-52.
- Anderson, J.L., Morrison J., 2005. Ilmenite, magnetite and peraluminous Mesoproterozoic anorogenic granites of Laurentia and Baltica. *Lithos* 80, 45-60.
- Anderson, J.L., Smith, D.R., 1995. The Effects of temperature and fO_2 on the Al-in-hornblende barometer. *American Mineralogist* 80, 549-559.
- Baker, L., Rutherford, M.J., 1996. The effect of dissolved water on the oxidation state of silicic melts. *Geochimica et Cosmochimica Acta* 60, 2179-2187.
- Baker, F., Wones, D.R., Sharp, W.N., Desborough, G.A., 1975. The Pikes Peak batholiths, Colorado Front Range, and a model for the origin of the gabbro-anorthosite-syenite-potassic granite suite. *Precambrian Research* 2, 97-160.
- Barros, C.E.M., Dall'Agnol, R., Barbey, P., Boullier, A.M., 1997. Geochemistry of the Estrela Granite Complex, Carajás region, Brazil: an example of an Archean A-type granitoid. *Journal of South American Earth Sciences*, 10, 321-330.
- Barros, C.E.M., Barbey, P., Boullier, A.M., 2001. Role of magma pressure, tectonic stress and crystallization progress in the emplacement of the syntectonic A-type Estrela Granite Complex (Carajás Mineral Province, Brazil). *Tectonophysics*, 343, 93-109
- Barros, C.E.M., Sardinha, A.S., Barbosa, J.P.O., Macambira M.J.B., 2009. Structure, petrology, geochemistry and zircon U/Pb and Pb/Pb geochronology of the synkinematic Archean (2.7 Ga) A-Type granites from the Carajás Metallogenic Province, northern Brazil. *The Canadian Mineralogist* 47, 1423-1440.
- Blundy, J.D., Holland, T.J.B., 1990. Calcic amphibole equilibria and a new amphibole-plagioclase geothermometer. *Contributions to Mineralogy and Petrology* 104, 208-224.
- Bogaerts, M., Scaillet, B., Liégeois, J.P., Vander Auwera, J., 2003. Petrology and geochemistry of the Lyngdal granodiorite (Southern Norway) and the role of fractional crystallizations in the genesis of the Proterozoic ferro-potassic A-type granites. *Precambrian Research* 124, 149-184.
- Bogaerts, M., Scaillet, B., Vander Auwera, J., 2006. Phase equilibria of the Lyngdal granodiorite (Norway): implications for the origin of metaluminous ferroangranitoids. *Journal of Petrology* 47, 2405-2431.
- Botelho, N.F., Moura, M.A., Teixeira, L.M., Olivo, G.R., Cunha, L.M., Santana, M.U., 2005. Caracterização geológica e metalogenética do depósito Cu ± (Au, W, Mo, Sn) Breves, Carajás. In: Marini, O.J., Queiroz, E.T., Ramos, B.W. (Eds.), *Caracterização de Depósitos Minerais em Distritos Mineiros da Amazônia*. DNPM, CT-MINERAL, FINEP, ADIMB. Cap. VI, pp. 339-389 (in Portuguese).

- Buddington, A.F., Lindsley, D.H., 1964. Iron-titanium oxide minerals and synthetic equivalents. *Journal of Petrology* 5, 310-357.
- Carmichael, I.S.E., 1991. The redox states of basic and silicic magmas: a reflection of their source regions. *Contributions to Mineralogy and Petrology* 106, 129-141.
- Clark, D.A., 1999. Magnetic Petrology of igneous intrusion: implications for exploration and magnetic interpretation. *Exploration Geophysics* 30, 5-26.
- Cuney, M., Friederich, M., 1987. Physicochemical and crystal-chemical controls on accessory paragenesis in granitoids: implications for uranium metallogenesis. *Bulletin de Minéralogie* 110, 235-247.
- Czamanske, G.K., Wones, D.R., 1973. Oxidation during magmatic differentiation, Finnmarka Complex, Oslo Area, Norway: Part 2, The mafic silicates. *Journal of Petrology* 14, 349-380.
- Dall'Agnol, R., Oliveira, D.C., 2007. Oxidized, magnetite-series, rapakivi-type granites of Carajás, Brazil: Implications for classification and petrogenesis of A-type granites. *Lithos* 93, 215–233.
- Dall'Agnol, R., Pichavant, M., Champenois, M., 1997. Iron-titanium oxide minerals of the Jamon granite, Eastern Amazonian region, Brazil: implications for the oxygen fugacity in Proterozoic A-type granites. *Anais da Academia Brasileira de Ciências* 69, 325-347.
- Dall'Agnol, R., Scaillet, B., Pichavant, M., 1999. An experimental study of a lower Proterozoic A-type granite from the eastern Amazonian craton, Brazil. *Journal of Petrology* 40, 1673-1698.
- Dall'Agnol, R., Teixeira, N.P., Rämö, O.T., Moura, C.A.V., Macambira, M.J.B., Oliveira, D.C., 2005. Petrogenesis of the Paleoproterozoic, rapakivi, A-Type granites of the Archean Carajás Metallogenic Province, Brazil. *Lithos* 80, 101-129.
- Dall'Agnol, R., Frost, C.D., Rämö, O.T. 2012. IGCP Project 510 A-type granites and related rocks through time: Project vita, results and contribution to granite research. *Lithos*, 151, 1-16.
- Dall'Agnol R., Oliveira D.C., Guimarães F.V., Gabriel E.O., Feio G.R.L., Lamarão C.N., Althoff F.J., Santos P.A., Teixeira M.F.B., Silva A.C., Rodrigues D.S., Santos M.J.P., Silva C.R.P, Santos R.D., Santos P.J.L. 2013. Geologia do Subdomínio de Transição do Domínio Carajás – Implicações para a evolução arqueana da Província Carajás - Pará. In: SBG, Simpósio de Geologia da Amazônia, 13, Anais, Belém, CDrom (in Portuguese).
- Deer, W.A., Howie, R.A., Zussman, J., 1992. *Rock-forming minerals*. London, 2nd Edition. Longmans , 696p.
- DOCEGEO (Rio Doce Geologia e Mineração - Distrito Amazônia) 1988. Revisão litoestratigráfica da Província Mineral de Carajás, Pará. In: Congresso Brasileiro de Geologia 35, Belém. Anexos. Belém, SBG. Vol. Província Mineral de Carajás-Litoestratigrafia e Principais Depósitos Minerais. 11-54 (in Portuguese).
- Eby, G.N., 1992. Chemical subdivision of the A-type granitoids: petrogenesis and tectonic implications. *Geology* 20, 641-644.
- Elliot, B.A., 2001. Crystallization conditions of the Wiborg rapakivi batholith, SE Finland: an evaluation of amphibole and biotite mineral chemistry. *Mineralogy and Petrology* 72, 305-024.

- Elliot, B.A., Rämö, O.T., Nironen, M., 1998. Mineral chemistry constraints on the evolution of the 1.88-1.87 Ga post-kinematic plutons in the Central Filand Granitoid Complex. *Lithos* 45, 109-129.
- Erdmann, S., Martel, C., Pichavant, M., Kushnir, A., 2014. Amphibole as an archivist of magmatic crystallization conditions: problems, potential, and implications for inferring magma storage prior to the paroxysmal 2010 eruption of Mount Merapi, Indonesia. *Contributions to Mineralogy and Petrology* 167, 1-23.
- Emslie, R.F., 1991. Granitoids of rapakivi granite-anorthosite and related associations. *Precambrian Research* 51, 173-192.
- Feio, G.R.L., Dall'Agnol, R., 2012. Geochemistry and Petrogenesis of the Mesoarchean Granites from the Canaã dos Carajás Area, Carajás Province, Brazil: Implications for the Origin of Archean. *Lithos* 154, 33-52.
- Feio, G.R.L., Dall'Agnol, R., Dantas, E., Macambira, M.J.B., Gomes, A.C.B., Sardinha, A.S., Santos, P., 2012. Geochemistry, geochronology, and origin of the planalto granite suite and associated rocks: implications for the neoproterozoic evolution of the Carajás Province. *Lithos* 151, 57-73.
- Feio, G.R.L., Dall'Agnol, R., Dantas, E.L., Macambira, M.J.B., Santos, J.O.S., Althoff, F.J., Soares, J.E.B., 2013. Archean granitoid magmatism in the Canaã dos Carajás area: Implications for crustal evolution of the Carajás province, Amazonian craton, Brazil. *Precambrian Research* 227, 157-185.
- Frost, B.R., 1991. Introduction to oxygen fugacity and its petrologic importance. In: Lindsley, D.H. (Ed.), *Oxide minerals: petrologic and magnetic significance*. Reviews in Mineralogy 25. Mineralogical Society of America, 1-9.
- Frost, C.D., Frost, B.R., Chamberlain, K.R., Edwards, B.R., 1999. Petrogenesis of the 1.46 Ga Sherman batholith, SE Wyoming: a reduced rapakivi-type anorogenic granite. *Journal of Petrology* 40, 1771-1802.
- Frost, B.R., Frost, C.D., Hulsebosch, T.P., Swapp, S.M., 2000. Origin of the charnockites of the Louis Lake batholith, Wind River Range, Wyoming. *Journal of Petrology* 40, 1771-1802.
- Frost, B.R., Frost, C.D., 2008. On charnockites. *Gondwana Research* 13, 30-44.
- Gabriel E.O., Oliveira D.C., 2014. Geologia, petrografia e geoquímica dos granitoides arqueanos de alto magnésio da região de Água Azul do Norte, porção sul do Domínio Carajás, Pará. *Boletim do Museu Paraense Emílio Goeldi. Ciências Naturais*, Belém, 9 (3): 533-564 (in Portuguese).
- Gaillard, F., Scaillet, B., Arndt, N.T., 2001. The effect of water and fO_2 on the ferric-ferrous ratio of silicic melts. *Chemical Geology* 147, 255-273.
- Gibbs, A. K., Wirth, K. R., Hirata, W. K., Olszewski, W. J. 1986. Age and composition of the Grão Para Group Volcanics, Serra dos Carajás. *Revista Brasileira de Geociências* 16, 201-211.
- Haggerty, S.E., 1981. Opaque mineral oxides in terrestrial igneous rocks. In: RUMBLE III, D.H. (Ed.), *Oxide minerals*. 2nd Ed. Reviews in Mineralogy 3. Mineralogical Society of America, 101-300.

- Haggerty, S.E., 1991. Oxide textures - a mini-atlas. In: Lindsley, D.H. (Ed.), *Oxide minerals: petrologic and magnetic significance*. Reviews in Mineralogy 25. Mineralogical Society of America, 129–219.
- Hammarström, J.M., Zen, E.A., 1986. Aluminium in hornblende: an empirical igneous geobarometer. *American Mineralogist* 71, 1297-1313.
- Harrison, T.M., Watson, E.B., 1984. The behavior of apatite during crustal anatexis: Equilibrium and kinetic considerations. *Geochimica et Cosmochimica Acta* 48, 1467-1477.
- Hollister, L.S., Grisson G.C., Peters, E.K., Stowell, H.H., Sisson, V.B., 1987. Confirmation of the empirical correlation of Al in hornblende with pressure of solidification of calc-alkaline plutons. *American Mineralogist* 72, 231-139.
- Huhn, S.B., Macambira, M.J.B., Dall'Agnol, R., 1999. Geologia e geocronologia Pb/Pb do granito alcalino arqueano planalto, região da Serra do Rabo, Carajás-PA. *Simpósio de Geologia da Amazônia*, 6, 463-466 (in Portuguese).
- Ishihara, S., 1981. The granitoid series and mineralization. *Economic Geology* 75, 458-484.
- Johnson, M.C., Rutherford, M.J., 1989. Experimental calibration of the aluminium-in-hornblende geobarometer with application to Long Valley caldera (California) volcanic rocks. *Geology* 17, 837-841.
- King, P.L., White, A.J.R., Chappell, B.W., Allen, C.M., 1997. Characterization and origin of aluminous A-type granites from the Lachlan Fold Belt, southeastern Australia. *Journal of Petrology* 38, 371-391.
- Klimm, K., Holtz, F., Johannes, W., King, P.L., 2003. Fractionation of metaluminous A-type granites: an experimental study of the Wangrah Suite, Lachlan Fold Belt, Australia. *Precambrian Research* 124, 327-341.
- Kosunen, P.J., 2004. Petrogenesis of mid-Proterozoic A-type granite: Case Studies from Fennoscandia (Finland) and Laurentia (New Mexico). PhD thesis, Department of Geology, University of Helsinki, Finland.
- Kowallis, B.J., Christiansen, E.H., Griffen, D.T., 1997. Compositional variations in titanite. *Geological Society of America. Abst. with Prog.* 29 (6), 402.
- Kretz, R., 1983. Symbols for rock-forming minerals. *American Mineralogist* 68, 277-279.
- Lamarão, C.N., Dall'Agnol, R., 2004. Química mineral de anfíbios e biotitas e condições de cristalização de granitoides paleoproterozóicos da região de Vila Riozinho, Província Aurífera do Tapajós, Cráton Amazônico. *Revista Brasileira de Geociências* 34, 95-108 (in Portuguese).
- Laurent, O., Rapopo, M., Stevens, G., Moyen, J.F., Martin, H., Doucelance, R., Bosq, C., 2014. Contrasting petrogenesis of Mg–K and Fe–K granitoids and implications for post-collisional magmatism: Case study from the Late-Archean Matok pluton (Pietersburg block, South Africa). *Lithos* 196-197, 131-149.
- Le Maitre, R.W., 2002. *A classification of igneous rocks and glossary of terms*. 1-193. 2 Edition, London.
- Leake, B.E., 1997. Nomenclature of amphiboles: Report of the Subcommittee on Amphiboles of the International Mineralogical Association Commission on New Minerals and Mineral Names. *Mineral Magazine* 61, 295-321.

- Loiselle, M.C., Wones, D.R., 1979. Characteristics and origin of anorogenic granite. Geological Society of America, abstracts with programs.11, 468p.
- Macambira, M.J.B., Lafon, J.M., 1995. Geocronologia da Província Mineral de Carajás; Síntese dos dados e novos desafios. Boletim do Museu Paraense Emílio Goeldi, Série Ciências da Terra, Belém 7, 263-287 (in Portuguese).
- Machado, N., Lindenmayer, Z., Krogh, T. E., Lindenmayer, D., 1991. U/Pb geochronology of Archean magmatism and basement reactivation in the Carajás Área, Amazon Shield, Brazil. *Precambrian Research*, 49, 329-354.
- Martin, R.F., 2007. Amphiboles in the igneous environment. *Reviews in Mineralogy and Geochemistry*. 67, 323-358.
- Miller, C.F., McDowell, S.M., Mapes, R.W., 2003. Hot and cold granites? Implications of zircon saturation temperatures and preservation of inheritance. *Geology* 31, 529–532.
- Moreto, C.P.N., Monteiro L.V.S. Xavier R.P., Amaral W.S., Santos T.J.S., Juliani C., Souza Filho C.R., 2011. Mesoarchean (3.0 and 2.86 Ga) host rocks of the iron oxide–Cu–Au Bacaba deposit, Carajás Mineral Province: U–Pb geochronology and metallogenetic implications. *Mineralium Deposita* 46, 789–811.
- Moreto, C.P.N., Monteiro, L.V.L., Xavier, R.A., Creaser, R.A., DuFrane, S.A., Tassinari, C.C.G., Sato, K., Kemp, A.I.S., Amaral, W.S., 2015. Neoproterozoic and Paleoproterozoic Iron Oxide-Copper-Gold Events at the Sossego Deposit, Carajás Province, Brazil: Re-Os and U-Pb Geochronological Evidence. *Economic Geology* 110, 809-835.
- Moore, G., Righter, K., Carmichael, I.S.E., 1995. The effect of dissolved water on the oxidation state of iron in natural silicate liquids. *Contributions to Mineralogy and Petrology* 120, 170-179.
- Moore, M., Davis, D.W., Robb, L.J., Jackson, M.C., Grobler, D.F., 1993. Archean rapakivi granite-anorthosite-rhyolite complex in the Witwatersrand basin hinterland, southern Africa. *Geology* 21, 1031 -1034.
- Nachit, H., Razafimahefa, N., Stussi, J.M., Carron J.P., 1985. Composition chimique des biotites et typologie magmatique des granitoides. *Comptes rendus de l'Académie des Sciences de Paris*, 301, 813 - 818.
- Nachit, H., 1994. Contribution à la typologie des granitoides, Petrogenèse et pétrologie structurale du batholite panafricain du cercle de tafrouste (boutonnière de Kerdous, Anti-Atlas occidental, Maroc), 465p.Thèse d'Etat, Université Ibhrou Zohor, Agadir.
- Naney, M.T., 1983. Phase equilibria of rock-forming ferromagnesian silicates in granitic systems. *American Mineralogist* 65, 639-653.
- Nardi, L.V.S., Bitencourt, M.F., 2009. A-type granitoids in post-collisional settings from southernmost Brazil: their classification and relationship with magmatic series. *The Canadian Mineralogist* 47, 1493–1504.
- Oliveira, D.C., Santos, P.J.L., Gabriel, E.O., Rodrigues, D.S., Faresin, A.C., Silva, M.L.T., Sousa, S.D., Santos, R.V., Silva, A.C., Souza, M.C., Santos, R.D., Macambira, M.J.B., 2010. Aspectos geológicos e geocronológicos das rochas magmáticas e metamórficas da região entre os municípios de Água Azul do Norte e Canaã dos Carajás – Província Mineral de Carajás. Congresso Brasileiro de Geologia, 45, Belém. CDrom (in Portuguese).

- Oliveira, M.A., 2003. Caracterização petrográfica, estudo de susceptibilidade magnética e natureza dos minerais óxidos de Fe e Ti do Granito Planalto, Serra dos Carajás-PA. Trabalho de Conclusão de Curso – Universidade Federal do Pará, Belém, 1-47 (in Portuguese).
- Oliveira, M.A., Dall'Agnol R., Althoff F.J., Leite A.A.S., 2009. Mesoarchean sanukitoid rocks of the Rio Maria Granite-Greenstone Terrane, Amazonian craton, Brazil. *Journal of South American Earth Sciences*, 27, 146-160.
- Oliveira, M.A., Dall'Agnol, R., Scaillet, B., 2010. Petrological constraints on crystallization conditions of Mesoarchean Sanukitoid Rocks, southeastern Amazonian craton, Brazil. *Journal of Petrology* 51, 2121–2148.
- Papoutsas, A., Pe-Piper, G., 2014. Geochemical variation of amphiboles in A-type granites as an indicator of complex magmatic systems: Wentworth pluton, Nova Scotia, Canada. *Chemical Geology* 384, 120-134.
- Prouteau, G., Scaillet, B., 2003. Experimental constraints on the origin of the 1991 Pinatubo dacite. *Journal of Petrology* 44, 2203-2241.
- Rajesh, H.M., Santosh, M., Wan, Y., Liu, D., Liu, S.J., Belyanin, G.A., 2014. Ultrahigh temperature granulites and magnesian charnockites: Evidence for Neoproterozoic accretion along the northern margin of the Kaapvaal Craton. *Precambrian Research* 246, 150-159.
- Rämö, O.T., Haapala, I., 1995. One hundred tears of rapakivi granite. *Mineralogy and Petrology* 52, 129-185.
- Rapopo, M., 2010. Petrogenesis of the Matok pluton, South Africa: implications on the heat source that induced regional metamorphism in the Southern Marginal Zone of the Limpopo Belt. Master Thesis - University of Stellenbosch, South Africa, 197p.
- Ridolfi, F., Renzulli, A., 2012. Calcic amphiboles in calc-alkaline and alkaline magmas: thermobarometric and chemometric empirical equations valid up to 1130 °C and 2.2 GPa. *Contributions to Mineralogy and Petrology* 163, 877–895.
- Ridolfi, F., Renzulli, A., Puerini, M., 2010. Stability and chemical equilibrium of amphibole in calc-alkaline magmas: an overview, new thermobarometric formulations and application to subduction-related volcanoes. *Contributions to Mineralogy and Petrology* 160, 45-66.
- Rieder, M., 1998. Nomenclature of the micas. *Mineralogical Magazine* 63, 267-279.
- Robinson, D.M., Miller, C.F., 1999. Record of magma chamber processes preserved in accessory mineral assemblages, Aztec Wash pluton, Nevada. *American Mineralogist* 84, 1346-1346.
- Rodrigues, D.S., Oliveira, D.C., Macambira, M.J.B., 2014. Geologia, geoquímica e geocronologia do Granito Mesoarqueano Boa Sorte, município de Água Azul do Norte, Pará – Província Carajás. *Boletim do Museu Paraense Emílio Goeldi. Série Ciências da Terra* 9, 597-633 (in Portuguese).
- Santos, D.R., Galarza, M.A., Oliveira, D.C., 2013. Geologia, geoquímica e geocronologia do Diopsídio-Norito Pium, Província Carajás. *Boletim do Museu Paraense Emílio Goeldi, Série Ciências da Terra* 8, 355-382 (in Portuguese).
- Santos J.O.S. 2003. Geotectônica do Escudo das Guianas e Brasil-Central. In: Bizzi, L.A. et al. (Ed.). *Geologia, tectônica e recursos minerais do Brasil: texto, mapas e SIG*. Brasília: CPRM-Serviço Geológico do Brasil, 169-226 (in Portuguese).

- Santos, P.A., Teixeira, M.F.B., Dall'Agnol, R., Guimarães, F.V., 2013. Geologia, petrografia e geoquímica da associação Tonalito-Trondhjemitó-Granodiorito (TTG) do extremo leste do subdomínio de transição, Província Carajás - Pará. *Boletim do Museu Paraense Emílio Goeldi, Série Ciências da Terra* 8, 257-290 (in Portuguese).
- Santos, P.J.L., Oliveira, D.C., 2014. Trondhjemitos da área de Nova Canadá: novas ocorrências de associações magmáticas tipo TTG no Domínio Carajás. *Boletim do Museu Paraense Emílio Goeldi. Série Ciências da Terra* 9, 635-659 (in Portuguese).
- Sardinha, A.S., Dall'Agnol R., Gomes, A.C.B., Macambira, M.J.B., Galarza, M.A., 2004. Geocronologia Pb-Pb e U-Pb em zircão de granitóides arqueanos da região de Canaã dos Carajás, Província Mineral de Carajás. *Congresso Brasileiro de Geologia*, 42. CDrom (in Portuguese).
- Sardinha, A.S., Barros, C.E.M., Krymsky, R., 2006. Geology, geochemistry, and U-Pb geochronology of the archaic (2.74 Ga) Serra do Rabo granite stocks, Carajás Province, northern Brazil. *Journal of South American Earth Sciences* 20, 327-339.
- Schmidt, M.W., 1992. Amphibole composition in tonalite as a function of pressure: Na experimental calibration of the Al-in-hornblende barometer. *Contributions to Mineralogy and Petrology* 110, 304-310.
- Schumacher, J.C., 1997. The estimation of ferric iron in electron microprobe analysis of amphiboles. In Leake, B.E., 1997 Nomenclature of amphiboles. Report of the Subcommittee on Amphiboles of the International Mineralogical Association Commission on New Minerals and Mineral Names. *European Journal of Mineralogy* 9, 623-651.
- Silva, A.C., Dall'Agnol, R., Guimarães, F.V., Oliveira, D.C., 2014. Geologia, petrografia e geoquímica de Associações Tonalíticas e Trondhjemiticas Arqueanas de Vila Jussara, Província Carajás, Pará. *Boletim do Museu Paraense Emílio Goeldi, Série Ciências Naturais* 9, 13-45 (in Portuguese).
- Souza, S. Z., Dall'Agnol, R., Althoff, F. J., Leite, A. A. S.; Barros, C. E. M., 1996. Carajás mineral province: geological, geochronological and tectonic constrasts on the Archaean evolution of the Rio Maria Granite-Greenstone Terrain and the Carajás block. In: *Symposium on Archaean Terranes of South America Platform, Brasília, 1996, Extended abstracts. SBG*, 31-32.
- Souza, Z.S., Potrel, H., Lafon, J.M., Althoff, F.J., Pimentel, M.M., Dall'Agnol, R., Oliveira, C.G., 2001. Nd, Pb and Sr isotopes of the Identidade Belt, an Archaean greenstone belt of the Rio Maria region (Carajas Province, Brazil): Implications for the Archaean geodynamic evolution of the Amazonian Craton. *Precambrian Research* 109, 293-315.
- Streckeisen, A.L., 1976. To each plutonic rock its proper name. *Earth Science Reviews* 12, 1-33.
- Sylvester, P.J., 1989. Post-collisional alkaline granites. *Journal of Geology* 97, 261-280.
- Tavares, F.M., 2015. Evolução geotectônica do nordeste da Província Carajás. *Dissertação do doutorado – Universidade Federal do Rio de Janeiro, Rio de Janeiro*, 1-115 (in Portuguese).
- Teixeira, M.F.B., Dall'Agnol, R., Silva, A.C., Santos, P.A. 2013. Geologia, petrografia e geoquímica do Leucogranodiorito Pantanal e dos leucogranitos arqueanos da área de Sapucaia, Província Carajás, PA: implicações petrogenéticas. *Boletim do Museu Paraense Emílio Goeldi, Série Ciências Naturais* 8, 291-323 (in Portuguese)

- Thomas, W. M., Ernst, W. G., 1990. The aluminum content of hornblende in calc-alkaline granitic rocks: a mineralogic barometer calibrated experimentally to 12 kbar. In: Spencer, R. J. & Shou, I.-M. (eds) Fluid-Mineral Interactions: A Tribute to H. P. Eugster. Geochemical Society Special Publication 2, 59-63.
- Vander Auwera, J., Bolle, O., Dupont, A., Pin, C., Paquette, J.L., Charlier, B., Duchesne, J.C., Mattielli, N., Bogaerts, M., 2014. Source-derived heterogeneities in the composite (charnockite-granite) ferroan Farsund intrusion (SW Norway). *Precambrian Research* 251, 141-163.
- Vasquez, L.V., Rosa-Costa, L.R., Silva, C.G., Ricci, P.F., Barbosa, J.O., Klein, E.L., 2008. Geologia e recursos minerais do estado do Pará: Sistema de Informações Geográficas – SIG: texto explicativo dos mapas geológico e tectônico e de recursos minerais do estado do Pará, 328p (in Portuguese).
- Watson, E.B., Harrison, T.M., 1983, Zircon saturation revisited: Temperature and composition effects in a variety of crustal magma types: *Earth and Planetary Science Letters* 64, 295–304.
- Whalen J.W., Currie K.L., Chappel B.W., 1987. A-type granites: geochemical characteristics, discrimination and petrogenesis. *Contributions to Mineralogical Petrology*, 95, 407-419.
- Wones, D.R., 1989. Significance of the assemblage titanite+magnetite+quartz in granitic rocks. *American Mineralogist* 74, 744-749.
- Wones, D.R., Eugster, H.P., 1965. Stability of biotite: experiment, theory, and applications. *American Mineralogist* 50, 1228-1272.
- Xavier, R.P., Monteiro, L.V.S., Souza Filho, C.R., Torresi, I., Carvalho, E.R., Dreher, A.M., Wiedenbeck, M., Trumbull, R.B., Pestilho, A.L.S., Moreto, C.P.N. 2010. The Iron Oxide Copper-Gold Deposits of the Carajás Mineral Province, Brazil: An Updated and Critical Review. In: Porter, T.M. (Org.) *Hydrothermal Iron Oxide Copper-Gold & Related Deposits: A Global Perspective, Advances in the Understanding of IOCG Deposits*. Adelaide: PGC Publishing, 2010, 3, 285-306.

SUPPLEMENTARY DATA

Table S1: Modal composition^a of the granites of the Planalto Suite.

GROUP 1 – Ilmenite-bearing granites																			
Mineral/Sample	Type area				Eastern of Canaã dos Carajás						Vila Feitosa								
	AMR-149 ⁽³⁾	AMR-145 ⁽³⁾	AMR-135 ⁽³⁾	AMR-162A	AMR-98A	AMR-116 ⁽³⁾	AMR-209 ⁽³⁾	AMR-118H	AMR-94A	AMR-117J	ARC-147 ⁽³⁾	AMR-137B	ARC-110	ARF-24	ARF-20	ARC-144 ⁽³⁾			
Facies	HBMzG	BHSG	BHMzG	HBMzG	HBLSG	BHSG	BHMzG	BHSG	HLMzG	BHMzG	BHMzG	BHSG	BHSG	BHSG	HBSG	BHMzG			
Alkali feldspar	21.3	40.0	31.7	24.2	40.8	34.5	36.6	47.4	41.6	30.4	21.5	29.6	37.4	57.9	49.0	27.9			
Plagioclase	16.6	14.6	19.1	36.0	13.6	16.4	21.0	10.6	25.0	19.8	31.0	12.2	7.0	15.6	22.4	29.9			
Quartz	34.5	38.2	39.4	34.2	41.2	42.5	32.2	29.4	32.2	27.8	34.8	30.5	43.2	19.8	20.8	24.6			
Amphibole	11.4	4.0	4.8	1.2	2.0	4.5	6.9	7.6	0.8	14.8	6.4	14.0	6.4	4.4	3.6	13.6			
Biotite	12.2	2.5	4.3	4.4	2.2	1.8	3.3	4.8	-	7.0	5.3	11.6	5.4	2.2	4.2	2.0			
Opaque minerals ¹	0.3	-	0.2	-	-	-	-	0.2	0.2	0.2	-	0.1	-	0.1	-	0.7			
Titanite	1.7	0.4	-	-	0.2	0.2	0.4	x	0.2	-	0.4	1.6	0.6	x	-	0.1			
Zircon	x	x	x	x	x	0.1	x	x	x	x	x	0.2	0.2	x	x	0.3			
Apatite	x	x	x	x	x	x	x	x	x	x	x	x	x	x	x	x			
Allanite	x	x	-	-	-	x	x	x	-	-	0.1	0.2	-	-	-	x			
Chlorite	-	-	-	-	-	-	-	-	-	-	-	-	-	-	-	-			
Muscovite	-	-	-	-	-	-	-	-	-	-	-	-	-	-	-	-			
Scapolite	-	-	-	-	-	-	-	-	-	-	0.2	-	-	-	-	0.8			
Tourmaline	-	-	-	-	-	x	x	-	-	-	-	-	-	-	-	-			
Felsic	72.4	92.8	90.2	349.8	95.6	93.5	89.8	87.4	98.8	78.0	87.3	72.5	87.8	93.3	92.2	82.7			
Mafic (M')	25.6	6.9	9.3	5.6	4.4	6.5	10.6	12.6	1.2	22.0	12.2	27.5	12.4	6.7	7.8	16.4			

GROUP 2 – Ilmenite-magnetite-bearing granites																						
Mineral/Sample	Type area				Eastern of Canaã dos Carajás								Vila Feitosa									
	AMR-151B ⁽³⁾	AMR-150	AER-82A ⁽³⁾	AMR-155A	AMR-152A ⁽⁷⁾	AMR-146 ⁽³⁾	AMR-137A ⁽³⁾	AMR-140*	AMR-155B ⁽³⁾	AMR-154A	AC-4b*	AC-16*	AC-6A*	AMR-177 ⁽²⁾	AMR-85A ⁽³⁾	AMR-171 ⁽³⁾	AER-72A ⁽³⁾	ARF-17 ⁽³⁾	ARC-109 ⁽³⁾	ARF-18	ARC-104 ⁽³⁾	ARC-148
Facies	BHMzG	BHLSG	BHMzG	HBAG	BHMzG	BHSG	BHMzG	BHMzG	BHSG	BHSG	BHSG	BHSG	BHMzG	HLAG	HSG	BSG	BLMzG	HBLSG	HBSG	HBSG	BMzG	HBMzG
Alkali feldspar	24.9	54.6	28.9	57.0	22.5	30.0	37.2	31.5	29.6	39.2	38.8	42.0	36.8	50.0	43.4	42.8	28.6	44.2	34.2	39.0	39.3	25.6
Plagioclase	17.6	21.4	18.6	6.4	18.3	21.5	17.1	21.5	19.7	18.4	16.3	19.9	21.3	2.1	10.6	16.3	34.3	15.2	7.6	12.6	18.4	34.3
Quartz	37.3	23.2	32.2	32.0	33.4	30.5	35.0	33.8	39.5	31.4	32.2	32.6	32.0	42.9	30.5	35.0	33.3	37.2	46.7	36.2	36.6	36.1
Amphibole	11.2	0.6	12.3	1.6	12.7	8.7	5.3	7.2	5.7	5.2	6.2	3.4	5.7	4.6	12.8	x	-	0.3	3.4	3.0	-	1.4
Biotite	5.6	0.2	4.1	2.6	9.6	1.5	2.4	4.7	3.6	0.8	4.8	1.9	3.2	-	x	5.7	3.1	1.8	5.5	3.4	2.1	1.8
Opaque minerals ¹	0.7	x	0.8	0.4	0.1	x	x	x	0.7	0.4	0.2	0.1	0.3	0.1	2.1	0.1	0.1	0.4	0.4	-	1.3	0.5
Titanite	2.3	x	1.3	x	x	0.3	x	1.3	1.0	x	1.5	0.1	1.0	-	-	-	0.2	0.2	0.4	-	-	-
Zircon	x	x	x	0.2	x	x	x	x	x	x	0.1	x	x	x	0.1	x	0.1	x	0.2	x	x	0.3
Apatite	x	x	x	x	x	x	x	x	x	x	x	x	x	x	0.2	x	0.1	x	x	x	x	x
Allanite	x	-	-	x	-	x	-	x	-	0.3	-	-	x	0.1	-	x	x	-	-	-	0.1	-
Chlorite	-	-	-	-	-	-	-	-	-	-	-	-	-	-	-	-	-	-	0.6	-	0.5	-
Muscovite	-	-	-	-	-	-	-	-	-	-	-	-	-	-	-	-	-	-	-	-	1.2	-
Scapolite	-	-	-	-	-	-	-	-	-	-	-	-	-	-	-	-	-	-	1.0	-	x	-
Tourmaline	-	-	-	-	-	-	-	-	-	-	-	-	-	x	x	x	x	-	-	-	-	-
Felsic	79.8	99.2	79.7	95.6	74.2	82.0	89.3	31.5	88.8	89.0	87.4	94.5	90.1	95.0	84.8	94.1	96.4	96.6	88.7	87.8	94.3	96.3
Mafic (M')	19.8	0.8	18.5	4.6	22.4	10.5	7.7	13.2	11.0	6.7	12.7	5.5	10.2	4.8	14.9	5.8	3.4	2.7	9.7	6.4	3.5	3.7

^a Compiled of Oliveira (2003); (2)Gomes (2003); (3) G. R. L. Feio (Write communication of unpublished data). a – Point counting with a minimum of 1500 points for thin section

1 – Ilmenite, magnetite, hematite, chalcopyrite and pyrite; (x) minerals found in the rock sample; (-) mineral not observed in the rock

Table S2: MS measurements for samples of the Planalto Suite.

Group 1	Sample	Provenance of the Sample	Facies	MS average	log MS (SI)
	AMR-162A	Type area	HBMzG	0.0102*10 ⁻³	-4.9914
	AMR-168A	Eastern of Canaã dos Carajás	x	0.0443*10 ⁻³	-4.3536
	AMR-168B	Eastern of Canaã dos Carajás	x	0.0530*10 ⁻³	-4.2757
	AMR-117G	Eastern of Canaã dos Carajás	x	0.0588*10 ⁻³	-4.2306
	AMR-164A	Eastern of Canaã dos Carajás	x	0.0608*10 ⁻³	-4.2161
	AMR-138	Type area	x	0.0644*10 ⁻³	-4.1911
	AMR-149*	Type area	HBMzG	0.0662*10 ⁻³	-4.1791
	AMR-98A	Eastern of Canaã dos Carajás	HBLSG	0.0728*10 ⁻³	-4.1379
	AMR-96	Eastern of Canaã dos Carajás	x	0.0750*10 ⁻³	-4.1249
	AMR-179	Eastern of Canaã dos Carajás	x	0.0823*10 ⁻³	-4.0846
	AMR-120A	Eastern of Canaã dos Carajás	x	0.0987*10 ⁻³	-4.0057
	ARC-147*	Vila Feitosa	BHMzG	0.1000*10 ⁻³	-4.0000
	AMR-117L	Eastern of Canaã dos Carajás	x	0.1007*10 ⁻³	-3.9970
	AMR-166A	Eastern of Canaã dos Carajás	x	0.1023*10 ⁻³	-3.9901
	AMR-133A	Type area	x	0.1168*10 ⁻³	-3.9326
	AMR-137B	Type area	BHSG	0.1211*10 ⁻³	-3.9169
	AMR-158	Eastern of Canaã dos Carajás	x	0.1251*10 ⁻³	-3.9027
	AMR-116*	Eastern of Canaã dos Carajás	BHSG	0.1281*10 ⁻³	-3.8925
	AMR-136	Type area	x	0.1282*10 ⁻³	-3.8921
	AMR-209	Eastern of Canaã dos Carajás	BHMzG	0.1306*10 ⁻³	-3.8841
	AMR-167	Eastern of Canaã dos Carajás	x	0.1332*10 ⁻³	-3.8755
	AMR-118H	Eastern of Canaã dos Carajás	BHSG	0.1387*10 ⁻³	-3.8579
	AMR-142	Type area	x	0.1393*10 ⁻³	-3.8560
	AMR-97	Eastern of Canaã dos Carajás	x	0.1428*10 ⁻³	-3.8453
	ARC-110	Vila Feitosa	BHSG	0.1461*10 ⁻³	-3.8353
	AMR-151A	Type area	x	0.1485*10 ⁻³	-3.8283
	AMR-118A	Eastern of Canaã dos Carajás	BHMzG	0.1510*10 ⁻³	-3.8210
	AMR-145	Type area	BHSG	0.1526*10 ⁻³	-3.8164
	AMR-166B	Eastern of Canaã dos Carajás	x	0.1704*10 ⁻³	-3.7685
	AMR-94A	Eastern of Canaã dos Carajás	HLMzG	0.2041*10 ⁻³	-3.6902
	AMR-117J	Eastern of Canaã dos Carajás	BHMzG	0.2118*10 ⁻³	-3.6741
	ARC-147	Vila Feitosa	BHMzG	0.2512*10 ⁻³	-3.6000
	ARF-24	Vila Feitosa	BHSG	0.2883*10 ⁻³	-3.5402
	AMR-135	Type area	BHMzG	0.3237*10 ⁻³	-3.4899
	ARF-20	Vila Feitosa	HBSG	0.3310*10 ⁻³	-3.4802
	ARC-144	Vila Feitosa	BHMzG	0.4042*10 ⁻³	-3.3934
	ARF-25	Vila Feitosa	x	0.6247*10 ⁻³	-3.2043

Continued table S2

Group 2	Sample	Provenance of the Sample	Facies	MS average	log MS (SI)
	ARF-19	Vila Feitosa	x	0.8036*10 ⁻³	-3.0950
	AMR-170A	Vila Feitosa	x	0.9003*10 ⁻³	-3.0456
	AMR-151B	Type area	BHMzG	1.0025*10 ⁻³	-2.9989
	ARF-22	Vila Feitosa	x	1.1324*10 ⁻³	-2.9460
	AC-4b	Type area	BHSG	1.1401*10 ⁻³	-2.9431
	AMR-140*	Type area	BHMzG	1.2947*10 ⁻³	-2.8878
	AC-16	Type area	BHSG	1.3757*10 ⁻³	-2.8615
	AMR-91B	Vila Feitosa	x	1.6262*10 ⁻³	-2.7888
	AMR-142A	Type area	x	1.7294*10 ⁻³	-2.7621
	AMR-150	Type area	BHLSG	2.0611*10 ⁻³	-2.6859
	ARF-17	Vila Feitosa	HBSG	2.2522*10 ⁻³	-2.6474
	AMR-141B	Type area	BHMzG	2.3327*10 ⁻³	-2.6321
	AMR-151D	Type area	x	2.5187*10 ⁻³	-2.5988
	AMR-85B	Eastern of Canaã dos Carajás	x	2.7076*10 ⁻³	-2.5674
	AER-82A	Type area	BHMzG	3.0611*10 ⁻³	-2.5141
	AMR-134A	Type area	x	3.1466*10 ⁻³	-2.5022
	ARC-109*	Vila Feitosa	HBSG	3.1488*10 ⁻³	-2.5019
	AMR-171C	Eastern of Canaã dos Carajás	BSG	4.0811*10 ⁻³	-2.3892
	GFMF-06	Vila Feitosa	HBSG	4.2358*10 ⁻³	-2.3731
	AMR-172B	Eastern of Canaã dos Carajás	x	4.6588*10 ⁻³	-2.3317
	AMR-155A	Type area	HBAG	4.7822*10 ⁻³	-2.3204
	AMR-177	Eastern of Canaã dos Carajás	HAG	5.2133*10 ⁻³	-2.2829
	AMR-153A	Type area	x	5.2588*10 ⁻³	-2.2791
	AMR-152A	Type area	BHMzG	5.4044*10 ⁻³	-2.2673
	ARC-141B	Vila Feitosa	BMzG	6.4355*10 ⁻³	-2.1914
	AMR-85A*	Eastern of Canaã dos Carajás	HSG	6.4611*10 ⁻³	-2.1897
	AMR-141A	Type area	x	6.4722*10 ⁻³	-2.1889
	AMR-171	Eastern of Canaã dos Carajás	BSG	6.5933*10 ⁻³	-2.1809
	AC-6A	Type area	BHMzG	6.6605*10 ⁻³	-2.1765
	ARC-77	Type area	x	6.8000*10 ⁻³	-2.1675
	AMR-146	Type area	BHMzG	7.1913*10 ⁻³	-2.1432
	AMR-152B	Type area	BHMzG	7.5022*10 ⁻³	-2.1248
	AMR-155B	Type area	BHMzG	7.8122*10 ⁻³	-2.1072
	AER-72A	Eastern of Canaã dos Carajás	BMzG	8.2966*10 ⁻³	-2.0811
	AMR-137A*	Type area	BHSG	8.5212*10 ⁻³	-2.0695
	ARF-18	Vila Feitosa	HBSG	9.8766*10 ⁻³	-2.0054
	AMR-154A	Type area	BHSG	11.3166*10 ⁻³	-1.9463
	ARC-104	Vila Feitosa	BMzG	11.8111*10 ⁻³	-1.9277
	ARC-112B	Vila Feitosa	BMzG	13.5500*10 ⁻³	-1.8681
	ARC-148	Vila Feitosa	HBMzG	15.7000*10 ⁻³	-1.8041

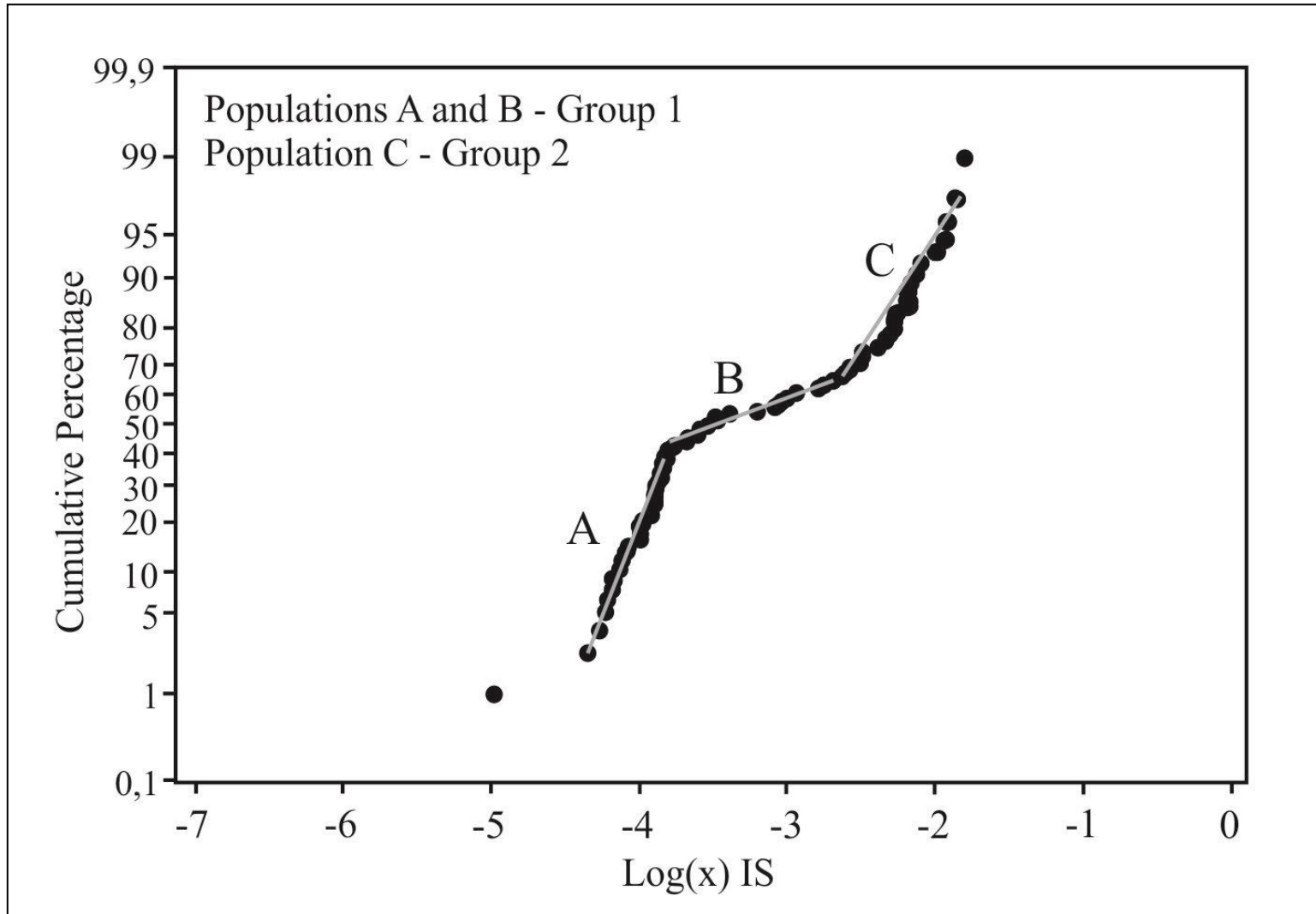
In bold. samples with chemical analyses and whole-rock FeOt/(FeOt+MgO) ratio; * Electron microprobe and scanning electron microscope analyses.

Table S3 - Representative chemical compositions of the granites of the Planalto suite.

Unit	PLANALTO SUITE												
Group	1					2							
Sample	ARC-147	ARC-144	AMR-209	AMR-149	AMR-116	AMR-152	ARC-109	AMR-137A	AMR-85A	AMR-140	ARF-17	ARC-104	AMR-177
Varieties	BHMzG	BHMzG	BHMzG	HBMzG	BHSG	BHMzG	HBSG	BHSG	HSG	BHMzG	HBSG	BMzG	HAG
SiO ₂	71.35	71.41	71.80	73.28	74.13	70.39	71.66	72.80	73.25	73.44	73.84	74.86	75.62
TiO ₂	0.38	0.52	0.28	0.41	0.25	0.64	0.44	0.38	0.29	0.32	0.30	0.20	0.14
Al ₂ O ₃	13.44	12.61	12.51	11.13	12.21	12.32	12.77	12.48	12.47	12.52	11.96	11.41	12.01
Fe ₂ O _{3t}	3.50	4.35	5.07	4.67	3.79	5.42	4.21	4.25	3.87	3.27	3.71	2.49	2.39
MnO	0.04	0.04	0.04	0.05	0.05	0.07	0.03	0.05	0.02	0.04	0.04	0.02	0.02
MgO	0.32	0.46	0.12	0.25	0.11	0.58	0.36	0.21	0.10	0.23	0.17	0.12	0.03
CaO	1.74	2.15	1.21	1.46	1.36	2.18	1.71	1.53	1.30	1.32	1.16	0.99	0.43
Na ₂ O	3.55	3.20	2.92	2.95	3.17	3.16	3.25	3.25	3.58	3.26	3.04	2.51	3.42
K ₂ O	4.55	4.01	5.20	3.49	4.65	3.93	4.49	4.04	4.21	4.45	4.75	5.03	5.09
P ₂ O ₅	0.09	0.10	0.04	0.05	0.03	0.13	0.09	0.04	0.04	0.04	0.04	0.02	<0.01
LOI	0.70	0.80	0.50	1.60	0.00	0.80	0.70	0.60	0.30	0.50	0.60	2.10	0.70
Total	99.66	99.65	99.69	99.34	99.75	99.62	99.71	99.63	99.43	99.39	99.61	99.75	99.85
Ba	1914	1842	1722	1765	1391	1624	1627	1814	4626	1142	1589	1488	499
Rb	94	101	132	85	134	97	117	120	71	158	127	124	67
Sr	167	169	88	161	96	204	145	173	92	137	101	88	36
Zr	356	465	399	462	393	595	487	502	499	387	432	303	316
Nb	15	19	22	19	16	26	21	24	7	24	26	24	11
Y	27	32	55	35	42	56	48	55	16	50	72	45	26
Hf	9	11	10	12	11	18	13	14	10	12	12	9	9
Ta	1	1	1	6	1	5	1	7	0	8	2	2	1
Th	15	22	14	11	12	10	24	14	5	27	44	19	14
U	4	5	6	3	2	2	4	4	1	6	7	6	3
Ga	18	17	20	19	20	23	18	22	16	21	18	17	17
La	28.4	43.1	43.1	56.7	63.0	81.7	64.4	84.4	29.2	99.0	118.4	68.0	78.0
Ce	78.6	87.0	97.6	107.6	130.5	179.6	130.4	162.7	58.8	203.0	237.3	133.5	148.7
Pr	7.5	10.9	12.3	11.2	15.6	19.5	16.3	17.2	7.0	20.0	27.3	16.4	17.0
Nd	29.4	43.2	51.5	42.3	63.5	77.4	62.5	62.8	28.0	74.1	101.1	61.5	63.0
Sm	5.8	8.1	10.1	8.7	10.7	13.8	10.6	11.6	4.8	12.1	15.2	10.4	8.9
Eu	1.6	2.2	2.2	2.1	2.1	2.4	1.8	2.5	2.7	1.8	1.9	1.6	1.1
Gd	5.2	6.9	10.0	7.0	9.1	10.8	8.9	9.8	3.8	9.3	12.2	8.9	6.6
Tb	0.9	1.1	1.6	1.0	1.4	1.7	1.5	1.5	0.6	1.3	1.9	1.4	0.9
Dy	5.1	5.9	9.5	6.2	7.7	9.8	8.4	9.2	3.0	8.4	10.5	7.9	5.2
Ho	1.0	1.2	1.9	1.3	1.6	2.0	1.6	1.8	0.6	1.7	2.3	1.5	0.9
Er	2.9	3.3	5.4	3.7	4.5	5.6	4.7	5.3	1.9	4.9	6.9	4.4	2.9
Tm	0.5	0.5	0.8	0.5	0.6	0.9	0.7	0.8	0.3	0.7	1.1	0.7	0.4
Yb	3.0	3.1	5.5	3.7	4.4	5.2	4.6	4.8	1.9	4.4	6.9	4.3	2.9
Lu	0.4	0.5	0.8	0.5	0.7	0.7	0.7	0.7	0.3	0.6	1.1	0.6	0.4
FeOt/(FeOt+MgO)	0.91	0.89	0.97	0.94	0.97	0.89	0.91	0.95	0.97	0.93	0.95	0.95	0.99
K ₂ O/Na ₂ O	1.28	1.25	1.78	1.18	1.47	1.24	1.38	1.24	1.18	1.37	1.56	2.00	1.49
Eu/Eu*	0.85	0.86	0.65	0.81	0.63	0.58	0.56	0.68	1.88	0.50	0.41	0.51	0.41
(La/Yb)N	6.88	9.91	5.60	10.90	10.29	11.18	10.13	12.51	11.14	16.07	12.40	11.37	19.03
A/CNK	0.96	0.93	0.99	0.99	0.96	0.92	0.96	1.00	0.97	1.00	0.98	1.00	1.01

BHMzG – Biotite-hornblende monzogranite; HBSG – Hornblende-biotite syenogranite; BHSG – Biotite-hornblende syenogranite; HSG – Hornblende syenogranite; HBMzG – Hornblende-biotite monzogranite; BMzG – Biotite monzogranite; BSG – Biotite syenogranite; HAG – Hornblende alkali-feldspar granite; opx - orthopyroxene; qtz – quartz.

Figure S1: Probability plot for samples of the Planalto Suite.



CAPÍTULO 3

3. CONCLUSÃO

A Suíte Planalto é composta de monzogranito, sienogranito, e álcali-feldspato granito com conteúdos variáveis de biotita e anfibólio. Clinopiroxênio é ausente ou ocorre localmente como cristais reliquiares envoltos por anfibólio.

Dois grupos têm sido distinguidos, tendo por base o comportamento magnético e os minerais óxidos de ferro-titânio: o Grupo 1 mostra baixos valores de suscetibilidade magnética ($SM \leq 0.6247 \times 10^{-3}$ SI) e ilmenita é o único mineral óxido Fe-Ti presente; o Grupo 2, com valores de suscetibilidade magnética moderados ($SM \geq 0.8036 \times 10^{-3}$) e magnetita associada com ilmenita.

Os dados de química mineral revelam que o anfibólio varia entre potássio-hastingsita e cloro-potássio-hastingsita e biotita se aproxima da composição annita. Anfibólio e mica mostram alta razão Fe/(Fe+Mg) (0,84 a 0,94 e 0,75 a 0,91, respectivamente) e são relativamente enriquecidos em Al quando comparados aos mesmos minerais de outros granitos ferrosos. A composição do plagioclásio é geralmente oligoclásio (An_{23-11}) e é similar nos porfiroclastos e nos finos cristais da matriz recristalizada. Grãos neoformados de composição albítica são também observados.

Estudos de petrologia magnética indicam que, o Grupo 1 do Planalto deriva de um magma reduzido que evoluiu em fugacidade de oxigênio abaixo do FMQ, onde o Grupo 2 cristalizou em condições ligeiramente mais oxidantes coincidente com aquelas do FMQ ou ligeiramente acima. Alternativamente, os granitos do Grupo 2 podem também ter sido formados em condições abaixo do FMQ e oxidado durante o estágio *subsolidus* ou metamórfico. Todavia, as condições globais se mantinham reduzidas para ambos os grupos a fim de explicar a alta razão Fe/(Fe+Mg) nos anfibólios, micas, e em rocha total.

As pressões obtidas pelo geobarômetro de Al em hornblenda não são conclusivas em função do caráter fortemente reduzidos dos granitos da Suíte Planalto e o reequilíbrio incerto dos anfibólios. Entretanto, evidências geológicas e petrográficas indicam pressões de 900-700 MPa para a origem dos magmas e pressões de colocação de 500-300 MPa.

O termômetro de saturação de zircão forneceu temperaturas iniciais de 897 a 854 °C e o geotermômetro de Ridolfi et al. (2010) temperaturas entre 910-831 °C, onde o termômetro de saturação de apatita indicou temperaturas muito menores (704-620 °C) para a Suíte Planalto. As temperaturas da apatita foram descartadas porque são muito menores que aquelas

geralmente admitidas para o estágio *solidus* em sistemas graníticos e devem provavelmente refletir a mobilidade do P durante o estágio *subsolidus*. O intervalo de temperatura de 910-850 °C (Table 2.6) foi admitido para a cristalização inicial da Suíte Planalto.

A dominância de anfibólio e biotita entre os minerais máficos da Suíte Planalto e a comum ausência de piroxênio indicam que o conteúdo de água no magma foi superior que 4 wt% podendo atingir mais que 7 % no peso.

A Suíte Planalto mostra fortes analogias mineralógicas e petrográficas com outros granitos ferrosos neoarqueanos da Província Carajás (Complexo Granítico Estrela e Serra do Rabo) e é conclusivo que foram formados em condições muito similares. Composições de anfibólio e biotita do Planalto e Estrela são bastante enriquecidos em Al e se mostram similar nesse aspecto ao pluton Matok nearqueano, localizado no Limpopo Belt. Essas características não são observadas nos granitos tipo-A proterozóicos tomados para comparação nesta pesquisa. Por outro lado, em termos de condição de fugacidade de oxigênio, os granitos Planalto se aproximam do batólito mesoproterozóico Wolf River, aos granitos Rapakivi da Finlândia e aos granitos paleoproterozoicos reduzidos a moderadamente oxidados, Suítes Velho Guilherme e Serra dos Carajás, respectivamente, e difere daqueles granitos oxidados (Suíte Jamon) da Província Carajás e também do Matok. Levando em consideração apenas os parâmetros de cristalização e ambientes geológicos, os granitos Planalto diferem significativamente de alguns exemplos clássicos de granitos tipo-A paleoproterozóico e mesoproterozóico. Por outro lado, mesmo se formando em diferente fugacidade de oxigênio, eles se aproximam em muitas características dos granitoides neoarqueanos Fe-K e Mg-K do Limpopo Belt, como exemplificado pelos granitoides Matok. O fato do Planalto e granitos similares de Carajás terem sido possivelmente formados em um ambiente colisional similar aqueles geralmente admitidos para Limpopo Belt e a íntima associação em ambas províncias com tais granitos e rochas charnockíticas, indicam que o ambiente geológico pode ter uma forte influência na natureza dos magmas granitoides neoarqueanos.

Finalmente, a composição mineralógica de anfibólio e biotita obtida tanto por EDS em MEV, quanto por WDS em Microsonda, são de maneira geral muito similar, levando em consideração apenas os elementos maiores. Si e Al^{IV} são os elementos com variações mais significantes. O Si apresenta teores mais elevados nas análises de EDS em MEV e conseqüentemente menores conteúdos de Al^{IV}. Entretanto, essa pequena variação no sítio octaédrico não provoca mudanças na classificação mineralógica de anfibólio e biotita,

demonstrando que, os conteúdos dos elementos maiores obtidos por EDS em MEV são próximos daqueles obtidos por WDS em Microsonda, portanto, confiáveis (Apêndice D e E).

REFERÊNCIAS

- Almeida J.A.C., Dall'Agnol R., Dias S.B., Althoff F.J. 2010. Origin of the Archean leucogranodiorite-granite suítes: evidence from the Rio Maria terrane and implications for granite magmatismo in the archean. *Lithos*, **120**: 235-257.
- Althoff F.J., Barbey P., Boullier A.M. 2.8-3.0 Ga Plutonism and deformation in the SE Amazonian craton: the Archean granitoids of Marajoara (Carajás Mineral province, Brazil). *Precambrian Research*, **104**: 187-206.
- Barros C.E.M., Dall'Agnol R., Barbey P., Boullier A.M. 1997. Geochemistry of the Estrela Granite Complex, Carajás region, Brazil: an example of an Archean A-type granitoid. *Journal of South American Earth Sciences*, **10**: 321-330.
- Barros C.E.M., Sardinha A.S., Barbosa J.P.O., Macambira M.J.B. 2009. Structure, petrology, geochemistry and zircon U/Pb and Pb/Pb geochronology of the synkinematic Archean (2.7 Ga) A-Type granites from the Carajás Metallogenic Province, northern Brazil. *The Canadian Mineralogist*, **47**:1423-1440.
- Costa J.B.S., Araújo J.B., Santos A., Jorge João X.S., Macambira M.J.B., Lafon J.M.A. 1995. Província Mineral de Carajás: aspectos tectono-estruturais, estratigráficos e geocronológicos. *Boletim Museu Paraense Emílio Goeldi, série Ciências da Terra*, **7**: 199-235.
- Cunha I.R.V. Petrologia Magnética e química mineral dos granitos da Suíte Planalto de Canaã dos Carajás, Província Carajás. Trabalho de Conclusão de Curso – Universidade Federal do Pará, Belém. 109 p.
- Dall'Agnol R., Lafon J.M., Macambira M.J.B. 1994. Proterozoic anorogenic magmatism in the Central Amazonian Province, Amazonian craton; geochronological, petrological and geochemical aspects. *Mineralogy and Petrology* **50**: 113-138.
- Dall'Agnol R., Pichavant M., Champenois M. 1997. Iron-titanium oxide minerals of the Jamon granite, Eastern Amazonian region, Brazil: implications for the oxygen fugacity in Proterozoic A-type granites. *Anais da Academia Brasileira de Ciências*, **69**: 325-347.
- Dall'Agnol R., Scaillet B., Pichavant M. 1999. An experimental study of a lower Proterozoic A-type granite from the eastern Amazonian craton, Brazil. *Journal of Petrology*, **40**: 1673-1698.
- Dall'Agnol R., Oliveira M.A., Almeida J.A.C., Althoff F.J., Leite A.A.S., Oliveira D.C., Barros C.E.M. 2006. Archean and Paleoproterozoic granitoids of the Carajás Metallogenic Province, eastern Amazonian Craton. In: Dall'Agnol, R., Rosa-Costa, L.T., Klein, E.L. (Eds.), Symposium on Magmatism, Crustal Evolution, and Metallogenesis of the Amazonian Craton. Belém, PRONEX-UFPA-SBGNO. 99–150 p. (Volume and Field Trip Guide).
- Dall'Agnol R., Oliveira, D.C. 2007. Oxidized, magnetite-series, rapakivi-type granites of Carajás, Brazil: Implications for classification and petrogenesis of A-type granites. *Lithos*, **93**: 215–233.

- Dall'Agnol R., Teixeira N.P., Rämö O.T., Moura C.A.V., Macambira M.J.B., Oliveira D.C. 2005. Petrogenesis of the paleoproterozoic, rapakivi, A-Type granites of the Archean Carajás Metallogenic Province, Brazil. *Lithos*, **80**: 01-129.
- Dall'Agnol R., Oliveira D.C., Guimarães F.V., Gabriel E.O., Feio G.R.L., Lamarão C.N., Althoff F.J., Santos P.A., Teixeira M.F.B., Silva A.C., Rodrigues D.S., Santos M.J.P., Silva C.R.P., Santos R.D., Santos P.J.L. 2013. Geologia do Subdomínio de Transição do Domínio Carajás – Implicações para a evolução arqueana da Província Carajás - Pará. In: SBG, SIMPÓSIO DE GEOLOGIA DA AMAZÔNIA, 13, Anais, Belém, CDrom.
- Feio G.R.L., Dall'Agnol R., Dantas E., Macambira M.J.B., Gomes A.C.B., Sardinha A.S., Santos P. 2012. Geochemistry, geochronology, and origin of the Planalto granite suite and associated rocks: implications for the Neoproterozoic evolution of the Carajás Province. *Lithos*, **151**: 57-73.
- Feio G.R.L., Dall'Agnol R., Dantas E.L., Macambira M.J.B., Santos J.O.S., Althoff F.J., Soares J.E.B. 2013. Archean granitoid magmatism in the Canaã dos Carajás area: Implications for crustal evolution of the Carajás province, Amazonian craton, Brazil. *Precambrian Research*, **227**: 157-185.
- Frost B.R., Frost C.D., Hulsebosch T.P., Swapp S.M. 2000. Origin of the charnockites of the Louis Lake batholith, Wind River Range, Wyoming. *Journal of Petrology*, **40**: 1771-1802.
- Frost B.R., Frost C.D. 2008. On charnockites. *Gondwana Research*, **13**: 30-44.
- Gabriel E.O., Oliveira D.C. 2013. Petrologia Magnética dos Granodioritos Água Azul e Água Limpa, Porção Sul do Domínio Carajás – Pará. *Geologia - USP, Série Científica*, **13** (4): 89-110.
- Gabriel, E.O., Oliveira, D.C. 2014. Geologia, petrografia e geoquímica dos granitoides arqueanos de alto magnésio da região de Água Azul do Norte, porção sul do Domínio Carajás, Pará. *Boletim do Museu Paraense Emílio Goeldi. Ciências Naturais*, **9** (3): 533-564.
- Gomes A.C.B. 2003. Geologia, Petrografia e Geoquímica dos granitoides de Canaã dos Carajás, SE do Estado do Pará. 2003. 199 f. Dissertação (mestrado) - Universidade Federal do Pará, Centro de Geociências, 160 p.
- Huhn S.B., Macambira M.J.B., Dall'Agnol R. 1999. Geologia e geocronologia Pb/Pb do granito alcalino arqueano planalto, região da Serra do Rabo, Carajás-PA. In: SIMPÓSIO DE GEOLOGIA DA AMAZÔNIA, 6. 1999 Manaus. *Boletim de Resumos Expandidos*. Manaus: SBG-NNO, **1**: 463-466.
- Le Maitre R. W., Streckeisen A., Zanettin B., Le Bas M.J., Bonin B., Bateman P., Bellieni G., Dudek A., Efremova S., Keller J., Lamere J., Sabine P.A., Schmid R., Sorensen H., Woolley A.R. 2002. *Igneous rocks: a classification and glossary of terms, recommendations of the International Union of Geological Sciences, subcommission of the Systematics of Igneous Rocks*. Cambridge University Press. 254 p.
- Leake B.E. 1997. Nomenclature of amphiboles: Report of the Subcommittee on Amphiboles of the International Mineralogical Association Commission on New Minerals and Mineral Names. *Mineral Magazine*, **61**: 295-321.

- Leake B.E., Wooley A.R., Arps C.E.S., Birch W.D., Burke E. A.J., Ferraris G., Grice J. D., Hawthorne F.C., Kisch H.J., Krivovichev V.G., Schumacher J., Stephenson N.C.N., Whittaker E.J.W. 2003. Nomenclature of amphiboles: Additions and revisions to the international mineralogical association's 1997 Recommendations. *The Canadian Mineralogist*, **41**: 1355-1362.
- Moreto C.P.N., Monteiro L.V.S. Xavier R.P., Amaral W.S., Santos T.J.S., Juliani C., Souza Filho C.R. 2011. Mesoarchean (3.0 and 2.86 Ga) host rocks of the iron oxide–Cu–Au Bacaba deposit, Carajás Mineral Province: U–Pb geochronology and metallogenetic implications. *Mineralium Deposita*, **46**: 789–811.
- Oliveira D.C., Santos P.J.L., Gabriel E.O., Rodrigues D.S., Faresin A.C., Silva M.L.T., Sousa S.D., Santos R.V., Silva A.C., Souza M.C., Santos R.D., Macambira M.J.B. 2010. Aspectos geológicos e geocronológicos das rochas magmáticas e metamórficas da região entre os municípios de Água Azul do Norte e Canaã dos Carajás – Província Mineral de Carajás, In: CONGRESSO BRASILEIRO DE GEOLOGIA, 45. 2010, Belém. *Anais... Belém*: SBG, 2010. CDROM.
- Oliveira M.A. 2003. Caracterização petrográfica, estudo de susceptibilidade magnética e natureza dos minerais óxidos de Fe e Ti do Granito Planalto, Serra dos Carajás-PA. Trabalho de Conclusão de Curso – Universidade Federal do Pará, Belém, 47 p.
- Pidgeon R.T., Macambira M.J.B., Lafon J.M. 2000. Th–U–Pb isotopic systems and internal structures of complex zircons from an enderbite from the Pium Complex, Carajás Province, Brazil: evidence for the ages of granulites facies metamorphism and the protolith of the enderbite. *Chemical Geology* **166**: 159–171.
- Rajesh H., Santosh M. 2004. Charnockite magmatism in southern India. *Indian Academy of Sciences-Earth and Planetary Sciences*, **113**: 565-585.
- Rajesh H.M., Santosh M., Wan Y., Liu D., Liu S.J., Belyanin G.A. 2014. Ultrahigh temperature granulites and magnesian charnockites: Evidence for Neoproterozoic accretion along the northern margin of the Kaapvaal Craton. *Precambrian Research*, **246**: 150-159.
- Ricci P.S.F. & Carvalho M.A. 2006. Rocks of the Pium-Area, Carajás Block, Brazil – A Deep seated High-T Gabbroic Pluton (Charnockitoid-Like) with Xenoliths of Enderbitic Gneisses Dated at 3002 Ma – The Basement Problem Revisited. In: *VIII Simpósio de Geologia da Amazônia*, CDroom.
- Rieder M. Nomenclature of the micas. 1998. *Mineralogical Magazine*, **63**: 267-279.
- Rodrigues D.D., Oliveira D.C., Macambira M.J.B. 2014. Geologia, geoquímica e geocronologia do Granito Mesoarqueano Boa Sorte, município de Água Azul do Norte, Pará – Província Carajás. *Boletim do Museu Paraense Emílio Goeldi. Série Ciências da Terra*, **9**: 597-633.
- Santos P.A. 2013. Geologia, petrografia e geoquímica da associação tonalito-trondhjemitogranodiorito (TTG) do extremo leste do Subdomínio de Transição, Província Carajás. Dissertação de mestrado. Universidade Federal do Pará, Belém, 133 p.
- Santos P.A., Teixeira M.F.B., Dall'Agnol R., Guimarães F.V. 2013. Geologia, petrografia e geoquímica da associação tonalito-trondhjemitogranodiorito (TTG) do extremo leste do Subdomínio de Transição, Província Carajás - Pará. *Boletim do Museu Paraense Emílio Goeldi, Ciências Naturais*, **8**: 257-290.

- Santos P.J.L., Oliveira D.C. 2014. Trondhjemitos da área de Nova Canadá: novas ocorrências de associações magmáticas tipo TTG no Domínio Carajás. *Boletim do Museu Paraense Emílio Goeldi. Série Ciências da Terra*, **9**: 635-659.
- Santos R.D., Galarza M.A., Oliveira D.C. 2013. Geologia, geoquímica e geocronologia do Diopsídio-Norito Pium, Província Carajás. *Boletim do Museu Paraense Emílio Goeldi, Série Ciências da Terra*, **8**: 355-382.
- Sardinha A.S., Dall’Agnol R., Gomes A.C.B., Macambira M.J.B., Galarza M.A. 2004. Geocronologia Pb-Pb e U-Pb em zircão de granitóides arqueanos da região de Canaã dos Carajás, Província Mineral de Carajás. In: SBG, CONGRESSO BRASILEIRO DE GEOLOGIA, 42, 2004. CDROM.
- Sardinha A.S., Barros C.E.M., Krymsky R. 2006. Geology, geochemistry, and U-Pb geochronology of the Archean (2.74 Ga) Serra do Rabo granite stocks, Carajás Province, northern Brazil. *Journal of South American Earth Sciences*, **20**: 327-339.
- Silva A.C., Dall’Agnol R., Guimarães F.V., Oliveira D.C. 2014. Geologia, petrografia e geoquímica de Associações Tonalíticas e Trondhjemiticas Arqueanas de Vila Jussara, Província Carajás, Pará. *Boletim do Museu Paraense Emílio Goeldi, Série Ciências Naturais*, **9**: 13-45.
- Silva F.F. 2011. Estudo de suscetibilidade magnética e minerais óxidos de Fe-Ti do magmatismo tipo Planalto da região de vila Feitosa, município de Canaã dos Carajás – Província mineral de Carajás. Marabá. Universidade Federal do Pará. Faculdade de Geologia. (Relatório técnico científico 19).
- Souza Z.S., Dall’Agnol R., Althoff F.J., Leite A.A.S., Barros C.E.M. 1996. Carajás Mineral Province: geological, geochronological and tectonic constrast on the Archean evolution of the Rio Maria Granito-Greenstone Terrain and the Carajás Block. In: SYMPOSIUM ON ARCHEAN TERRANES OF SOUTH AMERICA PLATAFORM, Df, Brasília. *Extended abstracts... SBG*, 31-32 p.
- Streckeisen A.L. 1976. To each plutonic rock its proper name. *Earth Science Reviews*, **12**: 1-33.
- Teixeira M.F.B., Dall’Agnol R., Silva A.C., Santos P.A. 2013. Geologia, petrografia e geoquímica do Leucogranodiorito Pantanal e dos leucogranitos arqueanos da área de Sapucaia, Província Carajás, PA: implicações petrogenéticas. *Boletim do Museu Paraense Emílio Goeldi, Série Ciências Naturais*, **8**: 291-323.
- Vander Auwera J., Bolle O., Dupont A., Pin C., Paquette J.L., Charlier B., Duchesne J.C., Mattielli N., Bogaerts M. 2014. Source-derived heterogeneities in the composite (charnockite-granite) ferroan Farsund intrusion (SW Norway). *Precambrian Research*, **251**: 141-163.
- Vasquez L.V., Rosa-Costa L.R., Silva C.G., Ricci P.F., Barbosa J.O., Klein E.L., Lopes E.S., Macambira E.B., Chaves C.L., Carvalho J.M., Oliveira J.G., Anjos G.C., Silva H.R. 2008. Geologia e recursos minerais do estado do Pará : Sistema de Informações Geográficas – SIG : texto explicativo dos mapas geológico e tectônico e de recursos minerais do estado do Pará. In: VASQUEZ M.L., ROSA-COSTA L.T. (Org.). Escala 1:1.000.000. Belém: CPRM, 2008b.

APÊNDICES

**APÊNDICE A - COORDENADAS DOS PONTOS AMOSTRADOS E ESTUDOS
REALIZADOS**

**TABELA A1 - COORDENADAS UTM DOS PONTOS AMOSTRADOS DA SUÍTE
PLANALTO COM SUAS RESPECTIVAS FÁCIES E ESTUDOS REALIZADOS.**

GR 1	Amostra	Lat (utm)	Long (utm)	Fácies	Petrografiaa	Geoquímicaa	EDS*	WDS**
	AMR-162A	9277660	638533	BHMzG	x			
	AMR-168A	9279020	637230					
	AMR-168B	9279020	637230					
	AMR-117G	9278502	628513					
	AMR-164A	9277992	638005					
	AMR-138	9292562	636407		x			
	AMR-149*	9289065	635459	HBMzG	x	x	x	x
	AMR-98A	9278352	635470	BHLSG	x			
	AMR-96	9278407	634664					
	AMR-179	9275100	633100					
	AMR-120A	9278935	628526					
	ARC-147*	9274442	606358	BHMzG	x	x	x	x
	AMR-117L	9278502	628513					
	AMR-166A	9270664	637370					
	AMR-133A	9291443	634670					
	AMR-137B	9292242	636202	HBSG	x			
	AMR-158	9276353	640662					
	AMR-116*	9278486	628384	BHSG	x	x	x	x
	AMR-136	9292978	635682					
	AMR-209	9279300	628526	BHMzG	x	x	x	
	AMR-167	9278953	637335					
	AMR-118H	9278962	628454	HBSG	x		x	
	AMR-142	9293020	637472					
	AMR-97	9278220	635079					
	ARC-110	9277068	613291	BHSG	x			
	AMR-151A	9290599	635933		x			
	AMR-118A	9278962	628454	BHMzG	x			
	AMR-145	9274074	605851	BHSG	x	x		
	AMR-166B	9270664	637370					
	AMR-94A	9278263	633657	HLMzG	x			
	AMR-117J	9278502	628513	BHSG	x			
	ARC-147	9274442	606358	BHMzG	x		x	
	ARF-24	9276960	613129	BHSG	x			
	AMR-135	9293026	635620	BHMzG	x			
	ARF-20	9276459	614188	HBSG	x			
	ARC-144	9273578	605787	BHMzG	x	x	x	
	ARF-25	9277290	612216		x			

Em negrito, amostras com análise química e razões FeOt/(FeOt+MgO) em rocha total; * análises por

**Microsonda Eletrônica e *Microscopia Eletrônica de Varredura. GR 1 = Granitos do Grupo 1.

GR 2	Amostra	Lat (utm)	Long (utm)	fácies	Petrografia	Geoquímica	EDS*	WDS**
	ARF-19	9276322	614338		x			
	AMR-170A	9280061	637472					
	AMR-151B	9290599	635933	BHMzG	x			
	ARF-22	9277142	614067	HBMzG	x			
	AC-4b	9292002	637683	HBSG	x	x		
	AMR-140*	9292743	636790	BHMzG	x	x	x	x
	AC-16	9290700	638551	BHSG	x			
	AMR-91B	9277978	631883					
	AMR-142A	9293020	637472					
	AMR-150	9288802	635498	HBLSG	x			
	ARF-17	9274390	614912	HBSG	x			
	AMR-141B	9293020	637472	BHMzG	x			
	AMR-151D	9290599	635933		x			
	AMR-85B	9275609	631255	HSG	x			
	AER-82A	9290425	636606	BHMzG	x			
	AMR-134A	9291590	634898					
	ARC-109*	9275089	612681	HBSG	x	x	x	x
	AMR-171C	9280270	637474	BSG	x			
	GFMF-06	9278170	610082	HBSG				
	AMR-172B	9280852	637330					
	AMR-155A	9290473	637546	HBAG	x			
	AMR-177	9276120	631990	HAG	x	x	x	
	AMR-153A	9290489	636557					
	AMR-152A	9290767	636356	BHMzG	x	x	x	
	ARC-141B	9272693	605534	BMzG	x			
	AMR-85A*	9275609	631255	HSG	x	x	x	x
	AMR-141A	9293020	637472					
	AMR-171	9280270	637474	BSG	x	x		
	AC-6A	9291837	636908	BHMzG	x			
	ARC-77	9291660	618604	BSG	x	x		
	AMR-146	9290069	635479	BHMzG	x			
	AMR-152B	9290767	636356	BHMzG	x			
	AMR-155B	9290473	637546	BHMzG	x			
	AER-72A	927437	638281	BMzG	x	x		
	AMR-137A*	9292242	636202	BHSG	x	x	x	x
	ARF-18	9276202	614553	HBSG	x			
	AMR-154A	9290459	637354	BHSG	x			
	ARC-104	9276039	614340	BMzG	x	x		
	ARC-112B	9278376	609428	BMzG	x			
	ARC-148	9276313	606238	HBMzG	x			

Em negrito, amostras com análise química e razões FeOt/(FeOt+MgO) em rocha total; * análises por **Microsonda Eletrônica e *Microscopia Eletrônica de Varredura. GR 2 = Granitos do Grupo 2.

APÊNDICE B - TABELAS COM ANÁLISES QUÍMICAS POR EDS EM MICROSCOPIA ELETRÔNICA DE VARREDURA DA SUÍTE PLANALTO.

APÊNDICE B.1 – ANÁLISES QUÍMICAS DE ANFIBÓLIO DA SUÍTE PLANALTO EM MICROSCOPIA ELETRÔNICA DE VARREDURA.

Amostra	AMR-147															
	C1_1.1	C1_1.2	C1_1.3	C1_1.4	C1_1.5	C1_1.6	C2_2.1	C2_2.2	C2_3.1	C2_3.2	C2_3.3	C2_3.4	C2_3.5	C2_3.6	C1_1.1	C1_1.2
Análise Mineral	Fprg	Fprg	Fprg	Fprg	Fprg	Fprg	Fprg	Fprg	Fprg	Fprg	Fprg	Fprg	Fprg	Fprg	Fprg	Fprg
SiO ₂	49,452	49,073	49,751	49,086	49,255	49,204	48,953	49,471	49,493	48,956	49,073	49,159	49,155	49,435	49,054	49,020
TiO ₂	0,939	0,696	0,947	0,891	0,872	0,911	0,782	0,824	0,976	0,797	0,862	0,852	0,867	0,907	0,912	0,792
Al ₂ O ₃	14,579	14,814	14,536	14,322	14,587	14,579	14,421	14,224	14,663	14,842	14,627	14,583	14,646	14,336	14,982	14,836
FeO	36,615	36,640	36,302	36,293	36,328	36,005	36,337	36,309	35,823	36,200	35,897	35,985	35,940	36,341	36,825	36,901
MgO	2,304	2,248	2,426	2,363	2,435	2,416	2,187	2,237	2,540	2,447	2,543	2,329	2,285	2,301	1,635	1,621
MnO	0,425	0,548	0,548	0,567	0,560	0,567	0,469	0,501	0,557	0,573	0,514	0,513	0,504	0,548	0,564	0,501
CaO	13,778	13,756	13,478	13,697	13,600	13,777	13,736	13,557	13,478	13,767	13,623	13,568	13,458	13,765	13,806	13,750
Na ₂ O	1,411	1,182	1,570	1,467	1,514	1,336	1,340	1,212	1,445	1,387	1,397	1,283	1,367	1,236	1,122	1,153
K ₂ O	3,111	3,202	3,013	3,048	3,050	3,085	3,184	2,997	3,095	3,054	3,045	3,049	3,080	3,045	3,287	3,115
TOTAL	122,616	122,157	122,572	121,733	122,203	121,879	121,409	121,332	122,068	122,022	121,581	121,321	121,300	121,914	122,187	121,689
Número de cátions baseado em 23 átomos de oxigênio																
Si	6,318	6,285	6,339	6,319	6,303	6,317	6,327	6,369	6,325	6,273	6,304	6,328	6,330	6,344	6,307	6,322
Al ^{IV}	1,682	1,715	1,661	1,681	1,697	1,683	1,673	1,631	1,675	1,727	1,696	1,672	1,670	1,656	1,693	1,678
Soma T	8	8	8	8	8	8	8	8	8	8	8	8	8	8	8	8
Al ^{VI}	0,513	0,521	0,522	0,492	0,503	0,523	0,524	0,527	0,534	0,515	0,518	0,541	0,553	0,513	0,578	0,577
Fe ³⁺	0,360	0,469	0,401	0,372	0,423	0,357	0,332	0,409	0,400	0,435	0,416	0,402	0,389	0,376	0,316	0,347
Ti	0,090	0,067	0,091	0,086	0,084	0,088	0,076	0,080	0,094	0,077	0,083	0,083	0,084	0,088	0,088	0,077
Mg	0,439	0,429	0,461	0,453	0,465	0,462	0,421	0,429	0,484	0,467	0,487	0,447	0,439	0,440	0,313	0,312
Mn	0,046	0,059	0,059	0,062	0,061	0,062	0,051	0,055	0,060	0,062	0,056	0,056	0,055	0,060	0,061	0,055
Fe ²⁺	3,552	3,454	3,467	3,534	3,465	3,508	3,595	3,500	3,428	3,444	3,440	3,471	3,481	3,524	3,643	3,633
Soma C	5	5	5	5	5	5	5	5	5	5	5	5	5	5	5	5
Ca	1,886	1,887	1,840	1,889	1,865	1,895	1,902	1,870	1,845	1,890	1,875	1,871	1,857	1,893	1,902	1,900
Na	0,114	0,113	0,160	0,111	0,135	0,105	0,098	0,130	0,155	0,110	0,125	0,129	0,143	0,107	0,098	0,100
Soma B	2	2	2	2	2	2	2	2	2	2	2	2	2	2	2	2
Na	0,235	0,181	0,228	0,255	0,240	0,227	0,238	0,172	0,204	0,235	0,222	0,192	0,198	0,200	0,181	0,188
K	0,507	0,523	0,490	0,500	0,498	0,505	0,525	0,492	0,504	0,499	0,499	0,501	0,506	0,499	0,539	0,512
Soma A	0,742	0,704	0,717	0,755	0,738	0,733	0,763	0,665	0,708	0,734	0,721	0,692	0,704	0,699	0,721	0,700
Fe/(Fe+Mg)	0,890	0,889	0,883	0,886	0,882	0,884	0,895	0,891	0,876	0,880	0,876	0,886	0,888	0,889	0,921	0,921
Mg/(Mg+Fe)	0,110	0,111	0,117	0,114	0,118	0,116	0,105	0,109	0,124	0,120	0,124	0,114	0,112	0,111	0,079	0,079

(Continuação)

Amostra	AMR-149														
	C1_2.1	C1_2.2	C1_2.3	C1_2.-4	C1_2.5	C1_2.6	C2_1.1	C2_3.1	C2_3.2	C2_3.3	C2_3.4	C2_3.5	C3_1.1	C3_1.2	C3_1.3
Análise Mineral	Fprg	Fprg	Fprg	Fprg	Fprg	Fprg	Hst	Fprg	Fprg	Hst	Fprg	Fprg	Fprg	Fprg	Fprg
SiO ₂	48,175	48,637	48,519	48,705	49,512	49,199	49,880	49,478	48,288	49,585	49,768	48,883	48,577	48,502	48,453
TiO ₂	0,500	0,454	0,435	0,427	0,804	0,904	1,121	1,288	0,642	1,268	1,181	0,973	1,216	1,213	1,036
Al ₂ O ₃	15,957	15,432	15,330	15,460	14,814	14,474	12,340	12,937	15,095	13,015	12,934	13,996	14,678	14,538	15,016
FeO	37,369	37,544	37,455	37,152	37,274	37,249	37,966	37,839	37,736	38,282	37,405	37,460	36,965	36,688	37,364
MgO	1,179	1,461	1,464	1,399	1,489	1,575	1,905	1,631	1,355	1,698	1,926	1,499	1,084	1,459	1,379
MnO	0,502	0,575	0,650	0,535	0,542	0,589	0,568	0,594	0,557	0,691	0,677	0,537	0,213	0,222	0,319
CaO	13,791	13,683	13,645	13,655	13,674	13,721	13,695	13,579	13,732	13,638	13,529	13,841	13,306	13,104	13,164
Na ₂ O	0,984	1,208	1,316	1,049	1,196	1,109	1,256	1,294	1,039	1,228	1,336	1,134	1,228	1,698	1,417
K ₂ O	3,623	3,398	3,356	3,489	3,183	3,248	2,683	2,784	3,503	3,063	2,889	3,003	3,314	2,985	3,237
TOTAL	122,080	122,390	122,169	121,870	122,487	122,068	121,414	121,424	121,946	122,467	121,645	121,325	120,581	120,409	121,384
Número de cátions baseado em 23 átomos de oxigênio															
Si	6,214	6,246	6,247	6,278	6,346	6,337	6,463	6,415	6,240	6,382	6,430	6,347	6,347	6,331	6,268
Al ^{IV}	1,786	1,754	1,753	1,722	1,654	1,663	1,537	1,585	1,760	1,618	1,570	1,653	1,653	1,669	1,732
Soma T	8	8	8	8	8	8	8	8	8	8	8	8	8	8	8
Al ^{VI}	0,639	0,582	0,573	0,627	0,584	0,534	0,347	0,392	0,538	0,356	0,399	0,489	0,607	0,568	0,557
Fe ³⁺	0,396	0,461	0,451	0,405	0,342	0,357	0,411	0,384	0,457	0,446	0,386	0,341	0,218	0,271	0,436
Ti	0,049	0,044	0,042	0,041	0,077	0,088	0,109	0,126	0,062	0,123	0,115	0,095	0,119	0,119	0,101
Mg	0,227	0,280	0,281	0,269	0,284	0,302	0,368	0,315	0,261	0,326	0,371	0,290	0,211	0,284	0,266
Mn	0,055	0,063	0,071	0,058	0,059	0,064	0,062	0,065	0,061	0,075	0,074	0,059	0,024	0,025	0,035
Fe ²⁺	3,634	3,571	3,582	3,600	3,654	3,655	3,703	3,718	3,620	3,674	3,655	3,726	3,820	3,734	3,605
Soma C	5	5	5	5	5	5	5	5	5	5	5	5	5	5	5
Ca	1,906	1,883	1,882	1,886	1,878	1,893	1,901	1,886	1,901	1,881	1,873	1,925	1,863	1,833	1,824
Na	0,094	0,117	0,118	0,114	0,122	0,107	0,099	0,114	0,099	0,119	0,127	0,075	0,137	0,167	0,176
Soma B	2	2	2	2	2	2	2	2	2	2	2	2	2	2	2
Na	0,152	0,183	0,211	0,148	0,175	0,170	0,217	0,211	0,161	0,187	0,207	0,211	0,174	0,262	0,180
K	0,596	0,557	0,551	0,574	0,520	0,534	0,443	0,460	0,577	0,503	0,476	0,497	0,552	0,497	0,534
Soma A	0,748	0,740	0,762	0,721	0,695	0,704	0,660	0,672	0,739	0,690	0,683	0,708	0,726	0,759	0,714
Fe/(Fe+Mg)	0,941	0,927	0,927	0,930	0,928	0,924	0,910	0,922	0,933	0,919	0,908	0,928	0,948	0,929	0,931
Mg/(Mg+Fe)	0,059	0,073	0,073	0,070	0,072	0,076	0,090	0,078	0,067	0,081	0,092	0,072	0,052	0,071	0,069

(Continuação)

Amostra	AMR-118-H												AMR-140		
	C4_2.1	C4_2.2	C4_2.3	C4_2.4	C1_2.1	C1_2.2	C1_2.3	C1_2.4	C1_2.5	C5_1.1	C5_1.2	C5_1.3	C4_1.1	C4_1.2	C4_1.3
Análise Mineral	Fprg	Fprg	Fprg	Fprg	Hst	Fprg	Fprg	Fprg	Fprg	Fprg	Fprg	Fprg	Fprg	Fprg	Fprg
SiO ₂	48,695	47,542	47,738	47,554	46,587	47,272	47,770	47,655	48,106	50,658	49,424	49,411	48,408	48,215	49,542
TiO ₂	0,927	0,726	0,757	0,724	1,056	0,842	0,907	0,916	1,124	0,956	0,754	0,692	0,410	0,527	0,817
Al ₂ O ₃	16,049	17,245	16,325	16,240	15,509	15,913	14,594	15,857	14,893	13,342	13,920	14,105	15,656	15,838	13,994
FeO	36,170	35,914	36,492	36,903	37,961	37,666	37,986	37,845	37,386	36,935	37,054	36,947	36,402	35,681	36,471
MgO	1,328	1,184	1,180	0,907	0,912	1,096	1,154	0,736	1,311	2,086	1,900	1,890	1,679	1,651	1,993
MnO	0,261	0,240	0,195	0,252	0,284	0,252	0,283	0,238	0,336	0,575	0,599	0,589	0,642	0,669	0,581
CaO	13,221	13,067	13,262	13,066	13,137	13,368	13,393	13,613	13,098	13,497	13,614	13,361	13,378	13,123	13,470
Na ₂ O	1,339	1,312	1,270	1,150	1,015	1,281	1,519	1,047	1,593	1,391	1,297	1,148	1,167	1,076	1,225
K ₂ O	3,189	3,839	3,613	3,638	3,531	3,599	2,902	3,723	3,083	2,137	2,706	2,937	3,163	3,119	2,773
TOTAL	121,178	121,068	120,832	120,434	119,992	121,290	120,510	121,630	120,930	121,576	121,267	121,081	120,906	119,899	120,866
Número de cátions baseado em 23 átomos de oxigênio															
Si	6,283	6,155	6,207	6,203	6,117	6,145	6,249	6,197	6,254	6,483	6,379	6,375	6,252	6,259	6,402
Al ^{IV}	1,717	1,845	1,793	1,797	1,883	1,855	1,751	1,803	1,746	1,517	1,621	1,625	1,748	1,741	1,598
Soma T	8	8	8	8	8	8	8	8	8	8	8	8	8	8	8
Al ^{VI}	0,724	0,786	0,708	0,700	0,518	0,583	0,499	0,627	0,535	0,495	0,497	0,519	0,635	0,682	0,532
Fe ³⁺	0,299	0,329	0,323	0,407	0,611	0,464	0,450	0,323	0,431	0,443	0,443	0,508	0,517	0,518	0,414
Ti	0,090	0,071	0,074	0,071	0,104	0,082	0,089	0,090	0,110	0,092	0,073	0,067	0,040	0,051	0,079
Mg	0,255	0,228	0,229	0,176	0,179	0,212	0,225	0,143	0,254	0,398	0,366	0,364	0,323	0,320	0,384
Mn	0,029	0,026	0,021	0,028	0,032	0,028	0,031	0,026	0,037	0,062	0,065	0,064	0,070	0,074	0,064
Fe ²⁺	3,604	3,559	3,644	3,618	3,558	3,631	3,706	3,792	3,633	3,510	3,556	3,478	3,414	3,355	3,527
Soma C	5	5	5	5	5	5	5	5	5	5	5	5	5	5	5
Ca	1,828	1,812	1,847	1,826	1,848	1,862	1,877	1,896	1,824	1,850	1,883	1,847	1,851	1,825	1,865
Na	0,172	0,188	0,153	0,174	0,152	0,138	0,123	0,104	0,176	0,150	0,117	0,153	0,149	0,175	0,135
Soma B	2	2	2	2	2	2	2	2	2	2	2	2	2	2	2
Na	0,162	0,142	0,167	0,117	0,106	0,184	0,262	0,160	0,226	0,196	0,207	0,134	0,143	0,096	0,172
K	0,525	0,634	0,599	0,605	0,591	0,597	0,484	0,618	0,511	0,349	0,445	0,483	0,521	0,516	0,457
Soma A	0,687	0,776	0,766	0,722	0,698	0,781	0,747	0,778	0,737	0,544	0,652	0,617	0,665	0,612	0,629
Fe/(Fe+Mg)	0,934	0,940	0,941	0,954	0,952	0,945	0,943	0,964	0,935	0,898	0,907	0,905	0,913	0,913	0,902

APÊNDICE B.2 - ANÁLISES QUÍMICAS DE BIOTITA DA SUÍTE PLANALTO EM MICROSCOPIA ELETRÔNICA DE VARREDURA

Amostra	ARC-140								AMR-118H								
Análise Mineral	C1_2.1 Bt	C1_2.2 Bt	C1_2.3 Bt	C1_2.4 Bt	C2_1.1 Bt	C2_1.2 Bt	C2_1.3 Bt	C3_1.1 Bt	C3_1.2 Bt	C3_1.3 Bt	C4_1.1 Bt	C4_1.2 Bt	C4_1.3 Bt	C1_1.1 Bt	C1_1.2 Bt	C1_1.3 Bt	C1_1.4 Bt
SiO₂	20,961	21,138	21,351	21,448	21,511	21,266	21,172	20,76	20,49	20,656	20,57	20,69	20,624	19,37	20,6	19,69	20,2
TiO₂	1,206	1,284	1,591	1,569	1,586	1,394	1,468	2,308	2,199	2,056	2,335	2,338	2,306	1,926	2,531	2,489	2,282
Al₂O₃	10,132	10,657	10,428	10,279	10,259	9,853	10,093	9,078	9,191	9,321	9,216	9,274	9,139	9,13	8,731	8,653	8,848
FeO	28,521	27,522	28,190	27,963	27,565	28,725	28,205	30,65	30,3	30,046	30,62	30,13	30,32	32,38	32,07	31,86	31,54
MgO	2,214	2,257	2,223	2,066	2,296	2,218	2,429	1,394	1,345	1,435	1,322	1,541	1,364	1,296	1,181	1,194	1,266
MnO	0,301	0,338	0,328	0,375	0,330	0,365	0,312	0,161	0,139	0,188	0,127	0,114	0,169	0,191	0,213	0,206	0,224
CaO	0,077	0,064	0,024	0,034	0,047	0,064	0,039	0,059	0,125	0,053	0,065	0,046	0,046	0,11	0,06	0,049	0,029
Na₂O	0,098	0,151	0,205	0,078	0,151	0,134	0,203	0,094	0,222	0,14	0,061	0,117	0,049	0,083	0,137	0,052	0,116
K₂O	9,773	9,971	10,335	10,116	10,193	10,219	10,153	9,405	9,599	9,533	9,257	9,486	9,468	7,897	9,722	9,022	9,229
TOTAL	73,283	73,382	74,675	73,928	73,938	74,238	74,074	73,910	73,617	73,428	73,571	73,732	73,485	72,381	75,243	73,210	73,741
Número de cátions baseado em 22 átomos de oxigênio																	
Si	5,776	5,758	5,755	5,816	5,816	5,809	5,766	5,782	5,747	5,7749	5,752	5,754	5,7728	5,599	5,734	5,653	5,717
Al^{IV}	2,224	2,242	2,245	2,184	2,184	2,191	2,234	2,218	2,253	2,2251	2,248	2,246	2,2272	2,401	2,266	2,347	2,283
Soma T	8	8	8	8	8	8	8	8	8	8	8	8	8	8	8	8	8
Al^{VI}	0,682	0,780	0,681	0,717	0,703	0,610	0,628	0,414	0,43	0,4877	0,435	0,439	0,4358	0,347	0,265	0,24	0,323
Fe	3,953	3,771	3,822	3,813	3,748	3,946	3,864	4,293	4,274	4,2248	4,307	4,214	4,2684	4,709	4,491	4,6	4,489
Ti	0,195	0,205	0,251	0,249	0,251	0,223	0,234	0,377	0,362	0,3371	0,383	0,381	0,3785	0,327	0,413	0,419	0,379
Mg	0,705	0,710	0,692	0,647	0,717	0,700	0,764	0,449	0,436	0,4635	0,427	0,495	0,4411	0,433	0,38	0,396	0,414
Mn	0,042	0,047	0,045	0,052	0,046	0,051	0,043	0,023	0,02	0,0269	0,018	0,016	0,0242	0,028	0,03	0,03	0,032
Soma C	5,577	5,513	5,492	5,479	5,465	5,530	5,534	5,556	5,521	5,54	5,570	5,546	5,5479	5,843	5,58	5,685	5,637
Ca	0,015	0,012	0,005	0,006	0,009	0,012	0,007	0,012	0,025	0,0104	0,013	0,009	0,009	0,022	0,012	0,01	0,006
Na	0,033	0,050	0,068	0,026	0,050	0,045	0,068	0,032	0,076	0,0478	0,021	0,04	0,0168	0,029	0,047	0,018	0,04
K	1,935	1,951	2,001	1,971	1,98	2,005	1,9865	1,882	1,934	1,9146	1,86	1,895	1,9038	1,64	1,945	1,861	1,876
Fe/(Fe+Mg)	0,849	0,841	0,847	0,855	0,839	0,849	0,835	0,905	0,907	0,9011	0,910	0,895	0,9063	0,916	0,922	0,921	0,916

(continuação)

Amostra	AMR-149													AMR-147								
	C1_1.1	C1_1.2	C1_1.3	C1_1.4	C1_2.1	C1_2.2	C1_2.3	C1_2.4	C1_2.5	C2_2.1	C2_2.2	C2_2.3	C2_2.4	C1_2.1	C1_2.2	C1_2.3	C1_2.4	C1_2.5	C2_2.1	C2_2.2	C2_2.3	
Análise Mineral	Bt	Bt	Bt	Bt	Bt	Bt	Bt	Bt	Bt	Bt	Bt	Bt	Bt	Bt	Bt	Bt	Bt	Bt	Bt	Bt	Bt	Bt
SiO ₂	21,07	20,896	21,06	20,81	20,46	19,587	20,57	20,969	20,271	20,26	20,933	20,566	20,941	21,62	21,589	21,38	21,68	21,55	21,508	21,75	21,62	
TiO ₂	1,641	1,539	1,609	1,474	1,455	1,266	1,436	1,447	1,324	1,361	1,602	1,412	1,46	1,815	1,669	1,966	1,786	1,837	1,391	1,457	1,39	
Al ₂ O ₃	9,095	9,167	8,874	9,055	8,992	9,213	9,06	8,955	8,98	9,182	8,901	9,399	9	9,353	9,401	9,168	9,219	8,9	9,407	9,016	9,18	
FeO	30,73	30,305	30,72	31,05	31,81	33,528	31,78	31,507	32,582	31,95	31,016	30,967	31,188	27,51	27,403	28,8	27,98	28,47	27,921	28,01	28,45	
MgO	2,097	1,952	2,041	2,057	2,101	2,116	2,124	1,952	1,879	2,262	2,146	2,505	2,205	2,995	3,061	3	3,145	3,052	3,164	3,224	3,151	
MnO	0,437	0,331	0,316	0,352	0,347	0,407	0,291	0,355	0,393	0,368	0,354	0,349	0,329	0,256	0,235	0,276	0,403	0,275	0,294	0,267	0,199	
CaO	0,01	0,095	0,019	0,04	0,069	0,112	0,106	0,048	0,07	0,218	0,109	0,068	0,049	0,091	0,069	0,056	0,083	0,04	0,047	0,055	0,126	
Na ₂ O	0,125	0,102	0,095	0,109	0,144	0,061	0,073	0,041	0,054	0,104	0,055	0,301	0,118	0,072	0,069	0,105	0,14	0,076	0,159	0,097	0,167	
K ₂ O	9,56	9,742	9,573	9,29	9,242	7,702	9,248	9,636	8,522	8,578	10,116	8,902	9,698	10,23	9,95	10,43	10,08	10,26	9,853	9,981	9,763	
TOTAL	74,765	74,129	74,306	74,234	74,618	73,992	74,681	74,910	74,075	74,281	75,232	74,469	74,988	73,942	73,446	75,179	74,515	74,455	73,744	73,858	74,051	
Número de cátions baseado em 22 átomos de oxigênio																						
Si	5,803	5,804	5,839	5,789	5,717	5,5643	5,728	5,8085	5,7161	5,669	5,7821	5,6883	5,7849	5,86	5,8696	5,783	5,851	5,86	5,8522	5,913	5,876	
Al ^{IV}	2,197	2,196	2,161	2,211	2,283	2,4357	2,272	2,1915	2,2839	2,331	2,2179	2,3117	2,2151	2,14	2,1304	2,217	2,149	2,14	2,1478	2,087	2,124	
Soma T	8	8	8	8	8	8	8	8	8	8	8	8	8	8	8	8	8	8	8	8	8	
Al ^{VI}	0,41	0,4547	0,401	0,411	0,333	0,2889	0,355	0,3908	0,3521	0,344	0,3415	0,3945	0,373	0,498	0,5303	0,366	0,44	0,38	0,5168	0,465	0,473	
Fe	4,256	4,2335	4,285	4,343	4,472	4,7904	4,451	4,3895	4,6208	4,496	4,3088	4,3077	4,3331	3,748	3,7471	3,918	3,797	3,894	3,8209	3,83	3,889	
Ti	0,265	0,2507	0,262	0,24	0,238	0,2109	0,235	0,235	0,2189	0,223	0,2595	0,229	0,2365	0,288	0,2661	0,312	0,283	0,293	0,2219	0,232	0,221	
Mg	0,667	0,6264	0,654	0,661	0,678	0,6945	0,683	0,6247	0,6122	0,731	0,6849	0,8005	0,7038	0,938	0,9615	0,938	0,981	0,959	0,9947	1,013	0,989	
Mn	0,062	0,047	0,045	0,05	0,05	0,0591	0,041	0,0503	0,0567	0,053	0,05	0,0494	0,0465	0,035	0,0327	0,038	0,056	0,038	0,0409	0,037	0,028	
Soma C	5,66	5,6122	5,645	5,705	5,771	6,0437	5,766	5,6903	5,8607	5,847	5,6447	5,7811	5,6929	5,508	5,5377	5,572	5,556	5,564	5,5952	5,577	5,6	
Ca	0,002	0,0185	0,004	0,008	0,014	0,0223	0,021	0,0093	0,0138	0,043	0,0211	0,0132	0,0095	0,017	0,0131	0,011	0,016	0,008	0,009	0,01	0,024	
Na	0,042	0,0346	0,032	0,037	0,049	0,0212	0,025	0,0139	0,0186	0,036	0,0186	0,1017	0,0398	0,024	0,0229	0,035	0,046	0,025	0,0529	0,032	0,055	
K	1,891	1,9439	1,907	1,856	1,856	1,5718	1,85	1,9175	1,7263	1,724	2,0073	1,7688	1,9246	1,992	1,9434	2,028	1,954	2,005	1,9259	1,949	1,906	
Fe/(Fe+Mg)	0,864	0,8711	0,868	0,868	0,868	0,8734	0,867	0,8754	0,883	0,86	0,8629	0,8433	0,8603	0,8	0,7958	0,807	0,795	0,802	0,7934	0,791	0,797	

APÊNDICE C - TABELAS COM ANÁLISES QUÍMICAS POR WDS EM MICROSSONDA ELETRÔNICA DA SUÍTE PLANALTO.

APÊNDICE C.1: ANÁLISES QUÍMICAS DE PLAGIOCLÁSIO DA SUÍTE PLANALTO EM MICROSSONDA ELETRÔNICA.

Amostra	AMR-140		AMR-149		ARC-109		AMR-85A		ARC-147		AMR-137A
	C6_1.3	C6_1.4	C5_1.3	C5_5	C5_1.3	C4_1.4	C6_1.1	C6_2	C3_1.1	C4_1.2	C5_1.4
tipo	olig	olig	alb	alb R	olig	olig R	olig	olig R	olig	olig	olig
SiO ₂	64,84	64,62	64,84	64,84	63,87	62,21	64,37	64,60	64,21	63,64	64,91
Al ₂ O ₃	21,99	21,89	20,81	20,27	22,12	23,28	22,03	22,00	22,10	22,43	21,69
FeO	0,09	0,03	0,03	0,00	0,08	0,03	0,00	0,03	0,00	0,00	0,08
CaO	2,23	2,11	1,21	0,81	3,06	4,41	2,92	2,76	2,71	3,08	2,33
Na ₂ O	10,76	10,51	11,35	11,49	9,90	9,27	10,47	10,22	10,19	10,16	10,43
K ₂ O	0,06	0,08	0,10	0,12	0,15	0,21	0,16	0,15	0,22	0,13	0,15
TOTAL	99,96	99,24	98,34	97,52	99,18	99,41	99,94	99,76	99,43	99,44	99,58
Si	11,43	11,46	11,60	11,68	11,36	11,09	11,38	11,41	11,39	11,30	11,48
Al	4,57	4,57	4,38	4,30	4,63	4,89	4,58	4,58	4,62	4,69	4,52
Fe	0,01	0,00	0,00	0,00	0,01	0,00	0,00	0,01	0,00	0,00	0,01
Ca	0,42	0,40	0,23	0,16	0,58	0,84	0,55	0,52	0,52	0,59	0,44
Na	3,68	3,61	3,93	4,01	3,41	3,20	3,59	3,50	3,50	3,50	3,58
K	0,01	0,02	0,02	0,03	0,03	0,05	0,04	0,03	0,05	0,03	0,03
Cátions	20,12	20,07	20,20	20,19	20,04	20,08	20,13	20,07	20,07	20,11	20,06
Sítio T	15,99	16,03	15,98	15,98	16,00	15,98	15,96	15,99	16,00	15,99	16,00
Sítio M	4,13	4,04	4,19	4,20	4,04	4,10	4,17	4,06	4,07	4,11	4,06
Albita	89	90	94	96	85	78	86	86	86	85	88
Anortita	10	10	6	4	15	21	13	13	13	14	11
Orthoclásio	0	0	1	1	1	1	1	1	1	1	1

*Complementam as análises apresentadas no Capítulo 2.

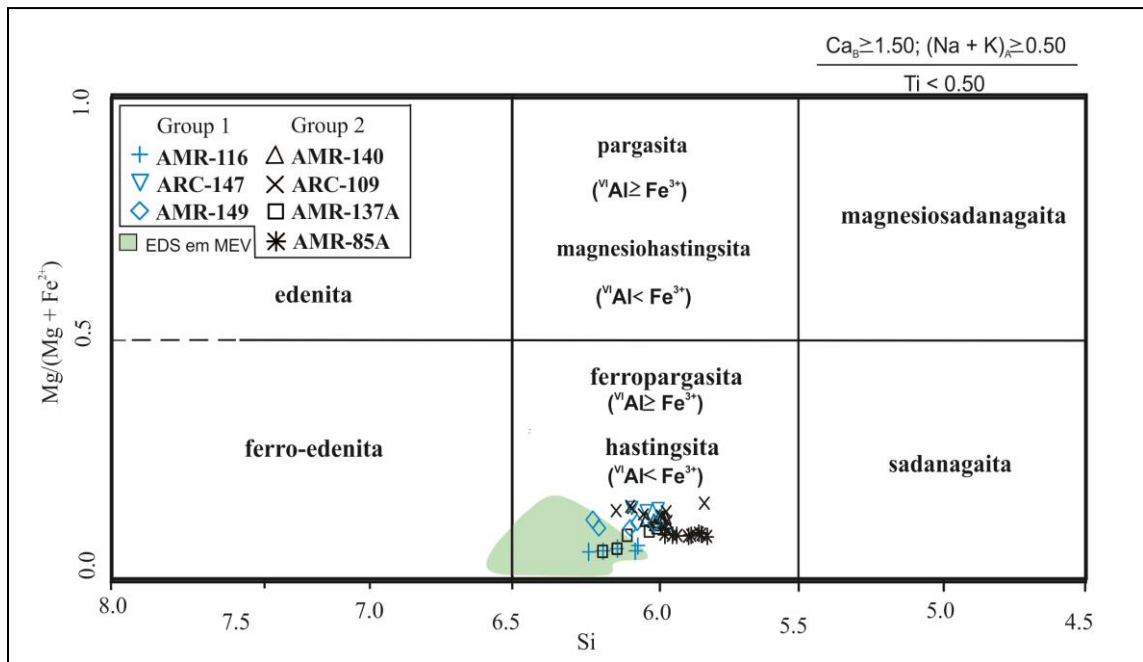
APÊNDICE C.2 - ANÁLISES QUÍMICAS DE ILMENITA E MAGNETITA DA SUÍTE PLANALTO EM MICROSSONDA ELETRÔNICA.

Sample	AMR149	AMR-85A		ARC-109	AMR-140	AMR-85A									
Mineral	Ilm	Ilm	Ilm	Ilm	Mgt	Mgt	Mgt	Mgt	Mgt	Mgt	Mgt	Mgt	Mgt	Mgt	Mgt
SiO ₂	0,03	0,05	0,02	0,01	0,11	0,05	0,05	0,05	0,08	0,12	0,08	0,03	0,03	0,07	0,03
TiO ₂	53,14	50,68	51,10	48,46	0,00	0,16	0,53	0,25	0,00	0,00	0,13	0,01	0,00	0,00	0,00
Al ₂ O ₃	0,00	0,00	0,00	0,00	0,04	0,05	0,07	0,07	0,10	0,11	0,07	0,17	0,09	0,10	0,11
FeO	41,24	47,37	47,49	47,59	90,42	92,06	91,74	92,04	92,17	92,12	91,82	92,47	92,07	92,37	92,53
Cr ₂ O ₃	0,00	0,02	0,00	0,00	0,00	0,00	0,02	0,01	0,00	0,03	0,00	0,00	0,02	0,02	0,05
MnO	5,96	2,65	2,89	4,01	0,01	0,01	0,00	0,00	0,00	0,00	0,00	0,00	0,00	0,00	0,00
MgO	0,01	0,01	0,00	0,01	0,00	0,00	0,00	0,00	0,00	0,00	0,00	0,00	0,00	0,02	0,00
CaO	0,11	0,00	0,00	0,00	0,06	0,05	0,08	0,00	0,00	0,00	0,05	0,00	0,01	0,02	0,04
Na ₂ O	0,00	0,02	0,00	0,03	0,00	0,00	0,03	0,08	0,02	0,04	0,00	0,01	0,04	0,02	0,02
K ₂ O	0,00	0,01	0,00	0,00	0,00	0,00	0,02	0,03	0,00	0,00	0,00	0,01	0,00	0,00	0,03
Total	100,49	100,80	101,49	100,09	90,63	92,38	92,53	92,52	92,37	92,41	92,15	92,69	92,26	92,62	92,80
Si	0,00	0,00	0,00	0,00	0,01	0,01	0,01	0,01	0,01	0,02	0,01	0,00	0,00	0,01	0,00
Al	0,00	0,00	0,00	0,00	0,01	0,01	0,01	0,01	0,02	0,02	0,01	0,03	0,01	0,02	0,02
Ti	3,34	3,22	3,23	3,14	0,00	0,02	0,05	0,02	0,00	0,00	0,01	0,00	0,00	0,00	0,00
Fe ⁺²	2,88	3,35	3,34	3,43	9,95	9,94	9,85	9,91	9,96	9,94	9,93	9,95	9,96	9,95	9,95
Cr	0,00	0,00	0,00	0,00	0,00	0,00	0,00	0,00	0,00	0,00	0,00	0,00	0,00	0,00	0,01
Mn	0,42	0,19	0,21	0,29	0,00	0,00	0,00	0,00	0,00	0,00	0,00	0,00	0,00	0,00	0,00
Mg	0,00	0,00	0,00	0,00	0,00	0,00	0,00	0,00	0,00	0,00	0,00	0,00	0,00	0,00	0,00
Ca	0,01	0,00	0,00	0,00	0,01	0,01	0,01	0,00	0,00	0,00	0,01	0,00	0,00	0,00	0,01
Na	0,00	0,00	0,00	0,00	0,00	0,00	0,01	0,02	0,01	0,01	0,00	0,00	0,01	0,01	0,01
K	0,00	0,00	0,00	0,00	0,00	0,00	0,00	0,01	0,00	0,00	0,00	0,00	0,00	0,00	0,00
Cátions	6,66	6,77	6,77	6,86	9,98	9,98	9,94	9,98	9,99	9,98	9,97	9,98	10,00	9,98	9,99

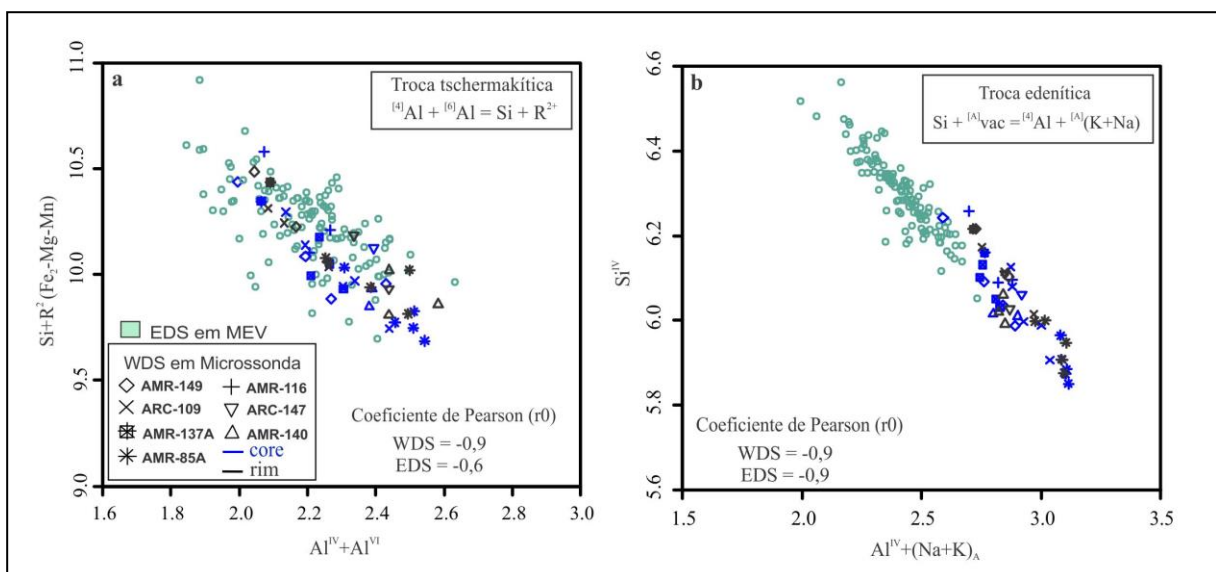
*Complementam as análises apresentadas no Capítulo 2.

APÊNDICE D - COMPARAÇÃO ENTRE AS ANÁLISES OBTIDAS POR EDS EM MEV E WDS EM MICROSSONDA ELETRÔNICA, PARA OS ANFIBÓLIOS DA SUÍTE PLANALTO.

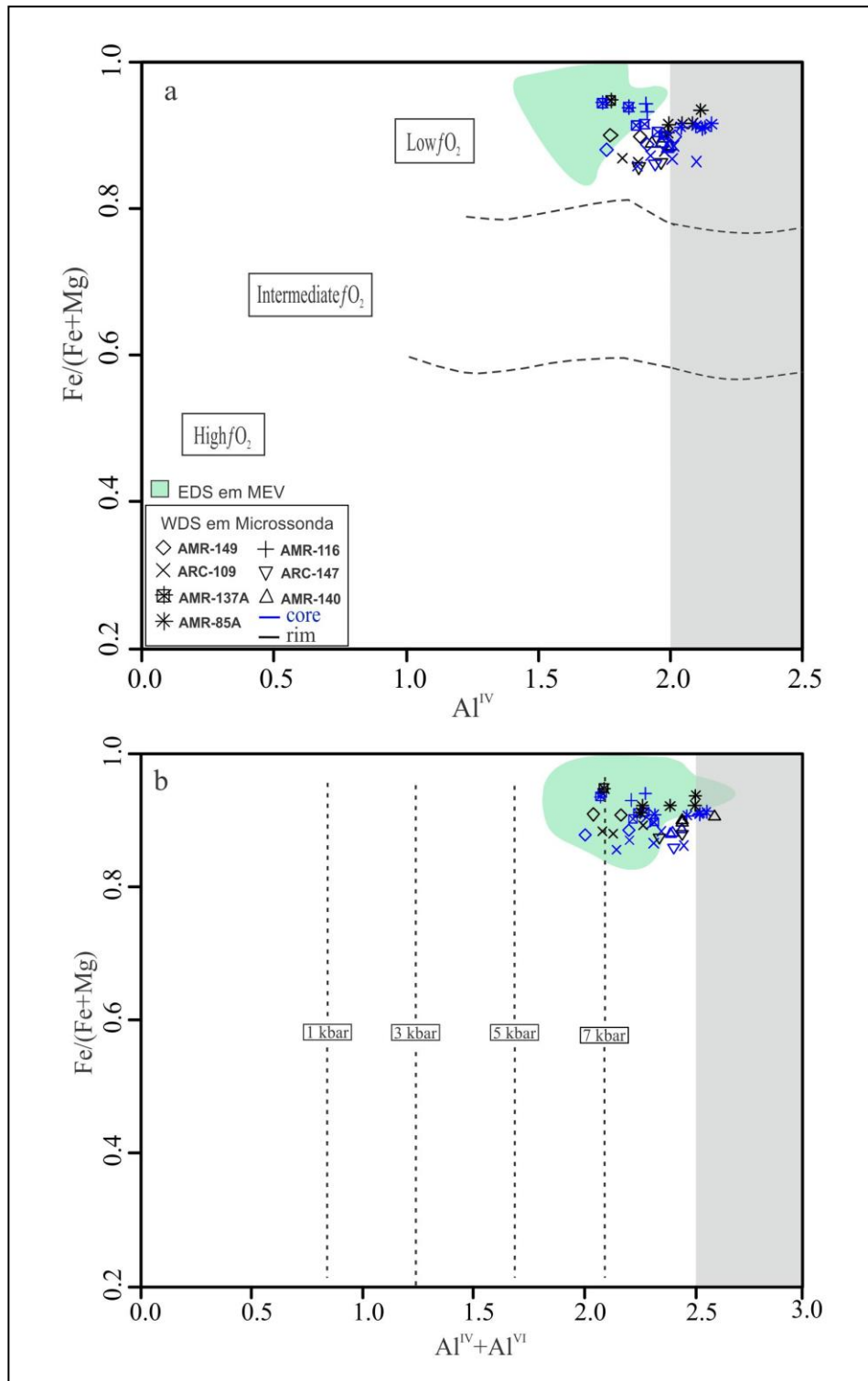
APÊNDICE D.1 - DIAGRAMA CLASSIFICATÓRIO DE LEAKE ET AL. (1997) PARA ANFIBÓLIOS DA SUÍTE PLANALTO.



APÊNDICE D.2 - DIAGRAMAS PARA AVALIAÇÃO DAS SUBSTITUIÇÕES (A) TSCHERMAKÍTICA E (B) EDENÍTICA EM ANFIBÓLIOS DA SUÍTE PLANALTO.

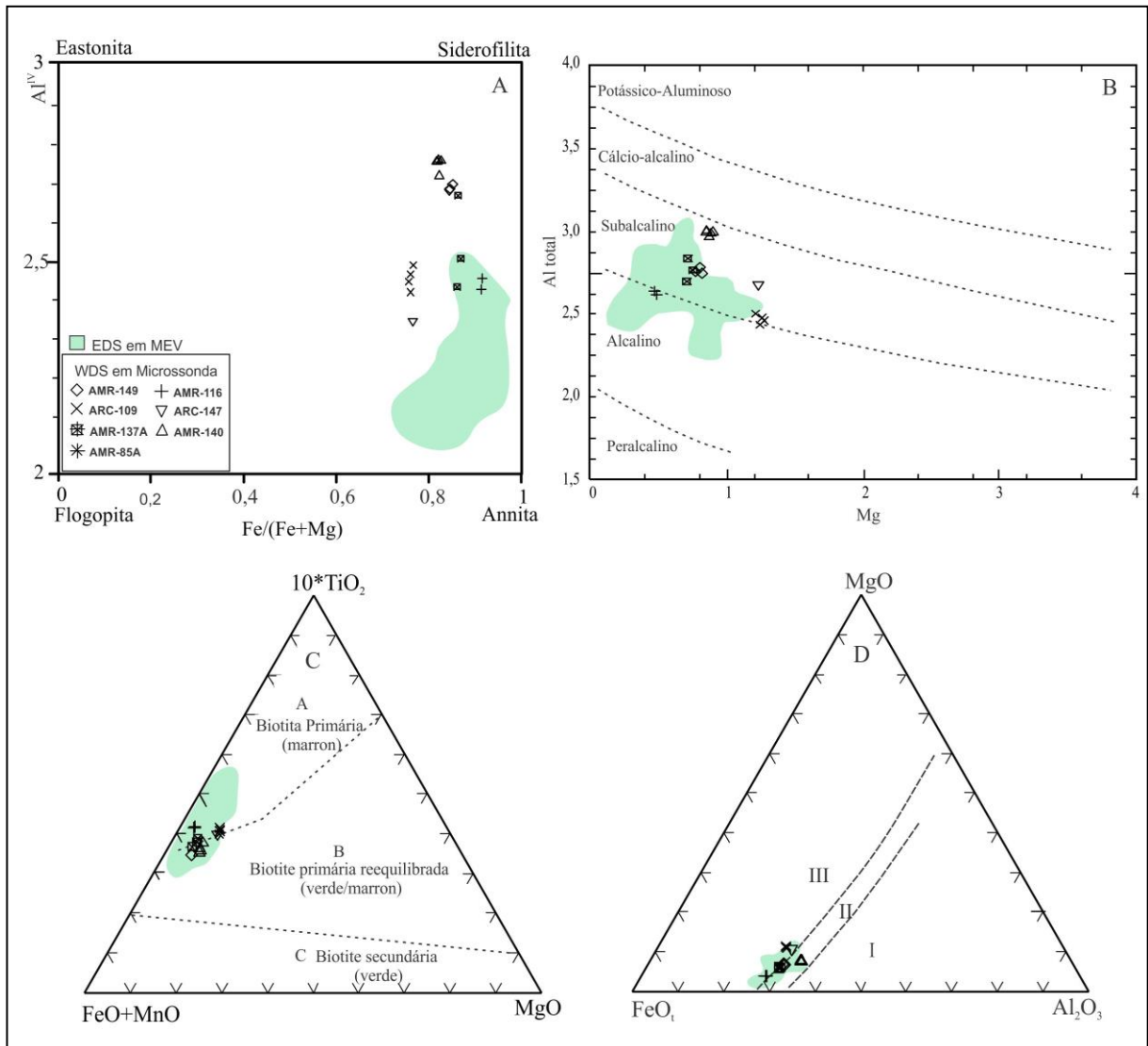


APÊNDICE D.3 - DIAGRAMAS CATIÔNICOS (A) $Fe/(Fe+Mg)$ VS. Al^{IV} E (B) $Fe/(Fe+Mg)$ VS. $Al^{IV} + Al^{VI}$ UTILIZADOS PARA ESTIMATIVA, RESPECTIVAMENTE, DE FUGACIDADE DE OXIGÊNIO E PRESSÃO, BASEADOS NA COMPOSIÇÃO DO ANFIBÓLIO. (FONTE DOS CAMPOS: ANDERSON & SMITH 1995).

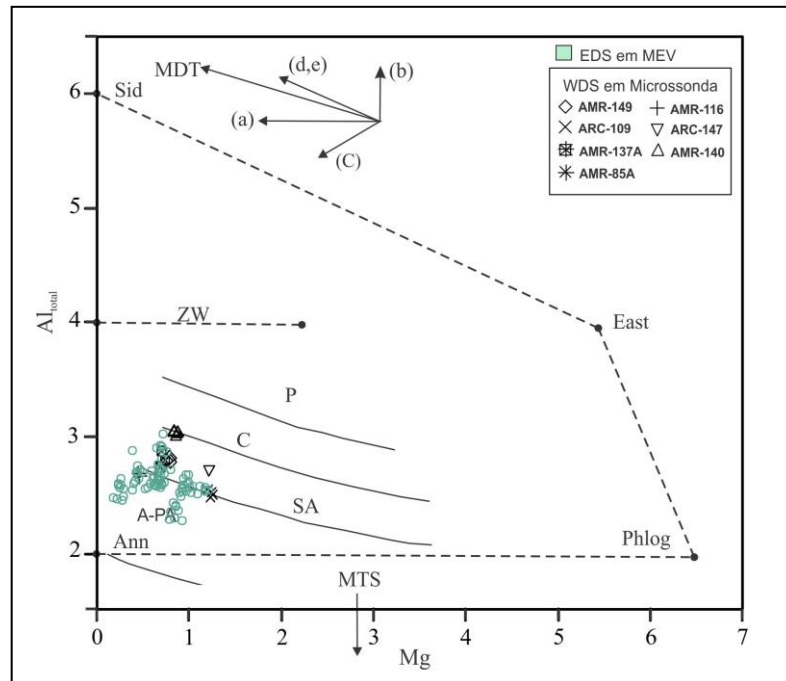


APÊNDICE E - COMPARAÇÃO ENTRE AS ANÁLISES OBTIDAS POR EDS EM MEV E WDS EM MICROSSONDA PARA BIOTITA DA SUÍTE PLANALTO.

APÊNDICE E.1: VARIAÇÕES COMPOSICIONAIS DAS BIOTITAS DOS GRANITOS DA SUÍTE PLANALTO: (A) DIAGRAMA $Al^{IV} - Fe/(Fe+Mg)$ (DEER ET AL.1992); (B) DIAGRAMA $Al_{TOTAL} \times Mg$ (NACHIT ET AL. 1985) PARA AS BIOTITAS, MOSTRANDO A AFINIDADE DAS BIOTITAS DA SUÍTE PLANALTO COM BIOTITAS DE ROCHAS SUBALCALINAS; (C) DIAGRAMA $(FeO+MnO)-(10*TiO_2)-MgO$ COM CAMPOS DE NACHIT (1994) MOSTRANDO A DISTRIBUIÇÃO DAS COMPOSIÇÕES QUÍMICAS DAS BIOTITAS ANALISADAS: (A) CAMPO DAS BIOTITAS MAGMÁTICAS PRIMÁRIAS; (B) CAMPO DAS BIOTITAS MAGMÁTICAS REEQUILIBRADAS; (C) BIOTITA SECUNDÁRIA; (D) DIAGRAMA $FeO-MgO-Al_2O_3$ (NOCKOLDS, 1947) MOSTRANDO AS COMPOSIÇÕES DE BIOTITAS EM DIFERENTES ASSOCIAÇÕES MINERAIS. CAMPOS: I – BIOTITA ASSOCIADA A MUSCOVITA, TOPÁZIO, FLUORITA ETC; II – BIOTITA QUE NÃO ACOMPANHA OUTRAS FASES MÁFICAS; III – BIOTITA ASSOCIADA A HORNBLENDA, PIROXÊNIO E/OU OLIVINA.



APÊNDICE E.2 - MEMBROS FINAIS DAS SÉRIES DE MICAS TRIOCTAÉDRICAS NO DIAGRAMA AL-MG (CF. STUSSI & CUNEY 1996): SID: SIDEROFILITA; EAST: EASTONITA; PHLOG: FLOGOPITA; ANN: ANNITA; MTS: MICA TETRASILÍCICA; ZW: ZINNWALDITA; (A), (B), (C), (D), (E) PRINCIPAIS SUBSTITUIÇÕES QUE OCORREM NAS BIOTITAS. AS BIOTITAS DA SUÍTE PLANALTO SÃO ANNITAS MAS APRESENTAM ENRIQUECIMENTO EM ALUMÍNIO, DAÍ O DESLOCAMENTO NO SENTIDO DA SIDEROFILITA.



APÊNDICE E.3 - DIAGRAMA $Fe/(Fe+Mg)$ VS $Al^{IV}+Al^{VI}$ MOSTRANDO A COMPOSIÇÃO DA BIOTITA DA SUÍTE PLANALTO.

